5-7-2010

Scalability study for robotic hand platform

Melissa Monahan

Scalability Study for Robotic Hand Platform

By

Melissa A. Monahan

A Thesis Submitted in Partial Fulfillment of the Requirement for Master of Science in Mechanical Engineering.

Approved by:

Department of Mechanical Engineering Committee:

Dr. Kathleen Lamkin-Kennard _____

Dr. Tuhin Das _____

Dr. Wayne Walter _____

Dr. Alan Nye, Dept. Representative _____

Industry Committee Member:

William Burton _____

Rochester Institute of Technology
Rochester, NY 14623
May 7, 2010

Permission to Reproduce the Thesis

Scalability Study for Robotic Hand Platform

I, Melissa Monahan, hereby grant permission to the Wallace Memorial Library of Rochester Institute of Technology to reproduce my thesis in the whole or part. Any reproduction will not be for commercial use or profit.

May 7, 2010

Abstract

The goal of this thesis project was to determine the lower limit of scale for the RIT robotic grasping hand. This was accomplished using a combination of computer simulation and experimental studies. A force analysis was conducted to determine the size of air muscles required to achieve appropriate contact forces at a smaller scale. Input variables, such as the actuation force and tendon return force, were determined experimentally. A dynamic computer model of the hand system was then created using Recurdyn. This was used to predict the contact (grasping) force of the fingers at full-scale, half-scale, and quarter-scale. Correlation between the computer model and physical testing was achieved for both a life-size and half-scale finger assembly. To further demonstrate the scalability of the hand design, both half and quarter-scale robotic hand rapid prototype assemblies were built using 3D printing techniques. This thesis work identified the point where further miniaturization would require a change in the manufacturing process to micro-fabrication.

Several techniques were compared as potential methods for making a production intent quarter-scale robotic hand. Investment casting, Swiss machining, and Selective Laser Sintering were the manufacturing techniques considered. A quarter-scale robotic hand tested the limits of each technology. Below this scale, micro-machining would be required. The break point for the current actuation method, air muscles, was also explored. Below the quarter-scale, an alternative actuation method would also be required. Electroactive Polymers were discussed as an option for the micro-scale.

In summary, a dynamic model of the RIT robotic grasping hand was created and validated as scalable at full and half-scales. The model was then used to predict finger contact forces at the quarter-scale. The quarter-scale was identified as the break point in terms of the current RIT robotic grasping hand based on both manufacturing and actuation. A novel, prototype quarter-scale robotic hand assembly was successfully built by an additive manufacturing process, a high resolution 3D printer. However, further miniaturization would require alternate manufacturing techniques and actuation mechanisms.

Acknowledgements

I would like to thank my thesis advisor, Dr. Kathleen Lamkin-Kennard for her direction, enthusiasm, and support of this project. Her dedication to this work is admirable and will certainly benefit RIT's Bioengineering advancements and provide exciting research for this Institution and future students.

I would also like to thank my thesis committee members Dr. Wayne Walter, and Dr. Tuhin Das, whose thoughtful feedback has made this a more complete project.

I greatly appreciate the help of Bill Burton, my engineering mentor who offered guidance with the dynamic modeling. He also provided me with the necessary encouragement to keep the project moving.

This work was generously supported by RIT faculty members John Wellin, who supported the experimental setups. John Bonzo, with manufacturing expertise and rapid prototyping services. Also Dr. Alan Raisanan, Dr. Denis Cormier, and Dr. Matthew Marshall with their insight and advice.

Finally I would like to thank my family and friends for whose support in everything I do, I am immeasurably grateful.

Table of Contents

Introduction

The problem of scalability aims to bridge the gap between a complex, life-size robotic hand and the less adept yet smaller-scale micro-manipulators available today. Taking some functionality of a life-sized robotic hand and scaling it down will result in a more sophisticated and precise tool for applications such as micro-surgeries. Robot assisted surgery is a developing field, marked by the need for precision. Currently, micro-manipulators are used in the laboratory for cell manipulation, covering a broad range of applications, but these devices lack the dexterity of the human hand. Thus the evolution of these tools, while promising, presents many developmental challenges for researchers today.

A micro-robotic hand could be capable of tasks similar to those of a human hand. This ability would give surgeons dexterous motions at the cellular scale during an operation procedure. While several advanced robotic hands exist, most are life-sized. Combining the additional degrees of freedom (DOF) that a life-size hand possesses, the micro-scale capabilities of micro-manipulators, and at some point the integration of haptic feedback would immeasurably advance the field of robotic micro-surgery. As a general term, "haptic" describes both force and tactile (touch) sensing.

The workings of the human hand are as amazing and complex as any other in the body. The design of our hands partially defines us as a species. When looked at strictly from an engineering perspective, one can identify a mechanical system of links, joints, and tendons (springs). This could be viewed as a major simplification, but it is these components that lend themselves to the field of robotics. Biomechanics and robotics are each vast and relevant topics. Combined, the slightly narrower field of BioRobotics has already experienced exciting and incredible success. Countless accomplishments include advances in robotic surgery, and these will continue to benefit patients of the future.

Literature Review

Several robotic hands currently exist in the literature today. These devices show a broad range of dexterity and accurately mimic the motion of the human hand at the life-size scale, but have not been successfully implemented at a smaller scale. The ultimate goal of the RIT Robotic Hand Platform is to perform tasks similar to those of a micro-manipulator, thus studying the state of the art in micro-manipulators and robotic surgery is of particular importance. Also, the main application of the RIT robotic hand is intended for robotic, cellular-scale surgery so inclusion of haptic feedback would introduce novel surgical capabilities. Many of the articles in the literature go hand in hand, however each has a unique point of view that in some way could be leveraged into a new robotic system for micro-surgery.

I. Current Hands

Many robotic hand designs exist and are the subject of much research, but the Shadow Hand (SH) is the most advanced. (Fig. 1) Developed by the Shadow Robot Company (London, UK), "The Shadow Hand is the closest robot hand to the human hand… providing comparable force output and sensitivity" [1]. Shadow Robot Company is able to make this claim based on the design as well as the incorporation of tactile elements on the fingers, seen in Figure 2.

Fig. 1 Shadow Hand [1]

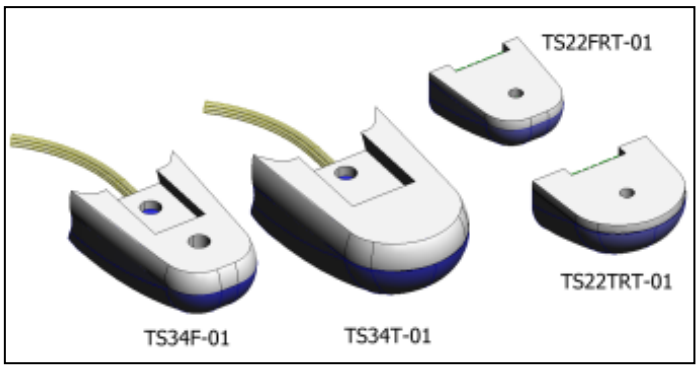

Fig. 2 Shadow Tactile Sensors [1]

The SH is actuated by forty air muscles that are attached to joints by artificial tendons, mimicking a human hand. Other technical specifications can be found on the Company's website. (www.shadowrobot.com)

The aspect that sets the Shadow Hand apart is the, "integrated touch sensing".

> The sensor uses Quantum Tunneling Composite (QTC) as the sensing medium. Each Sensor contains an on-board PSoC, which allows the user to actively control the range and sensitivity. This gives the sensor an unrivalled range, allowing plenty of useful feedback for control of manipulation tasks. The tactels are sensitive to loads ranging from 0.1N to 25N. This allows simultaneous control of both delicate handling and power grasping. The unique construction of Shadow Tactile Sensors allows custom sensors to be built to almost any dimensions allowing huge flexibility to fit your needs. [1]

Many applications are presented on the SH website (www.shadowrobot.com), however, the SH is mainly used by researchers studying grasping. Other applications include telepresence operations, rehabilitation and assistive technology, and ergonomic research. The tactels (which may be purchased separately) could possibly be incorporated on the RIT hand, should grasping research be necessary for further development of a mini-hand. NASA used the SH as inspiration for their own robotic hand design. [2]

NASA's Robonaut Hand is a key part of their Robonaut project. (Fig. 3) A humanoid robot is being developed for Extravehicular Activity (EVA), meaning spacewalks. One capability that would set this robot apart from a human astronaut would be increased dexterity in space. According to NASA, "Since we are attempting to model a human-like robot with human-like capabilities with Robonaut, we are using a human-like model for the development of our autonomous grasping capabilities" [2].

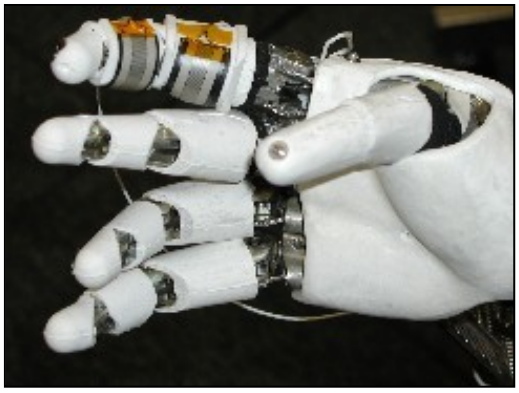

Fig. 3 Robonaut Hand [2]

The developers define success with the incorporation of tactile feedback in their robotic hand design. According to NASA, while looking into different sensor technologies, "we hope to

determine the critical sensor modalities that are required for the types of grasps and manipulation tasks we are interested in" [2].

The Robonaut Team was attempting to use force sensing resistors as tactile sensors. Work is still being done to determine the parameters that need to be measured during a grasping task. "Once we have a set of sensors capable of sensing the proper modalities, we then need to develop smart algorithms to determine what we are sensing" [2]. Other research focuses on tools to enable robotic hand designers to optimize their work. GraspIt! is a commercially available simulation program especially for robotic hand grasping.

Miller et al. [3] used GraspIt! to simulate a large number of different grasps, in order to determine the best grasp for a particular object. Then an analysis of each was conducted for various grasping tasks. More work is being done to advance the tool, such as the development of a deformable finger model that will "predict the geometric change in the contact regions and accurately compute contact forces between non-rigid bodies during grasping" [3]. GraspIt! stands apart as the only tool specifically focused on the analysis and visualization of robotic grasping.

The current robotic hands described above are examples of significant achievements in robotics and automation. The Shadow Hand boasts a variety of applications. These include grasping and ergonomic research, handling of delicate objects, rehabilitation and assistive technology, and telepresence operations. Almost all of these are essential aspects of a robotic surgical system. The Shadow Hand's ability to "manipulate delicate objects such as fruit and eggs" [3] parallels the need for a micro-manipulator to gently handle living tissues and cells. It is of importance to characterize the properties of the intended objects to be handled, especially in the case of biological cells.

In order to determine the appropriate forces for micro-manipulation, it is imperative to study a cell's mechanical properties and structure. This identifies requirements for micro-manipulators. Being able to quantify these properties automatically, while performing micro-manipulation tasks is important to researchers, since biological cells are greatly affected by experimental conditions. Girot et al. suggest that "since the reaction of the biological samples to stress vary greatly in a given lapse of time, it is important to monitor the characterization process continuously in an *in vitro* environment" [4]. Note that i*n vitro* "refers to the technique of performing a given experiment in a controlled environment

outside of a living organism" [5]. Girot et al. [4] described an experiment to prove that a cell's mechanical properties would change with and without the use of their clean room unit.

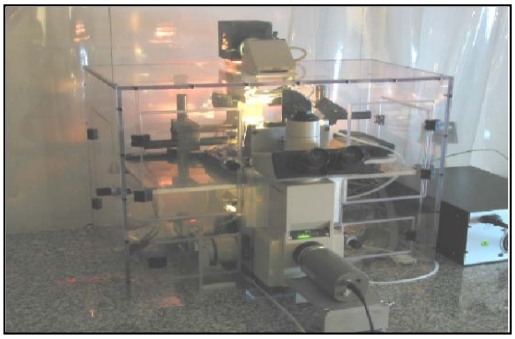

Fig. 4 FBM Experimental Setup [4]

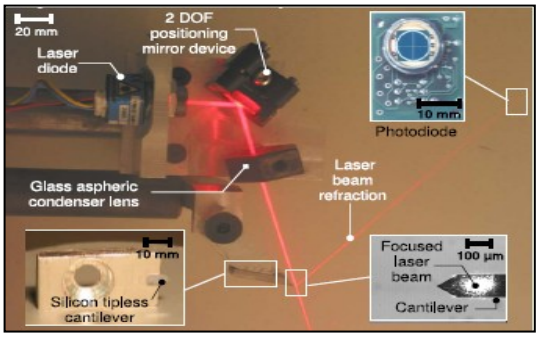

Fig. 5 Mechanical Sensing Unit [4]

Literature Review Summary Table: Current Hands			
Citation #	**Description**	**Significance**	**Related Figures**
[1]	Shadow Hand	Most advanced robotic hand, commercially available. Life-size, includes tactile feedback. Used primarily for grasping research.	Fig. 1 Shadow Hand Fig. 2 Shadow Tactile Sensors
[2]	Robonaut Hand	Life-sized robotic hand, developed by NASA for telepresence operations.	Fig. 3 Robonaut Hand
[3]	GraspIt! simulation tool	Modeling tool specific for robotic hand designs. Analyze poses of various grasping tasks.	
[4]	Force Bio-Microscope (FBM) used to characterize forces for micro manipulation	Experiments conducted *in vitro* to measure cell's mechanical properties, thus understand requirements for micro-manipulators that won't damage cells.	Fig. 4 FBM Experimental Setup Fig. 5 Mechanical Sensing Unit

II. Micro-Manipulators: Micro-grippers/Cell Manipulation

The following section covers the development of micro-manipulator tools, especially in the cases of gripping and cell manipulation. The earlier designs began with parallel plate, kinematic chain structures, and solving the inverse kinematic problem. This became the established procedure for later work. Inverse kinematics,

> Is the process of determining the parameters of a jointed flexible object (a kinematic chain) in order to achieve a desired pose. An articulated figure consists of a set of rigid segments connected with joints. Varying angles of the joints yields an indefinite number of configurations. The solution to the forward kinematic animation problem, given these angles, is the pose of the

> figure. The more difficult solution to the inverse kinematics problem is to find the joint angles given the desired configuration of the figure (i.e., end effector). [5]

Early work done by Grace et al. [6] foreshadowed work that has now been realized. According to Grace et al. "The initial operation mode will be open loop while future operation will be in a force-reflecting bilateral (macro-master/micro-slave) arrangement" [6].

The work done by Grace et al. [6] described the requirements and subsequent design of a parallel-structured micro-manipulator, to suit a specific application. For optical surgery, "micron-scale spherical movement of a glass micro-pipette tip inside the eye is required" [6]. Limitations of the current (1993) micro-manipulators forced Grace et al. [6] to pursue a six DOF design. The Jacobian matrix was used to map positions from the joints to endpoints. Mathematic software was used to solve the inverse kinematics problem, finding the joint positions as a function of endpoint coordinates. According to Grace et al. [6],

> This is straightforward for a parallel manipulator, because once the lengths are found by vector differences, the inverse Jacobian is then obtained by symbolically differentiating with respect to the joint positions. From this state, endpoint position and geometry values can be supplied, and the inverse Jacobian evaluated and inverted to give the Jacobian. [6]

Grace et al. [6] planned to include force sensing at the end effector, and eventually a more advanced master-slave setup.

In 2007, Ramadan et al. [7] presented a mathematical solution for the inverse kinematics problem of their hybrid micro-nano manipulator hand. The hybrid structure of the hand refers to two parallel kinematics chains that are connected in series. Each finger module was attached to a plate and had a glass pipette end effector, seen in Figure 5. Together these "fingers" of the hand produce a chopstick-like motion. Based on the mathematical solution, a simulation program was developed to optimize the workspace volume by varying the design parameters. Next, CAD geometry was made based on the optimal design parameters. (Fig. 6) A limited analysis of the hand was done in ANSYS and appeared to have a good correlation with the theoretical values.

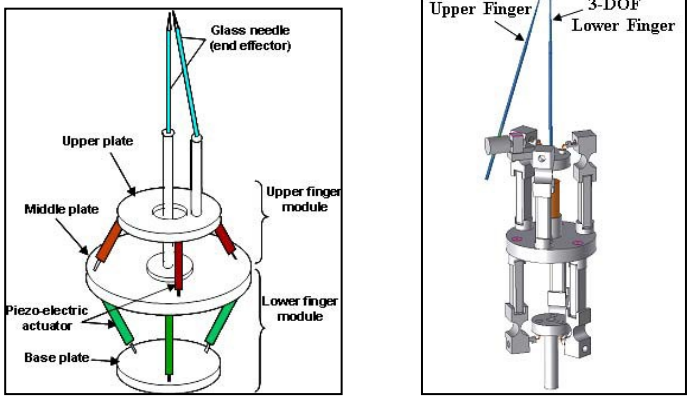

Figs. 5 & 6 In-Series Two-Fingered Micro-Nano Hybrid Manipulator Hand [7]

The proposed hardware setup for the hand used two computers, one for controlling the hand and the other for image processing. The xy-coordinates of the end effector were located with an image processing system. The fingertips of the hand were controlled either with a keyboard or joystick. Future work proposed in the study included further ANSYS analysis, as only two of the legs were simulated to predict the hand's range of motion. Also, there were no results presented that described the hand actually manipulating a micro or nano-scale object. Furthermore, no anticipated applications for the design were presented.

Han et al. [8] introduced a micro-gripper capable of manipulating a small object such as a glass micro bead, and potentially a cell. Operation of the gripper was made possible for an aqueous environment. A piezo-resistive sensor was integrated into the gripper to sense gripping-force. The resistor in the sensor varied according to the force on the micro-gripper. Thus, for a given applied force, the force on the cell and thus the deformation of the cell could be determined.

Important considerations for the micro-gripper were operation in water, and limiting damage to the cell. Various types of micro-gripper designs were mentioned including adhesion, absorption, and mechanical types. The mechanical type was identified as one that is not significantly affected by an aqueous environment and capable of controlling gripping force with a force sensor.

The shape of the micro-gripper was determined by numerical analysis. The length and thickness dimensions of the micro-gripper made up the range/domain. When the gripping force was applied, if the deflection of the cantilever was larger than the micro

object, it was difficult to grip. This set the guidelines for the largest feasible deflection, based on a cancer cell size of 20µm.

It was unclear which equation was being used by Han et al. [8] to determine the stresses on the cantilever. Although the reader might assume it is the following:

$$\delta = \frac{3\sigma(1-\nu)}{E}\left(\frac{L}{t}\right)^2$$

"Stoney's formula is one of the key equations to understanding the behavior of MEMS cantilevers. Cantilever end deflection δ is related to applied stress σ, where ν is Poisson's ratio, E is Young's modulus, L is the beam length and t is the cantilever thickness" [5]. From the equation it was determined that the maximum stress on the cantilever would not exceed the yield strength. The length and thickness of the cantilever were subsequently chosen.

The bursting force of a cell is within a few µN, thus the grippers must be sensitive to this degree. According to Han et al. "The piezo-resistive sensor uses the change of electrical resistivity due to the strain variation according to the applied force. The resistance change is expressed as the summation of the multiplication of the resistivity and the stress in the longitudinal and transverse direction" [8].

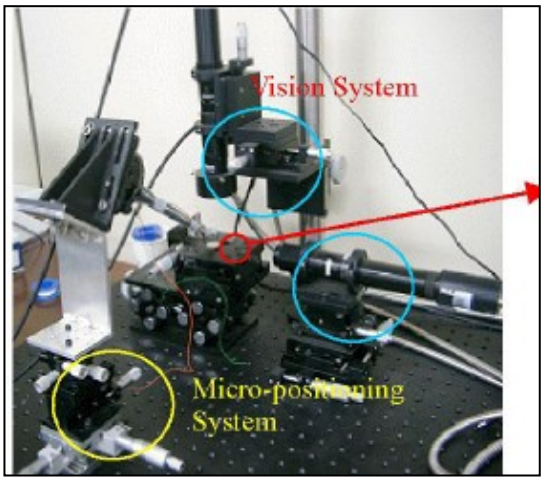

Fig. 7 Micro-gripper system [8]

Fig. 8 Magnified micro-gripper [8]

Shown in Figures 7 and 8, the complete system included a vision system, micro-positioning system, and micro-gripper. An experiment showed that micro-glass beads could be manipulated both in air and water. The gripper was more successful in the aqueous environment due to the following adhesive forces: Van der Waals, surface tension, electrostatic. "As the force given by the AFM tip on the end of the gripper is increased, the

change of the resistance of the piezo-resistive sensor is measured" [8]. It was found that the "applied force is proportional to the rate of change of the resistance which is smaller than the design value" [8]. This conclusion verified the expected outcome.

Tam et al. [9] and Wejinya et al. [10] focused on specific aspects of micro-manipulation tools. Tam et al. [9] worked to determine the possibility of using flexure joints for micro-manipulators. Whereas Wejinya et al. [10] looked at controlling the suction force of a pneumatic end effector used in micro-manipulation tasks. Favre-Bulle et al. [12] described a creative approach to the control of a unique micro-gripper. It included many complex concepts which may reduce the potential for its realization. However, it is these extraordinary ideas which have enabled the many technological advances in the medical and robotics fields.

Tam et al. [9] discussed existing two DOF flexure joint configurations as well as a novel two DOF design. The new design may lead to the development of a three DOF manipulator and corresponding six DOF system. "The general objective is to develop an inexpensive, high resolution multiple degrees-of-freedom micro-manipulation system with maximum repeatability and precision using a completely mechanical concept called flexure joint" [9].

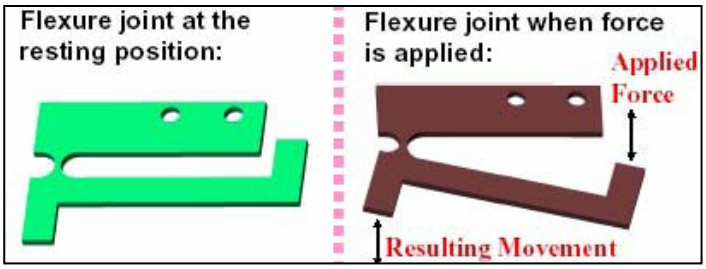

Fig. 9 One DOF Flexure Joint [9]

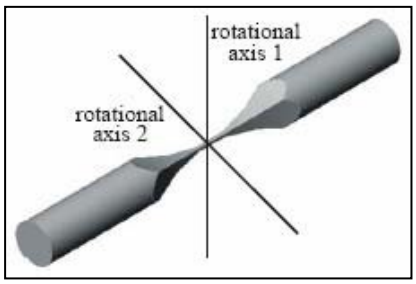

Fig. 10 Two DOF Flexure Joint [9]

A flexure joint operates similarly to a lever system, where a macro-motion input is reduced to a micron output displacement. (Fig. 9) The scaled-down motion is based on some fixed design reduction ratio. Given that a single flexure joint produces one rotational DOF, the problem becomes determining the number of joints required. To be considered was the overall system size and the operating workspace, based on potential applications. The joints were actuated by piezo-ceramic discs connected in parallel. When a voltage was applied the discs expanded. In general, "Piezoelectricity is the ability of some materials (notably crystals and certain ceramics) to generate an electric potential in response to applied mechanical

stress" [5]. When coupled to a flexure joint, the expansions of the discs acted as the input force for the system.

Previous work was reviewed by Tam et al. [9], beginning with the basics of flexure joint behavior. When an input force is applied, the joint flexes at the pivot only causing elastic deformation of the material. (Fig. 10) With the addition of more flexure joints, both a higher reduction ratio and more DOF become available. Two disadvantages of the multiple-DOF flexure joint are manufacturability and the delicate nature of the joint. Using several one DOF joints connected in parallel was simpler, and mitigated these design problems.

Two versions of a three DOF design were presented, one of which is represented in Figure 11. Trigonometric calculations were done to determine the size of the work space. Analysis was completed in ANSYS to find the optimum flexure thickness. The benefits and costs of two types of actuation were then compared. Piezoelectric actuation provides precise motion at a small scale with the ability to generate large forces. This is an expensive method compared to a lead screw assembly. For this work, lead screw actuation was chosen based on its cost-effectiveness.

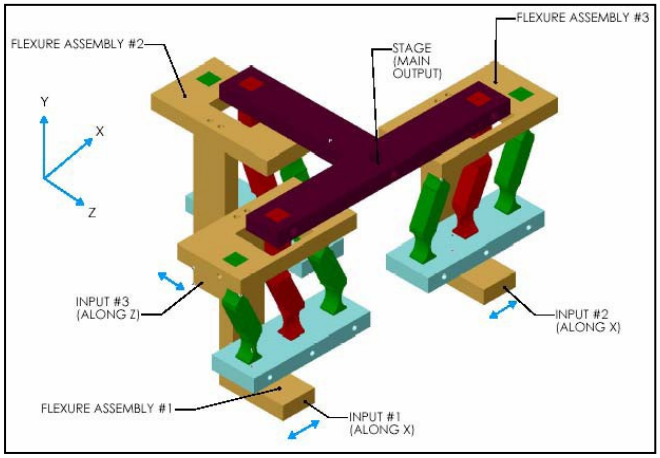

Fig. 11 Possible Three DOF Model [9]

Next, manufacturing methods were discussed for the flexure joints. It was decided to machine the joints by a wire EDM cutter. A prototype of the entire assembly was designed and modeled in FEA to determine the workspace. The ultimate goal of this work was to develop a six DOF system to increase flexibility of the end effector.

Basic concerns when developing a gripping tool for micro-manipulation include precision control of the force used to hold a micro-object. Too much force will damage a delicate object such as a living cell, but too little force would not accomplish the task. A

micro-tool must be small itself due to the workspace restrictions of its applications. For micro-assembly applications, it is important that micro-tool be simple and inexpensive. These aspects of a grasping tool are outlined as requirements for the RIT robotic hand.

The focus of the research by Wejinya et al. [10] was the exploration and development of an effective, efficient solution for micro-assembly and micro-manipulation. The design of the tool was based on the pneumatic vacuum/pressure mechanism. Effectively controlling the suction force and pressure of the tiny latex tube end effector was essential. In order to accomplish this, "a high sensitivity PVDF beam sensing buffer is built between the micro-tube and micro-pump" [10]. A closed-loop system including the end effector, micro-pump, and PVDF sensing buffer were integrated to provide the required precision forces for micro-manipulation. (Fig. 12) Note that, "Polyvinylidene Difluoride, or PVDF is a highly non-reactive and pure thermoplastic fluoropolymer" [5].

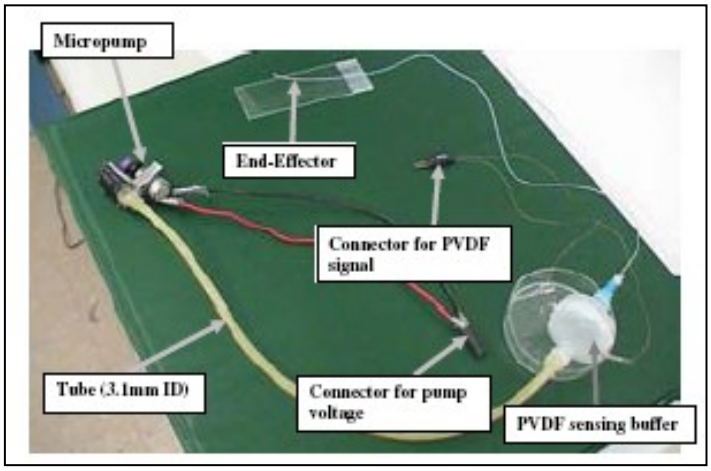

Fig. 12 Pneumatic End Effector System [10]

Wejinya et al. [10] returned to fundamentals in order to describe how the pneumatic end effector would work. Capillary force is the force that results from surface tension, and was used to calibrate the capillary-like end effector. The working principle of the pneumatic system was also described. "When voltage is applied to the micro-pump, the free tube end can generate micro suction or pressure force due to vacuum or pressure action provided by the micro-pump" [10].

Based on the flow rates, the PVDF sensing buffer detects the suction/pressure force generated by the micro-pump. "The deformation of the sensor beam is caused by the suction/pressure force acting at the middle of the beam strip in the sensing buffer" [10]. The unit piezoelectric equation was found based on the piezoelectric transverse effect and

assumptions. Also, assuming that the PVDF film was constrained on both ends and external force was applied in the middle of the beam, the stress on the beam can be calculated. A dynamic relationship between the sensing output voltage and the suction/pressure force was described. The resulting equation referred to the force in the sensing buffer itself. To obtain the force at the end effector, the cross-sectional areas of the tube and sensing buffer were taken into account. The research of these authors lead to a patent for an end effector for nano-manufacturing which claims, "The end effector is comprised of: a micro-pump fluidly coupled to a micro-tube; a piezoelectric sensing structure disposed in the micro-tube; and a processing circuit electrically coupled to the sensing structure for determining the force of the micro-fluidic flowing through the micro-tube [11]."

Favre-Bulle et al. [12] presented an uncommon solution to micro-manipulation problems, utilizing a tentacle design for the micro-gripper with many links and joints. It also, "introduces a novel approach for the kinematic coordination of mechanical robot micro-grippers on the basis of neural networks" [12]. The hyper-redundant robot design made controlling the gripper a challenge. To compensate for this, the authors used an "optimized geometrical path generator in order to teach dynamic neural nets a certain motion behavior, dependent on distance sensor signals" [12]. Sensors were located near the joints of the gripper, and detected the distances to the object being gripped. It was demonstrated that the neural network was able to learn the procedure for gripping, manipulating the links to wrap around the object.

According to the CalTech Robotics group,

> Robot manipulators which have more than the minimum number of degrees-of-freedom are termed "kinematically redundant" or simply "redundant". Redundancy in manipulator design has been recognized as a means to improve manipulator performance in complex and unstructured environments. "Hyper-redundant" robots have a very large degree of kinematic redundancy, and are analogous in morphology and operation to snakes, elephant trunks, and tentacles. There are a number of very important applications where such robots would be advantageous. [13]

Favre-Bulle et al. [12] took inspiration from nature's examples of hyper-redundant systems, and aimed to leverage previous work done with control methods to look at micro-

manipulation limitations in a new way. Optical range finder and "nearest-neighbor" (capacitative or ultrasonic) sensors were considered as options for detecting the distance to an object's surface. Due to the limitations of both working at the micro-scale, and with high conductivity objects, a capacitative sensor was selected. However, it was noted that the distance information attained was used to "roughly estimate the object's contour. For a certain manipulator configuration, the distance values allow to build a coarse model of the object contour, which is transformed into a set of spline functions" [12].

The shape controller described by Favre-Bulle et al. [12] uses the computed torque method to produce torque signals in order to move the manipulator and achieve a desired shape. Trajectory coordination was then utilized, where a grasp planner "calculates a reference vector for the shape controller at each time step in the wrapping sequence" [12]. Several approaches to plan the wrapping trajectories included genetic, geometric, and a neural network approach. "The neural network receives off-line training from a geometrical trajectory generator" [12]. However, by means of this procedural knowledge, the neural network learned the principles of the wrapping sequence with consideration of the received sensory information from the object. Where, "Procedural knowledge is the knowledge exercised in the performance of some task" [5]. The neural nets were then capable of generalization. This hyper-redundant micro-gripper design and complicated control system have not yet been realized. Many problems must be addressed before these concepts could be experimentally tested. These include concerns of friction, structural stability, and drive dynamics.

A variety of micro-robotic systems have been developed that control or operate grasping tools. Applications of these devices include cell injection and cell manipulation. The manipulation of single cells is performed for a variety of biological applications and may one day extend to single-cell surgery. Common practice involves observing the object which is suspended in liquid through an inverted microscope with end effectors attached to the microscope. It is important that the end effectors do not hinder visibility, thus glass capillaries are used. However, this system limits movement of the object to the boundaries of the microscope stage.

Truper et al. presented a micro-robot system that can, "hold, lift, transport, and release cells" [14], without being restricted to the microscope space. The proposed micro-

robot accommodates three different end effectors, the switching of which is done by rotating the robot platform. Another advantage of this modular concept was that the object could be approached from different angles. (Fig. 13)

The system included a mobile platform that transported the other components to their designated position. This was done by piezoelectric actuation of roller spheres. The manipulator unit was comprised of three moveable tables, driven with high precision by electromagnetic micro-motors, seen in Figure 14. Piezoelectric stacks were used for fine positioning of the end effector mounting frame located on top of the tables. Table position was measured by LVDT sensors, while image processing determined overall robot movement. A capillary was used as an end effector along with a micro-pump to accomplish pick/place and cell injection tasks.

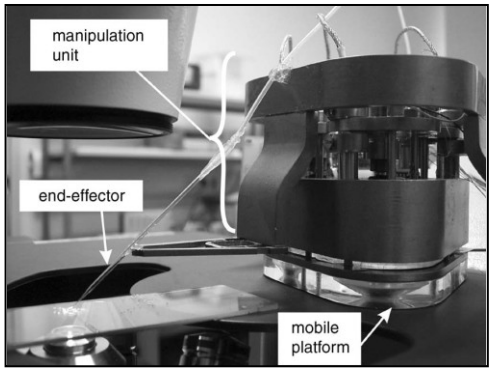

Fig. 13 Mobile micro-robot with pipette for cell manipulation on stage of inverted microscope [14]

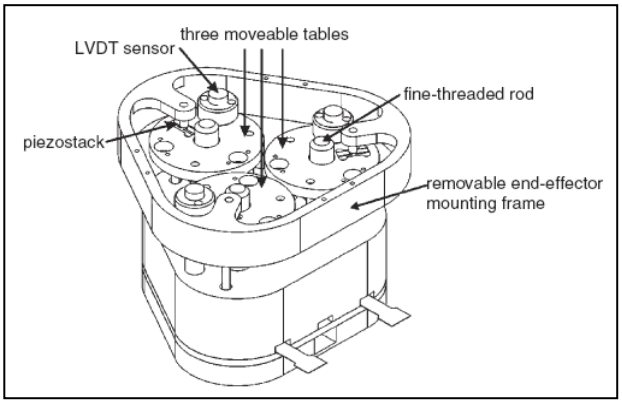

Fig. 14 Manipulator Unit [14]

The goal for Truper et al. [14] of automated cell manipulation tasks was met by several important requirements for measuring both manipulator and target positions. "The position of the object plane is measured by using a focus index algorithm that detects and correlates edges in the microscope image. If the target objects are in focus, they can be tracked with the help of a geometric model-finder algorithm" [14]. To determine the position of the end effector, another focus index algorithm was used. Two approaches for positioning during cell transport and sorting were discussed by Truper et al. [14]

The picture sequence in Figure 15 visually describes a cell transportation experiment. Frame by frame, a cell was lifted, moved, and lowered to the desired position. To further the automation of cell manipulation, Truper et al. planned to establish "more sophisticated algorithms for the recognition of and distinction between different types of cells" [14].

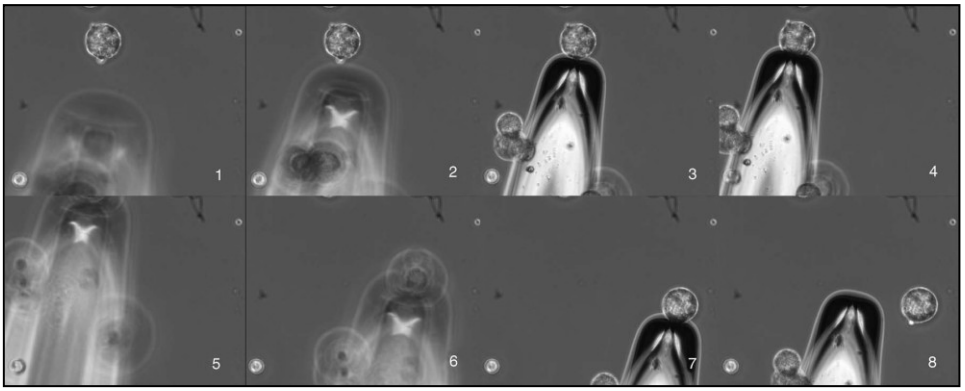

Fig. 15 Sequence of handling (lifting and transporting) with the capillary [14]

Brufau et al. described a "multi-micro robot manipulating system to handle μm-sized objects as well as smaller nano-scale objects" [15]. The purpose was to automate the manipulation of these small scale objects, with nanometer precision. Depending on the attached tool, a cluster of small (cm^3) mobile autonomous robots could carry out a range of tasks. For example, "an AFM (atomic force microscope) probe for local measurements, a silicon chip with an injection needle for cell injection, and a microgripper for micromanipulation" [15]. (Fig. 16)

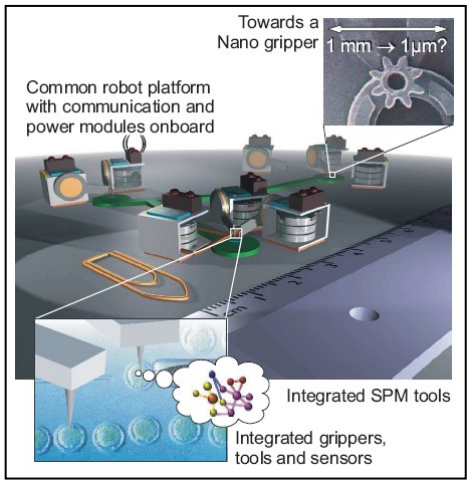

Fig. 16 MICRoN Project Overview [15]

This work preceded a more specific cell injection application described by Tagliareni et al. [16]. Brufau et al. [15] focused more on locomotion, positioning, and electronics systems as well as inclusion of an AFM tool for cell manipulation. This tool can image the 3D structure of biological specimens in their environment, allowing for real-time monitoring of biological processes. "This tool is also used to study the mechanical properties of cells"

[15]. It used a sharp tip to investigate the mechanical forces and associated cell deformations related to cell processes.

Data collected using an AFM may be useful to determine requirements for allowable micro-gripper forces. The AFM force sensor is an optical lever which operates by,

> …reflecting a laser beam off the cantilever. Angular deflection of the cantilever beam causes a two-fold larger angular deflection of the laser beam. The reflected laser beam strikes a position-sensitive photodetector consisting of two side-by-side photodiodes. The difference between the two photodiode signals indicates the position of the laser spot on the detector and thus the angular deflection of the cantilever. [15]

For two reasons, force measurements with an optical sensor require a large size AFM. The first reason is due to the distance between the reflected beam and the photodiode. Second, the size of its different components presents limitations. Thus, while this tool is desirable and adequate in a laboratory setting, it may not be applicable to real time surgical operation situations.

An extension of the work described by Brufau et al. [15] above was the development of a fully automated cell manipulation system, used as a tool for the micro-injection of living cells. (Fig. 17) The three subsystems of the cell manipulation system are the electronics, a micro-robot cluster with an integrated micro-fluidic SyringeChip, and infrared communication.

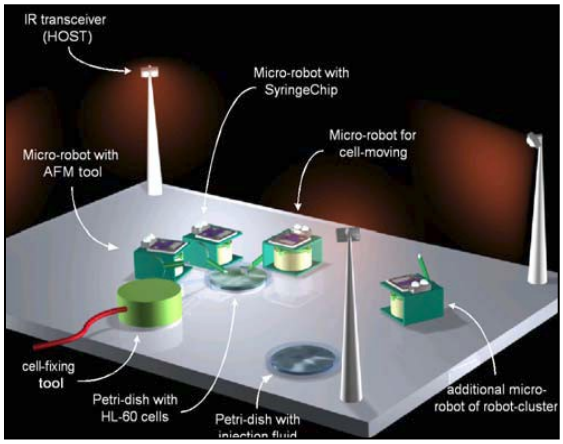

Fig. 17 Infrared controlled robot cluster performing a biological cell manipulation (3D model) [16]

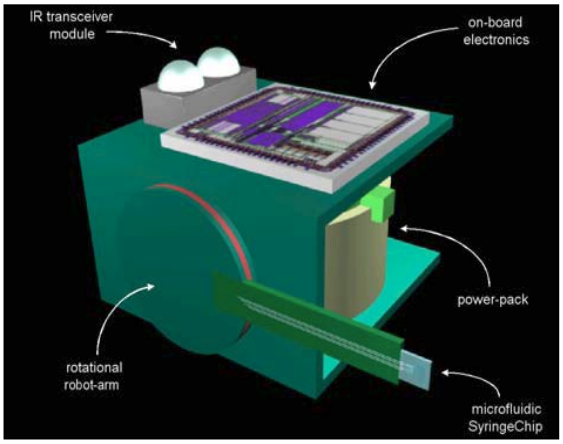

Fig. 18 3D Model of a MiCRoN Robot [16]

These subsystems were built with the intention of integration into a MiCRon robot. (Fig. 18) "A MiCRoN robot consists of a power supply module, a locomotion unit, an arm with an attached tool, an infrared transceiver, and the robot's control and actuation electronics" [16].

The micro-injection process involves treating each individual cell manually with a drawn glass capillary, the operation of which depends on the skill of the micro-manipulator technician. The necessity for precision in these tasks leads to the desire to automate these operations. The advantage of using mobile micro-sized robots as presented by Tagliareni et al. was the increased "flexibility due to the variety of tools" [16].

Several micro-robots, each equipped with a tool, were required to complete the cell manipulation process. For example, the SyringeChip robot (that performs the actual cell injection of liquid) contains a micro-needle, an integrated liquid reservoir, and a thermo-pneumatic actuator. The cluster worked toward the common goal, and each individual robot was controlled by the host computer. This setup was summarized as a single-master, multi-slave system. The electronics system used three circuit boards to coordinate the remotely controlled tasks of the micro-robots. Finally, in order to maximize mobility, infrared transmissions were used for wireless communication.

Although the entire cluster of robots was not yet built, this system was one example where micro-manipulators, in conjunction with other micro-robots, were used to complete the specific task of cell injection. Here the micro-gripper robot was a supporting tool in the cell manipulation process.

Li and Xi [17] presented several accomplishments towards the development of a robotic system potentially capable of performing single-cell surgeries. Li and Xi [17] have developed MEMS polymer grippers with the tested ability to grip 500μm size cells in water. Also, a probe-etching technique that can shape fiber probes into various tip geometries was presented. A PVDF force sensing system with sub-μN resolution was developed. When combined, these technologies may present advances for several applications including bio-manipulation and injection as well as single-cell surgery.

The ability to rotate a single cell is desirable for a micro-injection process. Li and Xi's goal was to develop a "micro-gripper system that can be eventually used to manipulate and isolate cells controllably, and enable localized cell probing and measurement" [17]. The applications of micro-pipettes are limited by their size. Currently they are used to "transport

micro-electrodes into cells to obtain an electrical signal and to inject fluid into cells" [17]. Decreasing the tip size of micropipettes would greatly increase the variety of applications. Techniques developed for Scanning Near-field Optical Microscopy have shown the possibility of a nano-scale tip for cell surgery. In order to use the nano-tips, the robotic system must be optimized for precise motion. At this point in 2004, Li and Xi acknowledged that "effective methods on micro force sensing and control are still lacking" [17].

Development of the underwater micro-gripper began with the problem of actuation. Although thermal actuators have several inhibiting features, the authors have accounted for these. [17] In general, thermal actuators require a high power input and dissipate significant heat energy that may kill biological cells. The actuation voltage is also relatively high, and will induce electrolysis in the solution environment. Using a polymer material called Parylene C for the micro-gripper alleviated these major problems. A tri-layered thermal actuator was made by encapsulating a thin film metal heater with Parylene C. "Parylene C is bio-compatible, has excellent thermal and electrical insulation properties, and has a relatively large coefficient of thermal expansion" [17]. One limitation of the material is its low melting point.

Experiments were conducted to evaluate two methods for inducing a temperature change in the thermal actuator. The first involved passing a current through the resistive heater, where the second method heated the actuator by raising the temperature of the surroundings. Fabrication involved combining "a sacrificial boundary etching technique with a well known and simple chemical probe etching process (Turner's Method)" [17]. This fabrication process, called the KL process, was also used to make smaller micropipettes seen in Figure 19.

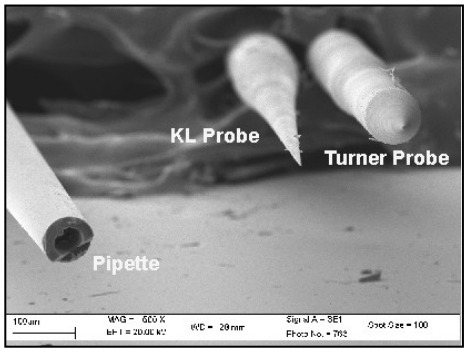

Fig. 19 SEM picture of KL probe, Turner probe, and conventional pipette [17]

Another component developed by Li and Xi [17] was a force sensor system using an *in situ* PVDF piezoelectric sensor. PVDF film was used to fabricate sensors that detect real time micro-forces during a manipulation process. With the addition of custom electronics, the force signal was extracted with great efficiency. Experiments using the PDVF sensors showed that the sensitivity of the system was adequate for picking up cell-probing signals. [17] It was found that the KL probes caused less damage than a Turner probe during a cell injection process. In other words, the nano-tips could penetrate cell membranes with less mechanical resistance.

Different methods have been investigated for actuating robotic systems by Tie, Lin, and Cunxi [18] and Wang et al. [19]. These allowed a glimpse into the wide variety of scientific concepts being considered to enable the highest precision movements. Powerful magnetic forces are used in medical imaging applications and are being investigated as a method for driving a robot. Other novel methods of using smart materials such as electroactive polymer actuators are also active areas of research, as by Wang et al. [19].

Typically, servo motors drive the robotic systems used in micro-manipulation tasks. Limitations of this transmission method include friction, wear and tear, and clearance. Robots driven by shape memory alloys are vulnerable to environmental variation. Piezoelectric drivers have the disadvantages of high voltage requirements and poor connections between layered piezo-ceramics.

Tie, Lin, and Cunxi [18] aimed to mitigate these problems and achieve higher precision by using magnetic force as the driver for a robotic system. However, the single DOF slider that was proposed as the manipulator seemed like it would not have the functionality of other robotic systems. Displacement of the slider was measured to indicate a sensed force. The control system used the displacement measurements to adjust output voltage of the electric magnets so that the slider was dynamically balanced in place. Support boards for the manipulator were affixed with four magnets each. Increasing and decreasing the magnetic forces of each magnet moved the manipulator to the desired position. A simple displacement experiment was conducted, and it seemed the system was less intuitive than its more common counterparts. However the authors concluded that, “the robot control precision and velocity characteristics can meet the requirement of the micro-manipulator robot” [18].

EAPs, another robotic actuation method under investigation, are

> …polymers whose shape is modified when a voltage is applied to them. They can be used as actuators or sensors. As actuators, they are characterized by the fact that they can undergo a large amount of deformation while sustaining large forces. Due to the similarities with biological tissues in terms of achievable stress and force, they are often called artificial muscles, and have the potential for application in the field of robotics, where large linear movement is often needed. [5]

Wang et al. [19] introduced a parallel architecture in order to bridge the gap between the limits of EAPs and the application of micro manipulators. This particular architecture was defined by "handling objects using multiple polymer actuators in order to greatly enhance their load carrying ability… A significant technical challenge presented by micro-manipulators based on artificial muscle actuators is the nonlinearity of actuator dynamics" [19].

Literature Review Summary Table: Micro-Manipulators, Part 1			
Citation #	**Description**	**Significance**	**Related Figures**
[6]	Parallel structured micro-manipulator for optical surgery	Described six-DOF micro-manipulator design, and mathematics for finding the joint positions as functions of endpoint coordinates.	
[7]	Hybrid mirco-nano manipulator hand	Two fingered hand producing chopstick-like motion. Used mathematic simulation to optimize workspace volume.	Fig. 5 & 6 In series two-fingered micro-nano hybrid manipulator hand
[8]	Micro-gripper with force sensor	Piezo-resistive sensor was integrated into micro-gripper, shape of sensor determined by numerical analysis. Sensitive enough to grip glass micro bead in aqueous environment.	Fig. 7 Micro-gripper system Fig. 8 Magnified micro-gripper
[9]	Use of flexure joints to increase DOF for micro-manipulator	Joints were piezo-ceramic discs connected in parallel, description of flexure joint behavior.	Fig. 9 One DOF Flexure Joint Fig. 10 Two DOF Flexure Joint Fig. 11 Possible Three DOF Model

Literature Review Summary Table: Micro-Manipulators, Part 2			
Citation #	**Description**	**Significance**	**Related Figures**
[10]	Pneumatic end effector for micro-manipulator	Used capillary force to calibrate end effector. PVDF sensor detected pressure generated by micro-pump. System capable of controlling forces for micro-manipulation.	Fig. 12 Pneumatic End Effector System
[12]	Hyper-redundant robotic micro-grippers	Redundant, more DOF. Shape controller and neural network approach to manipulator control.	
[14]	Micro-robot system, modular concept	System capable of accommodating three different end effectors for automated cell manipulation. Capillary end effector and micro-pump used for cell injection tasks.	Fig. 13 Mobile micro-robot with pipette for cell manipulation on stage of inverted microscope Fig. 14 Manipulator Unit Fig. 15 Sequence of handling with the capillary
[15]	MiCRoN: Cluster of mobile robots to carry out tasks	Cell injection and micro-manipulation done with Atomic Force Microscope probe, used to study mechanical properties of cells.	Fig. 16 MiCRoN project overview
[16]	Continuation of work with MiCRoN cluster of mobile robots	Fully automated cell manipulation for cell injection.	Fig. 16 MiCRoN project overview Fig. 17 Infrared controlled robot cluster performing a biological cell manipulation Fig. 18 3D model of a MiCRoN robot
[17]	MEMS poly-grippers for gripping cells	PVDF force sensing system, for use in rotating single cells for cell injection. Used Turner's Method for development of small micropipettes, "KL probe" cause less damage to cells during injection process.	Fig. 19 SEM picture of a KL probe, a Turner probe, and a conventional micropipette
[18]	Magnetic force to drive robotic system	Increase and decrease magnetic forces to control position of micro-manipulator.	
[19]	Micro-manipulators using EAP actuation	Handling objects using EAPs as actuation method	

The key technologies discussed in the Micro-Manipulators section focused on the unique aspects of handling cells. The challenges faced are of relevance to the development of the RIT micro-hand, which is designed to apply in robotic micro-surgeries. These

considerations for actuation, operation in an aqueous environment, and increased dexterity are all important for future work related to the RIT Robotic Hand Platform.

III. Robotic Surgery

The concept of a master-slave setup is the basis for the majority of robotic surgery systems. The surgeon operates a master device, whose movements are translated to the slave manipulator. This concept has enabled "tele-"surgery, where the surgeons may conduct an operation miles away from the patient. This incredible feat means that specialists could reach more patients in need. In theory, all surgery performed with this kind of setup can be considered tele-surgery to some extent, whether the surgeon is five feet or five hundred miles away.

Mamoru Mitsuishi, whose name appears on several of the following articles, has been working on tele-surgery systems for over a decade. [20] [21] His work began with a proof of concept micro-handling experiment. Force information from the remote site was transformed to auditory information at the operator site. A few years later a surgeon successfully completed a suturing procedure of an artificial blood vessel. The micro-surgery was performed remotely via tele-monitoring, with the surgeon 700 km from the operation site. This advance and many others were made possible by the continued development of micro-robotic surgical systems. The master-slave setup has since seen continuous advancement. As of 2007, Mitsuishi was working on advanced force feedback control for minimally invasive surgery. [21]

Mitsuishi et al. [20] described a micro-robotic surgery system, with the ability to be operated over the Internet. "Another feature of the system is the transformation of multi-axis force to auditory information," [20] thus allowing the surgeon to hear when the end effector is contacting an object. Two objectives of robotic surgery are to reduce both the load on the surgeon as well as operating time.

The key technologies presented by Mitsuishi et al. [20] were a vision system and slave manipulator. The combination of these, "allow for high accessibility to small objects independent of the approach angle" [20]. A diagram of the system is seen in Figure 20. The enabling technologies included the SEM which was "specially adapted to produce a stereo image of the object being manipulated in real-time" [20]. Second was the pair of micro-

manipulators (three DOF each) and the robotic tool-handler, equipped with a single-axis force sensor. Actuation was achieved with piezoelectric elements. Strain gauges were used for force feedback to the master system.

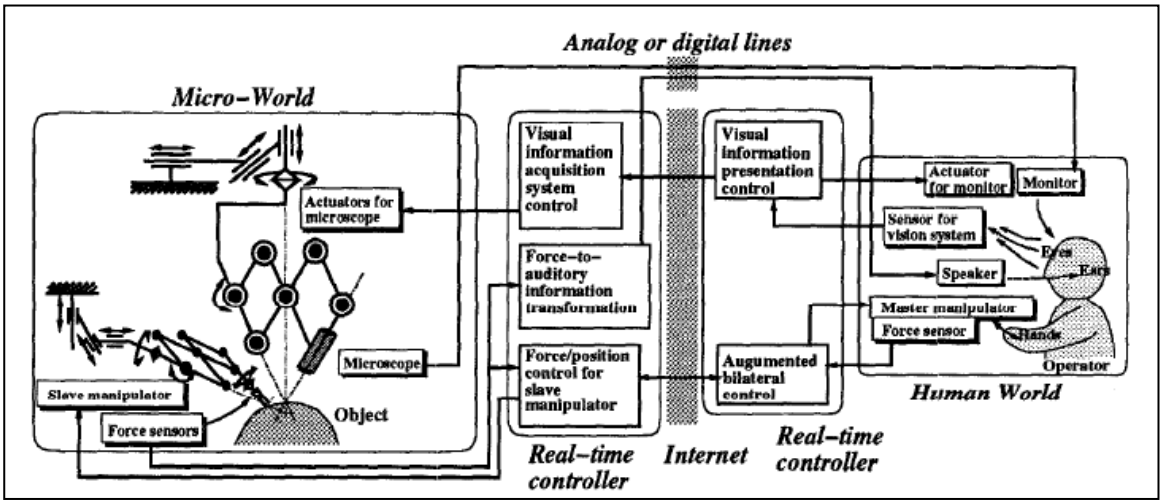

Fig. 20 System construction for a tele-micro-surgery system [20]

Mitsuishi et al. [21] have also implemented a master-slave micro-manipulator system for performing tele-surgery. In this system, contact forces measured by a multi-axis force/torque sensor at the tip of the tool were converted to an audible signal. "The frequency of the sound is controlled as proportional to the absolute value of the force information because a human operator is more sensitive to the frequency change than the amplitude change. If the frequency of the measured multi-axis force exists in an audible range, it is effective directly to amplify the force information" [21]. Thus the surgeon operating remotely could hear the force he was exerting on the target object. One substantial limitation of the system was an "unreachable" area of the workspace due to the design of the mechanical manipulator.

A robotic surgery system described by Ikuta, Yamamoto, and Sasaki [22] took the master-slave setup a step further, enabling surgeries in "deep and narrow" spaces of the body. Mainly the applications included neurosurgery, and other surgeries where accessibility is limited. Similar to a catheter procedure, a guide tube was inserted into the difficult to reach surgical site. The slave micro-manipulator was inserted by this path. An endoscope inserted the same way relayed the images necessary to perform the micro-surgery.

In order for the micro-manipulator to be placed via the guide tube, the tip and the drive unit were separate. Thus a micro-wire was used to transmit the movements through the

flexible portion of the slave unit. These concepts were tested and improved on with several prototype iterations. Suturing experiments were conducted on chicken livers to validate the effectiveness of the latest prototype. “By improving the driving property, degree of freedom in movement, and operability of the tip manipulator, a prototype of a total system with dramatically improved performance was created” [22].

Berkelman et al. [23] focused on the development of a miniature force sensor. The sensor could be mounted to a handheld device or robotic end effector and measure forces in 3D. Berkelman et al. saw the potential for, “the application of this force sensor, in combination with a second sensor, to perform robotically assisted 62.5:1 amplified force reflection for micro-manipulation” [23]. With force requirements in the sub-mN range for certain applications, Berkelman et al. [23] set out to supplement visual feedback with a robotic force amplification system. The ability of surgeons to sense the micro-forces was known to “significantly increase safety, minimize damage to tissues, improve outcomes of existing procedures, and enable new procedures” [23]. The sensor design requirements were based on several important factors. Considering the micro-surgical applications intended, the sensor must be small enough and have an appropriate performance range. In order to attain the tight tolerances required, the parts for the sensor were made using wire-cut EDM machining.

“Typical conventional multi-axis force sensors contain a set of elastic beams arranged in a cross configuration and instrumented with strain gauges” [23]. Here, a double cross design was adopted so that the sensor could achieve isotropic sensitivity at the tool tip. (Fig. 21) This configuration of two vertically separated flexure beam crosses “adds stiffness in response to torques from radial forces at the tip but not to axial forces” [23]. Thus, varying the separation between the cross beams made the sensor “uniformly sensitive to forces in all directions at the instrument tip” [23]. Figure 22 shows the sensor assembled with instrument tip and housing.

Strain gauges measure a change in resistance across the surface of a flexed beam. Here eight strain gauges were wired together in four half-bridge configurations. The bridge signals and force load vector were calibrated to obtain a least-squares matrix transform. Temperature effects were a concern for variation in strain gauge resistance and variations

between strain gauges. Thus, calibration within a thermal chamber to determine compensation values for thermal variation was recommended. [23]

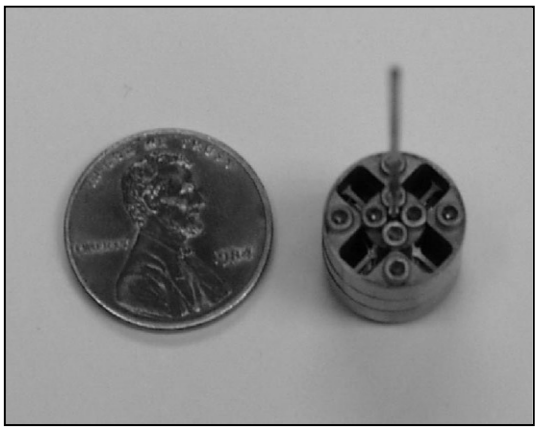

Fig. 21 Assembled Sensor [23]

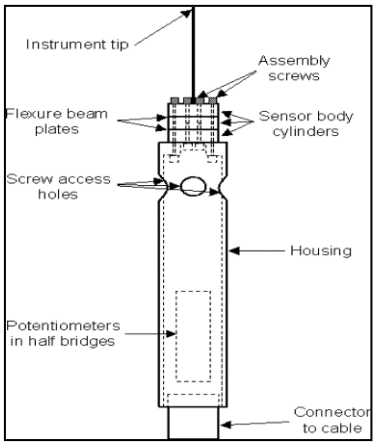

Fig. 22 Sensor with Instrument Tip and Housing [23]

In order to perform a force scaling experiment, a robotic system was used where both the user and robot held a surgical instrument. The interaction forces of each were sensed independently. Here a six-axis force/torque sensor measured the operator's forces on a handle and forces at the instrument tip were measured by the miniature sensor. It was shown that, "the robot reacts to changes in the tip force of less than 5mN, amplifying these forces with a gain of 62.5 to the instrument handle" [23]. Thus the surgeon could easily perceive the tiny forces.

The MicroHand robotic surgery system is a master-slave setup with force/toque sensors that provides force feedback to the surgeon. [24] An animal experiment proved the validity of the tool. The slave manipulator of the MicroHand has both a left and right hand, each driven with cables. Several operation tools can be attached to the end of the manipulator. These are easily interchangeable, and provide the various abilities of cutting, gripping, suturing and knotting. Prototype surgical tools are shown in Figure 24. Also, at the end of the manipulators is a six-dimension force/torque sensor enabling detection of forces between the tool and its target object.

Overall, the slave manipulator is separated into a macro-part, which allowed the tool to be positioned quickly, and the micro-part described above, which produced more precise operations. The master system used was the commercially available PHANToM Desktop, a haptic interface for the micro-manipulator. This system "provides precision positioning input and high fidelity force-feedback output" [25]. The surgeon was able to remotely feel the

interactive forces of the manipulator. However, the 3D torque feedback was lost due to limitations of the PHANToM Desktop.

Fig. 23 MicroHand System [24]

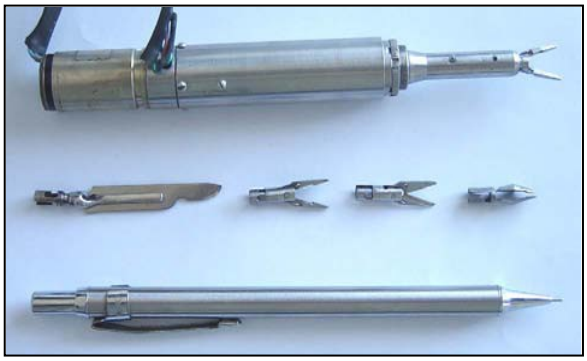

Fig. 24 Prototype of Surgical Tools [24]

The joint design of the manipulator is split into joints for position, and joints for posture. A circular-shaped guide aides the posture of the manipulator and allows rotation of the surgical tool. The cable driven structure of the positioning joints was described. Next the various micro-surgical tools were listed. These are easily changeable via a spring-loaded mechanism, seen in Figure 25. For the case of the micro-gripper, a torsion spring in the design allows for more flexibility while manipulating tissue and organs.

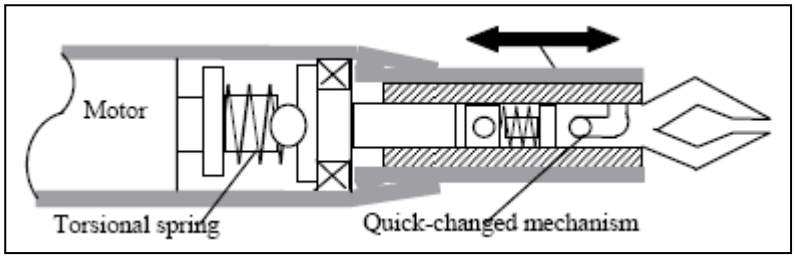

Fig. 25 Schematic of Gripper [24]

The master system was made to control the torque motors of the MicroHand manipulators and also to record the encoders directly. A closed-loop diagram was included to show how the sensor detects force. These forces were mapped to the PHANToM Desktop, where the moments of the joints were calculated, "based on force equilibrium principles and multi-factor arithmetic" [24]. The force feedback enables surgeons to sense small forces that would otherwise be undetectable. The ability to amplify these small interaction forces will reduce the risk of damage to biological tissue. The control system for the MicroHand included the force feedback function, image collection, and display. A multi-view image system provided the surgeon with the necessary information to operate the surgical tools.

The surgical system that Misuishi et al. [21] was developing ten years prior was by 2007 a reality, and applications were extended to minimally invasive surgeries (MIS). Now, "the system transmits the total environment of the operating room and reduces the load applied to soft tissues by approximately 30% by implementing an augmented force presentation capability for the surgeon" [26]. No longer is the surgeon limited to auditory force data, but able through augmentation techniques to physically perceive forces. Force reflecting joystick devices allowed surgeons to feel forces as the robot does, such as one might experience during a virtual reality simulation.

Fig. 26 Master Manipulators [26]

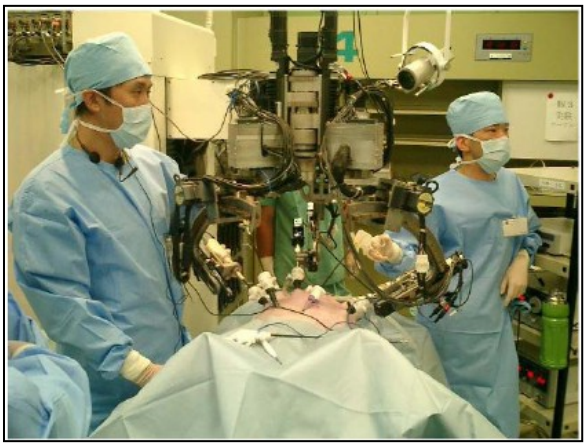

Fig. 27 Slave Manipulators [26]

Mitsuishi, known for work in tele-surgery pointed out that, "minimally invasive surgery is fundamentally tele-operated, even if the actual distance between the surgical filed and a surgeon is small" [26]. For this case as well as robotic micro-surgery in general, the importance of high-quality visual and force feedback is paramount.

The MIS system for an internal organ consisted of a master-slave system connected by a computer network. (Fig. 26) Figure 27 shows the slave manipulators holding forceps and an endoscope. "The information generated by the surgeon's operation of the master manipulators is transformed into position and attitude information and these are transmitted to the slave manipulators" [26]. Foot pedals were used to switch data transmission, motion correspondence, and magnification ratio, from master to slave manipulators.

"The link driven, multiple DOF forceps consists of an end effector and a drive," [26] three DOF for translation and one DOF for rotation. When manipulating an organ or blood vessel, caution must be exercised due to the delicate nature of the living tissue. Excessive force causes damage, but the small forces required are imperceptible to the surgeon.

Grasping forces were augmented by adding a damper element to the force reflection controller. The equation for the damper is $D_m=G_dF_s$, where D_m is the damper element, G_d is a constant that converts the slave force (F_s) to the master side. "It generates viscosity impedance to the master manipulator when contact occurs between the slave manipulator and an object. G_d is determined by considering the operator's sensation and the mechanical properties of the grasped object" [26]. One application for the system was total knee arthroplasty, for which Mitsuishi described the tool path.

While the previous work by Mitsuishi [26] presented an overview of robotic surgery and its ties with MIS, the work done by Mitsuishi et al. [27] next focused on the full force feedback control and augmentation modes mentioned above. Mitsuishi et. al described how a "gain scheduling algorithm provides the operator with maximum-allowable force perception" [27]. A more in depth understanding of surgical tasks revealed that forces in some directions are more important to perceive than others. "With the consideration of the performed task and tissue mechanical properties, the reaction force in those directions will be amplified," [27] resulting in seven total force augmentation modes. The surgeon could automatically switch between these modes as needed. Other works were mentioned including the *da Vinci* system, motion scaling, hand tremor cancelling, and various experiments. However, this work went a step further enabling the surgeon to feel as well as visualize the contact of micro-manipulator and target object.

An overview of the MIS system was given, with main components including the master, slave, control/communication, and audio/visual subsystems. Beginning with the master manipulator, the device had two 7-DOF arms with parallel linkage and wrist mechanisms for translation, rotation and grasping motions. The slave manipulator had three arms, with five DOF at the forceps tip (3 translational, 1 rotational, 1 grasp). The design of which was described as follows, "Combinations of the simple parallel plate structures made up multi-axis force sensor unit. The attached strain gauges measure the force-induced surface strain, which is converted to an electrical voltage signal" [27]. Force sensors were used to measure the forces of the grippers and slave manipulator.

Transformation of the motions from master to slave manipulators was done through the endoscope coordinate frame, "to ensure that his hand motion corresponds to the forceps movement seen from the endoscope screen" [27]. In the force feedback loop, the surgeon's

motion was scaled down by a factor of three by means of a transformation matrix. Then the force at the forceps tip was reported back by inverting the matrix. (Fig. 28)

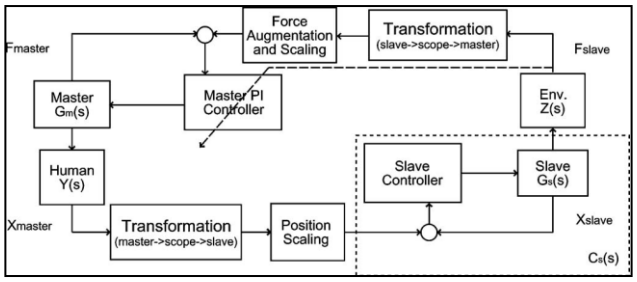

Fig. 28 Master–slave system controller block diagram [27]

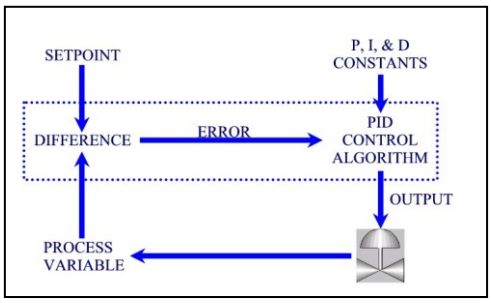

Fig. 29 How a PID controller works [28]

Proportional-integral gain scheduling, shown in Figure 29, locally controlled force feedback at the master side. Integral control was shown to minimize the time to perception of the contact force. "Control gain scheduling based on the reaction force between the slave and the tissue is proposed" [27] to remedy the inherent instability of integral control. An example of lowering the forceps was given to describe why force augmentation in the negative z-direction would be beneficial. This way, forces exerted on the tissue as the manipulator was moved downward were better perceived. It was also noted that, "proper force-feedback augmentation for different performed tasks and tissue mechanical properties are necessary" [27]. Figure 30 displays which DOF were subject to force amplification for each of the seven augmentation modes. The modes are representative of surgical tasks such as grasping & pushing, and lifting & pulling/probing.

Mode No.	Force amplification direction for soft, delicate tissue	Force amplification for normal tissue
1. grasping / spreading	grasping direction	no augmentation
2. pushing / pulling	z direction	no augmentation
3. lifting up/ tapping	x-z plane	no augmentation
4. grasping & pushing /grasping & pulling	grasping & z direction	no augmentation
5. grasping & lifting /grasping & tapping	grasping & x-z plane	no augmentation
6. grasping & lifting & pulling / grasping & probing	grasping & x-y-z direction	no augmentation
7. lifting & pulling / probing	x-y-z direction	no augmentation

Fig. 30 Force Feedback Augmentation Modes [27]

Using foot pedals to switch between these modes was found to be too disruptive to the surgeon's concentration. Automatic mode switching was achieved by a control algorithm. "The basic idea is that a suitable force-feedback augmentation mode is

determined from the force signal pattern and the motion of the forceps at that moment and past interval" [27]. Several preliminary experiments confirmed the efficiency of the switching algorithm and benefits of the augmentation modes.

As research continues, one must be aware of the current capabilities of robotic surgery. "In 1999, ZEUS® made history in the world's first robotic-assisted beating-heart bypass surgery, by Douglas Boyd, MD" [29]. The system, developed by Computer Motion Inc., includes a master console and three robotic arms, seen in Figure 31. Spoken commands position the endoscope, so that the surgeon is free to operate the master handles. The movements are scaled down and filtered to achieve high precision when performing an operation.

Fig. 31 ZEUS® Surgical System [29]

Fig. 32 The *da Vinci*® S™ Surgical System [30]

A similar concept to ZEUS, the *da Vinci*® Surgical System, is currently available through Intuitive Surgical Inc. (Fig. 32) The two companies, Computer Motion and Intuitive Surgical, merged in 2003. The *da Vinci*® system enables surgeons to provide minimally invasive procedures for major surgeries. Miniature slave instruments and a camera are inserted through small incisions. The surgeon operates the master device seen in Figure 32. To the right side of the picture, the robotic instruments are seen attached to a patient side table. The website (www.davincisurgery.com) described the system's operation, "state-of-the-art robotic and computer technologies scale, filter and seamlessly translate your surgeon's hand movements into precise micro-movements of the *da Vinci*® instruments" [30]. While the system has been effective in tens of thousands of surgeries, it currently does not include haptic feedback.

Yang et al. identified the need for high precision and tremor-free control which could be met by Robot Assistant Micro-Surgery (RAMS) system, which employs a "multi-axis

motion planning method" [31]. Yang et al. [31] first looked at typical surgical applications in order to determine basic motions for assistant robots. Next, several planning methods including the spline curve (S-curve) were compared. S-curve planning along with Intercross Polygon Approximation was applied to RAMS motion planning. Finally the validity and efficiency of the system was verified with simulation and an animal experiment.

As observed by Yang et al. [31], the general surgical process began with locating the surgical grippers and adjusting them close to the target. The grippers held open the membrane of the "vessel", the position and pose were precisely regulated. Typical operations were grouped into two categories, single-joint motion and multi-joint motion. After completing these observations along with a study of working space in micro-surgery, a robotic system with a master-slave control was developed.

The master hands were made of two 6-D mice that can each sense force in six dimensions. The slave system consisted of two manipulators each built with both macro and micro-mechanisms. The larger mechanism moves the end effectors into the surgical field with three translational DOF. The smaller mechanism was designed for the precise motions, with six DOF including three for translation and three for rotation.

Two complimentary control modes were provided, master-slave and human-machine interface (HMI). These can be instantaneously switched. The more intuitive master-slave control allowed the surgeon better real time performance. The HMI on the other hand was able to preset joint positions in order to operate motion planning in joint space.

A next step for these developing systems may be the miniaturization of the robots themselves. The concept of an ingestible robotic system capable of re-configuring itself inside the body might be hard to swallow. But today, endoluminal capsules are used in medical diagnosis. These capsules containing a miniature video camera are swallowed by the patient, and images are transmitted back to the doctor. Other types of biomedical sensors can be swallowed to measure various physiological parameters. [5] Pak et al. [32] looked into an actuator concept to enable re-configurable micro-robots. Once the RIT hand is miniaturized, this concept might be one of the options available for actuation.

Cutting-edge work by Pak et al. [32] looked to move beyond the current micro-robotic systems to the future of hand-held and endoluminal systems. Pak et al. [32] envisioned a system of several robotic modules capable of re-configuring themselves once

inside the body. The swallow-able modules would be specifically designed for stomach surgery, where size limitations are based on the esophagus.

Pak et al. [32] designed a Silicone Bourdon Tube (SBT) which made use of the pressure produced via the Bourdon effect, which creates a mechanical displacement. (Fig. 33) "The Bourdon effect arises as a curved hollow tube with an elliptical cross section is inflated. As the internal pressure increases the cross section becomes more circular, causing the tube to straighten and displacing the tip" [32].

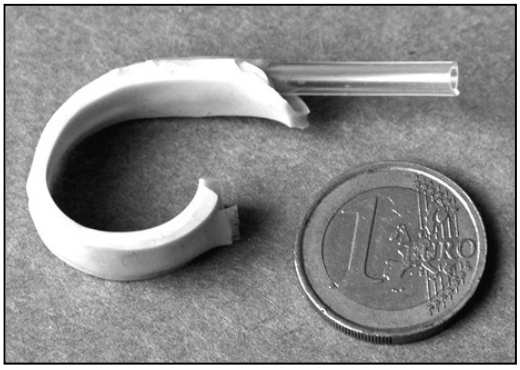

Fig. 33 SBT Prototype [32]

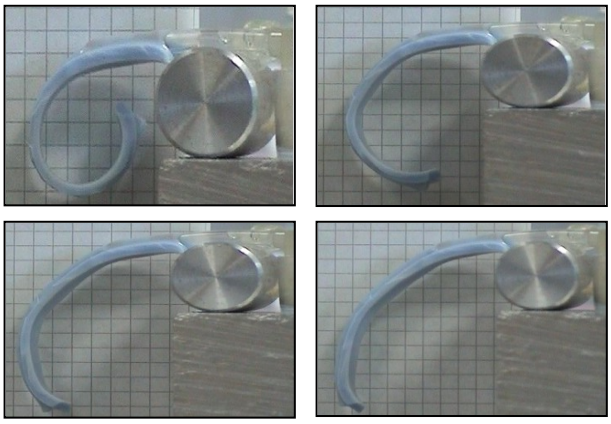

Fig. 34 SBT as it is pressurized via electrolysis [32]

Although the Bourdon tube is commonly used in pressure gauges, there are not many analytical models available. Pak et al. [32] developed a simple, idealized model that relates pressure to radius of curvature. Approximations and several simplifying assumptions were made, and the model was analyzed using ANSYS. A small Bourdon tube and electrolysis box was made in order to verify the model results. Although larger than desired, the setup provided proof of concept and was designed such that customized fabrication would allow for miniaturization.

Experiments to test the SBT's shape as well as a force experiment were carried out. Using a syringe to pressurize the SBT, a camera captured the radius of curvature data. This experiment showed a change in shape/extension of the tube. A force experiment was set up to prove that the SBT was capable of generating the necessary level of force. Next, the SBT was pressurized by electrolysis for a second set of experiments designed to evaluate the shape of the tube. Figure 34 shows the SBT as it changes shape. This pressurization method showed similar results to the syringe. However, the energy absorbed by the electrolysis reaction will limit efficiency.

The work by Pak et al. showed that, "the SBT exhibits remarkable linearity with respect to both pressure and charge applied, due to geometric effects being dominant over other potentially non-linear effects. The effect of geometry is the relationship between the cross section profile change and the resulting axial SBT curvature change" [32]. The issue of power consumption was recognized for future work.

Literature Review Summary Table: Robotic Surgery, Part 1			
Citation #	**Description**	**Significance**	**Related Figures**
[20]	Tele-micro-surgery system	Master-slave robotic surgery setup capable of operation over the Internet. Vision system and slave manipulator were key technologies.	Fig. 20 System construction for a tele-micro-surgery system
[21]	Continuation of tele-micro surgery system	Tele-system used force feedback with auditory information.	
[22]	Micro-surgery robot for deep and narrow space	For applications such as neurosurgery, micromanipulator is placed via a guide tube.	
[23]	Miniature force sensor	Sensor mounted to handheld device or robotic end effector to measure forces in 3D.	Fig. 21 Assembled Sensor Fig. 22 Sensor with instrument tip and housing
[24], [25]	MicroHand surgery system with force feedback	Slave manipulator operated with cables, capable of interchanging tools. Master system used PHANToM Desktop haptic interface for the micro-manipulator.	Fig. 23 MicroHand System Fig. 24 Prototype of Surgical Tools Fig. 25 Schematic of Gripper
[26]	Tele-micro-surgery system, now with force feedback	Force reflecting joystick, surgeons feel forces as the robot does. Grasping forces augmented by damper element.	Fig. 26 Master Manipulators Fig. 27 Slave Manipulators
[27], [28]	Tele-micro-surgery system, augmentation modes	Description of augmentation modes. Surgeons capable of switching between modes, able to feel and visualize the contact of micro-manipulator and target object.	Fig. 28 Master-slave system controller block diagram Fig. 29 How a PID controller works Fig. 30 Force Feedback Augmentation Modes

Literature Review Summary Table: Robotic Surgery, Part 2			
Citation #	**Description**	**Significance**	**Related Figures**
[29]	ZEUS ®: Robot assisted surgery	Spoken commands position endoscope, surgeon operated master handles, motions scaled down for high precision.	Fig. 31 ZEUS® Surgical System
[30]	*da Vinci* Surgical System	Master-slave setup for minimally invasive surgery, many successful surgeries.	Fig. 32 The *da Vinci*® S™ Surgical System
[31]	Robot Assistant Micro-Surgery system with motion planning	Locate surgical tools and adjust them close to target. Master-slave setup with human machine interface.	
[32]	Ingestible, re-configurable miniature robots	Endoluminal capsules with miniature video cameras swallowed by patient. Leverage technology for robots to re-configure inside the body for stomach surgery. Silicone Bourdon Tube design proposed.	Fig. 33 SBT Prototype Fig. 34 SBT as it is pressurized via electrolysis

Development of the robotic surgery master-slave setup has continued to improve, beginning with auditory feedback and leading to commercially available surgical techniques. Including aspects of this research will be required to enable success of the RIT robotic hand. Force and touch feedback are essential to the advancement of precision surgical applications. The RIT Robotic Hand Platform has identified enhanced dexterity and the inclusion of haptic feedback as differentiating factors to the current technologies. Scaling a robotic hand with the dexterity of the human hand is another step towards this ultimate goal of a tool for micro-surgeries.

IV. Haptic Feedback

The majority of related work above included some reference to force feedback. The importance of haptic feedback is indicated by the amount of related research being conducted and would likely be a requirement for the RIT micro-hand. Experiments were done to verify that force feedback is indeed a benefit to a robotic surgery system. For example, the experiments described by Kitagawa et al. [33] were conducted to demonstrate that incorporating force feedback into a robot assist system improves performance. Three methods for knot tying were compared. These were hand, instrument (needle drivers), and robot (*da Vinci*) ties shown in Figures 35-37. Both experienced surgeons and medical residents completed the tying exercises.

Kitagawa et al. [33] stated three hypotheses concerning the accuracy, repeatability and required skill for each method. The reader must keep in mind that both the hand and instrument methods have natural tactile and/or force feedback. The size limitations of a surgeon's hand make instrumental methods a necessity for certain tasks. A robotic system with the "feel" (force feedback) of an instrument should theoretically have better performance. This claim could be validated by showing that the instrument method is more accurate and repeatable than the current robotic method.

The first claim by Kitagawa et al. [33] was that while the hand and instrument ties have similar applied force magnitudes, the robot would not. Showing this would indicate that higher accuracy of applied forces could be achieved with force feedback.

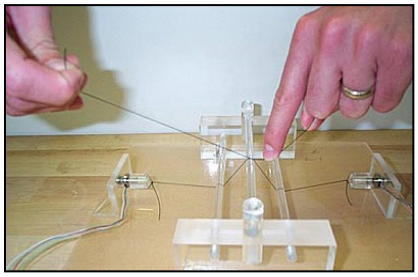

Fig. 35 Hand Ties [33]

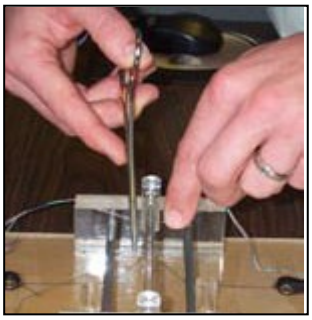

Fig. 36 Instrument Ties [33]

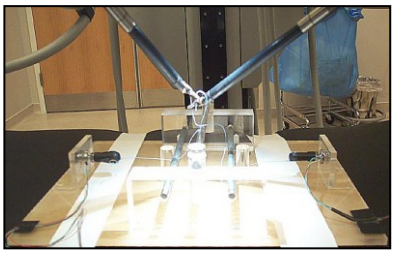

Fig. 37 Robot Ties [33]

Data showed that the instrument method was worse than hand ties, although slightly better than robotic ties. Thus it could not be concluded that a robotic system with similar force feedback to an instrument would match the performance of a human hand.

Second, Kitagawa et al. [33] hypothesized that the standard deviation (SD) of force would be higher for robot ties, where hand and instrument SD would be similar and lower. This would show that repeatability is better with an instrument as opposed to the robot. The claim that hand and instrument ties exhibit similar SD was validated. It was also shown that robot ties did have a lower repeatability than hand ties. From the data analysis it could be concluded that the repeatability of a robotic system would improve with force feedback.

Finally, the third claim by Kitagawa et al. [33] was that novice knot tiers would have higher SD's than experienced surgeons. Using the robot should decrease the gap in performance between the skill levels. In the case of hand ties, the experienced group had a much lower SD than the novices. However, for both the instrument and the robot ties these

methods were not statistically different between the skill levels. Thus it could not be said that force feedback is required for a robot to bridge the gap between skill levels.

Pillarisetti et al. [34] dealt with the limitations of cell-injection techniques due to poor control of cell-injection force. One limitation of conventional cell manipulation techniques was that they could not provide force feedback to an operator. An automated cell injection system was developed by Pillarisett et al. [34], and capable of measuring forces in the μN range. Results showed that operators able to feel the cell-injection force lead to a higher success rate in cell-injection tasks than with visual feedback alone.

Individual cell manipulation is a common process in several biomedical areas. In this case, "the potential application involves regional or target specific delivery of genetic material within a cell or embryo" [34]. The success rate of injection tasks would be improved with haptic and visual feedback from the cell. "Typical transgenic organisms are created by introducing modified genetic material mechanically, one cell at a time" [34]. Several attempts using various techniques have been undertaken by researchers to automate cell manipulation. Pillarisetti et al. [34] aimed to combine force and visual feedback to improve cell-injection tasks.

A nano-manipulator acted as the cell injection unit and a micro-manipulator was the cell holding unit. PVDF film was used to develop the force sensor for measuring cell injection forces. "A theoretical model for the PVDF film is developed and compared with the experimental calibration," [34] in a separate paper. "A linear relationship is established between the applied force and the corresponding integral voltage output from the charge amplifier" [34].

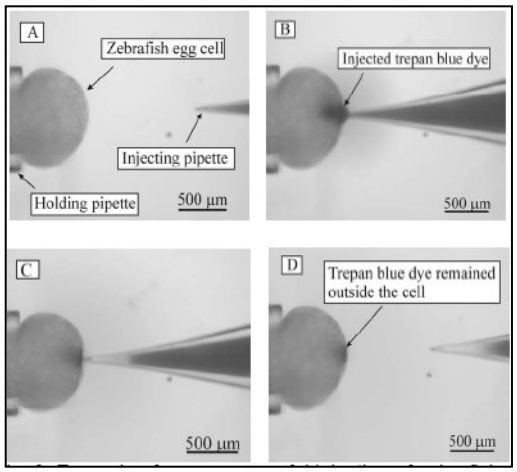

Fig. 38 Unsuccessful injection, vision feedback [34]

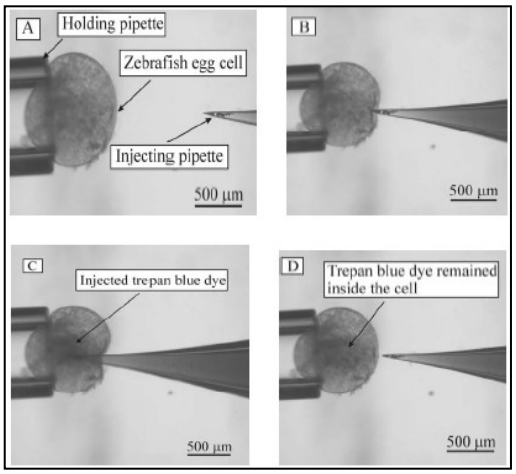

Fig. 39 Successful injection, vision & force feedback [34]

Zebrafish egg cells (diameter 600-700 μm) were used for the following experiments. Figure 38 shows an example of an unsuccessful injection of a zebrafish egg cell with visual feedback alone. Figure 39 shows an example of a successful injection, using both vision and force feedback. First, the human subject was to accomplish a cell injection task using only visual feedback. Then the same experiment was done but force feedback was added to the visual. In this case a haptic interface device was used. When contact was made with the cell, the subject would perceive an apparent increase in force. Experimental results with statistical significance revealed that the addition of force feedback increased the success of the cell injection tasks.

The theory presented by Riviere, Ang, and Khosla [35] behind a handheld micro-device was that the master system is not required. Attempts to duplicate the DOF and functions of a human arm for robotic surgery are difficult, as seen in much of the literature. In turn, the design of a handheld tool could focus on such tasks as tip positioning accuracy. Here, the device "detects its own motion and deflects its tip for active compensation of the erroneous component of the movement" [35]. Besides greatly reducing the cost of a robotic system, this concept was more intuitive and would require less training. A drawback of this approach is common to that of other robotic systems, the time delay, in this case from estimating undesired movement.

Functions of the device would include motion sensing, filtering, and tip deflection for compensation. The prototype tool made by Riviere, Ang, and Khosla [35] was capable of canceling 3D tremor, or involuntary shaking. Tremor was approximated as a sinusoid and canceled by a system based on the weighted-frequency Fourier linear combiner. The system also used inertial sensing and piezoelectric actuation to achieve tremor compensation.

Davies et al. [36] compared an active-constraint medical robot (Acrobot assist system) and conventional surgery. According to the Acrobot website (www.acrobot.co.uk), "Acrobot provides precision surgical systems for computer-assisted 3D planning, surgical navigation and surgeon-controlled robotic surgery" [37]. Hands-on robotic surgery was described as the surgeon holding a force-controlled handle located near the tip of the robot. This setup is rare as the master was located directly on the slave manipulator. Low impedance on the slave manipulator ensured that forces exerted could be directly felt by the surgeon. (Fig. 40)

Fig. 40 Acrobot System [36]

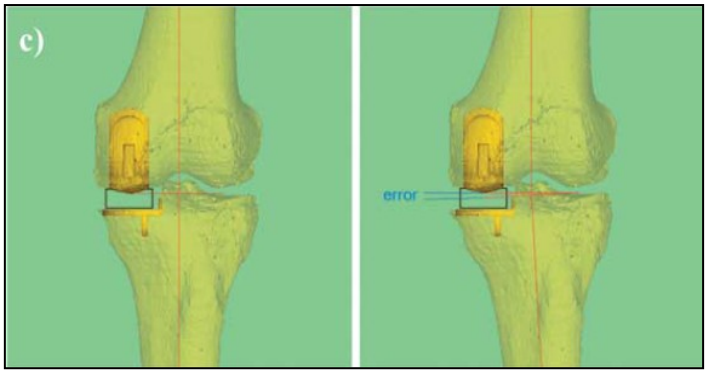

Fig. 41 Close-up views of joint illustrating angular error [36]

The principle task of Acrobot is that of a rotary cutter, the force feedback allows the surgeon to distinguish between hard and soft tissue. A "safe region" was pre-determined and defined a space where the robot was safe to move and cut. The robot was thus actively constrained to the safe region however allowance was provided for the surgeon's judgment during a procedure.

Davies et al. [36] then addressed the issues concerning the justification for robotic surgery. The needs for cost-effectiveness and simplicity were highlighted. Next the Acrobot system was put to the test. The components of the system included a preoperative CT-based planner, an intra-operative registration and cutting facility, and a postoperative accuracy check. After performing 13 assisted knee surgeries and 15 performed with conventional methods, the results were compared. Success was determined by a specified difference between planned and achieved joint lines. (Fig. 41) The Acrobot had a 100% success rate while the conventional method achieved only 40% success. Cases using Acrobot also had increased postoperative improvement of about three times that of the conventional cases.

Limitations of this study include the absence of long-term follow-up. One surgeon performed the Acrobot procedures, while four different surgeons carried out the conventional surgeries. This could add to the variation seen in the results of the conventional method. The article admitted that "we still do not know how accurate the surgeon needs to be to obtain reliably good results" [36].

Literature Review Summary Table: Haptic Feedback			
Citation #	**Description**	**Significance**	**Related Figures**
[33]	Incorporation of force feedback for improved performance	Experiment of tying sutures via hand, instrument, robot (*da Vinci* ®). Investigated accuracy, repeatability, required skill. Hand and instrument methods have natural force feedback. Results showed force feedback improved performance.	Fig. 35 Hand Ties Fig. 36 Instrument Ties Fig. 37 Robot Ties
[34]	Automated cell injection system	Capable of measuring forces, patients who could feel cell-injection force lead to higher success rates than visual feedback alone.	Fig. 38 Unsuccessful injection with vision feedback Fig. 39 Successful injection with vision and force feedback
[35]	Tremor cancelling for handheld robotic device	Handheld device does not require a master system. Focus on tip position accuracy despite natural tremors of human hand. More intuitive system.	
[36], [37]	Acrobot assist system	Surgeon holds a force-controlled handle near the tip of the robot. Master system located on slave manipulator. Compared Acrobot assisted surgeries with conventional, more success with Acrobot (100% versus 40%).	Fig. 40 Acrobot System Fig. 41Cloes-up views of joint illustrating angular error

The Haptic Feedback section described experiments proving the importance of haptic feedback in surgical devices. As stated above, the inclusion of haptic feedback on the RIT robotic hand is identified as important future work. This topic is further addressed in the last section of this paper, Recommendations for Future Work.

Statement of Work

Advanced robotic hands exist, and are primarily designed for life-size applications. However there is a large technological gap between designs such as the Shadow Hand, and micro-manipulators. The tools available for cell manipulation lack dexterity, and the ability to control the amount of force is paramount. The ultimate goal of the RIT robotic hand is to provide dexterous motion at the cellular scale. The current life-size RIT hand shown in Figure 1 below provided a starting point for a scalability study. Experimentation with the existing hand coupled with a dynamic computer model that predicted contact forces could be

used to optimize the grasp of the hand on an object at various scales. Understanding the grasping forces is an essential first step in the development of a micro-scale dexterous hand.

Future work for the RIT Platform includes controls for the miniature robotic hand. Finally, further advancement for medical robotics and cell-manipulation lies in haptic feedback. While integrating the necessary feedback into the RIT hand may take time, it would eventually be necessary for the intended application of robotic surgery. Keeping all of this in mind, the first step for the RIT hand was a scaling project, which was the objective of this thesis work.

The goal of this thesis project was to assess the limitations of scalability for the RIT robotic hand design. This was accomplished by developing simulations of the force generating properties of the robotic hand, and comparing results with experimental setups. Test procedures were developed to support validation of the dynamic model. The thesis work identified the point where further miniaturization would require a change in the manufacturing process and/or actuation technique. A prototype robotic hand was fabricated at the smallest level of scalability.

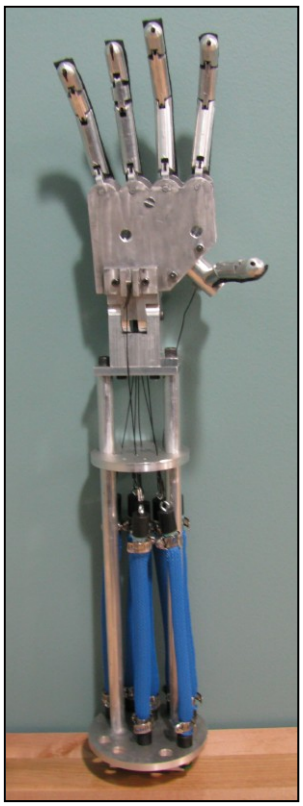

Fig. 1 RIT Robotic Grasping Hand [38]

Description of Robotic Hand Design

The Scalability Study began with an existing robotic hand designed by an RIT, Senior Design Team [38], which is life-size and referred to as "full-scale". (Fig. 1) This design was first reviewed for potential changes that would better support a scalable robotic hand. The overall design was evaluated, and then several changes were made to the geometry.

The RIT hand design was modeled after a human hand, with each of the five fingers represented. (Fig. 2) Each finger includes three phalanges, except the thumb which has two, for a total of 14 links. A human hand has three types of joints, the metacarpophalangeal (MCP) joint, proximal interphalangeal (PIP) and distal interphalangeal (DIP) joint. (Fig. 3) Motions of the human finger joints include flexion, and extension. In the case of the MCP joints, the additional motions include abduction, adduction, and some axial rotation. The RIT hand is simplified to a grasping function, where each joint is approximated as a hinge, exhibiting only flexion and extension. Here the metacarpal bones are approximated as a set of parallel plates shaped like the palm. This simplification removed the abduction, adduction, and eliminated axial rotation of the MCP joints of which a human hand is capable.

Fig. 2 RIT Senior Design Team Robotic Hand [38]

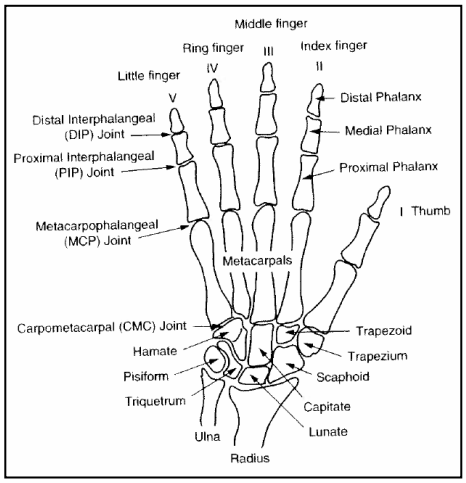

Fig. 3 Bones and joints of the right hand [40]

The grasping motion of the hand is actuated by pneumatic air muscles and wires. The Senior Design Team focused on improving the design of the air muscles. "The air muscles are completely new, and uniquely designed for higher pressures… and greater reliability than previous air muscle designs" [39]. Aluminum was selected as the hand material due to its strength, corrosion resistance, and machinability. On the back of the robotic hand (palm side

facing down), strips of foam rubber with adhesive were attached to each finger. The rubber acts as a spring return or tendon, which opposes the force due to the wire.

Solid Model of Robotic Hand

In order to make any changes to the RIT hand design, it was necessary to recreate the CAD geometry. The original CAD files were not compatible with the CAD software (NX) that was used for this thesis project. With this opportunity, the geometry was optimized to more closely match the anatomical average sizes for each phalange. In order to establish a rough estimate for the average length of male and female fingers, the overall lengths of the author's fingers (female) were measured. These lengths were averaged with the overall lengths of the RIT hand's finger dimensions, which were based on a male. For consistency the finger lengths were all measured from the centerline of the joints. (Fig. 4)

The average for each finger length for both male and females was used to calculate individual phalange lengths, using a table from the book *Biomechanics of the Upper Limbs* [40]. (Table I) The "anatomically optimized" phalange length results are found in Table II. Details of the calculation of the phalange lengths are found in Appendix A. The dimensions in Table II are used for the CAD geometry recreated in NX. In Figure 5, the index finger measures 98 mm or approximately 3.8 inches.

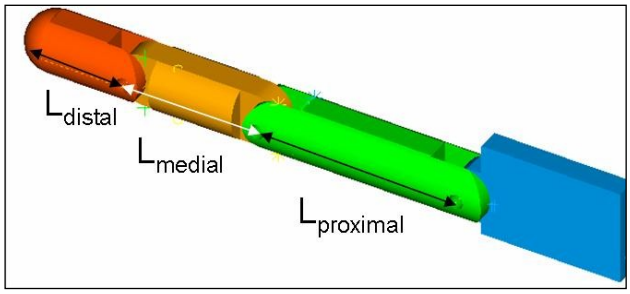

Fig. 4 (above) Phalange Length Measurements

Table I (right) reproduced from *Biomechanics of the Upper Limbs* [40]

Phalange Lengths as Percent of Hand Length for Males and Females			
Phalanx	**Proximal**	**Medial**	**Distal**
Thumb	17.1	--	12.1
Index	21.8	14.1	8.6
Middle	24.5	15.8	9.8
Ring	22.2	15.3	9.7
Little	17.7	10.8	8.6

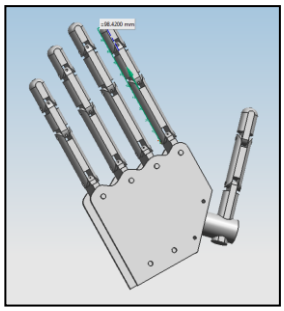

Fig. 5: NX CAD geometry

Lengths (in)					
Phalanx:	**Thumb**	**Index**	**Middle**	**Ring**	**Little**
Proximal	1.5	1.9	2.1	1.9	1.6
Medial	n/a	1.2	1.4	1.3	1
Distal	1	0.7	0.8	0.8	0.8
total*=	2.5	**3.8**	4.3	4	3.4

Table II Optimized Phalange Lengths

Dynamic Computer Model

One key goal of this project was to create a dynamic computer model of the hand system to be used as a tool for assessing a scaled robotic hand design. The first step in the development of the dynamic model involved the characterization of forces acting on the hand using a basic free body diagram (FBD). In this case, the FBD was used to provide an overview of which inputs were needed to most accurately model the hand as a dynamic system. Since the RIT hand functions with a grasping motion, the action of each finger is the same. Thus only the FBD of the index finger was drawn. See Appendix B for the FBD and related assumptions.

Forces due to mass, friction, the wire (actuation), and the foam rubber were identified as the significant contributors to the dynamic system. While it is easy to quantify the mass, the other forces involved require further investigation. Both the foam rubber material stiffness and the wire pull force create moments about the joints which oppose each other's motion. Thus the spring constant of the foam rubber material was of importance, as well as the amount of force exerted by the wire to pull on the finger links.

Characterization of Inputs

The FBD was drawn with the assumption that there is an actuating force provided by the air muscles. This force will be referred to as the wire pull force and was measured in the Air Muscle Pull Force Test. The wire pull force represents the amount of force used to fully contract the hand. As the air muscles are contracted by compressed air, they generate a pull force on the distal phalange via the connected wire that is strung through each finger link. In order to determine this actuation force, the air muscles were measured in several states, while at rest, fully contracted but unattached, and fully contracted when attached to the robotic hand.

The setup for the Pull Force Test was comprised of a BiSlide positioning slide, load cell, strain gage transducer amplifier, and analog data acquisition with Labview interface. The load cell was fixed to the base of the slide and a sample air muscle was connected. The opposite end of the air muscle was connected to a sliding mechanism. The position of the sliding mechanism was first calibrated by entering a number of steps into Labview and measuring the distance the slide travels from a fixed point. The displacement of the slide

correlated linearly with the number of steps entered into Labview, according to the data plotted in Figure 6.

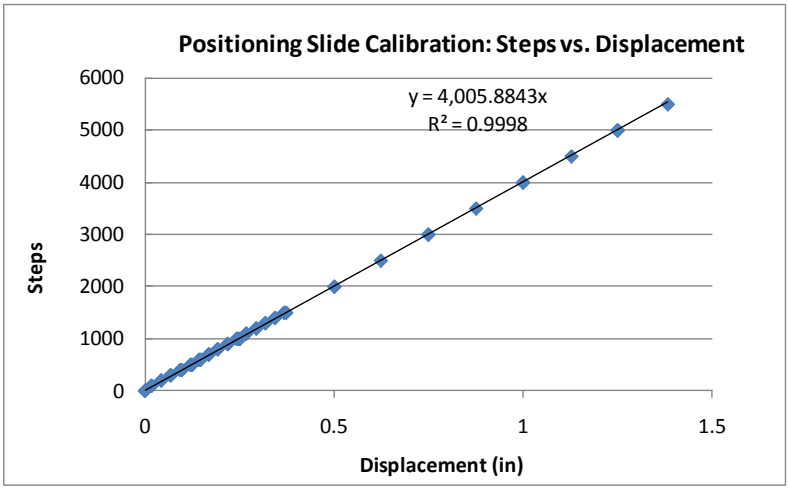

Fig. 6 Positioning Slide Calibration

The length of the air muscle was measured in the resting state, where no pressure was applied. Before being attached to the positioning slide, the air muscle was then pressurized using an air compressor to contract the muscle. A pressure gage and valve was used to control the air pressure to 60 psi. This pressure was determined to produce the best results for contracting the air muscles and hand, according to the Senior Design Team. [39] The length of the contracted air muscle was recorded. Figures 7 and 8 show examples of an air muscle in the resting state and in the fully contracted state.

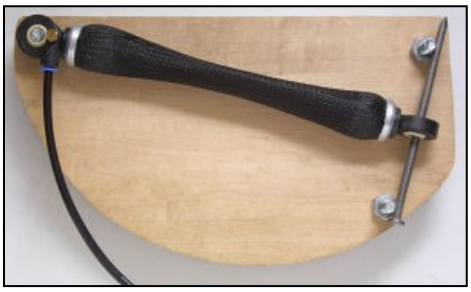

Fig. 7 Resting state [1]

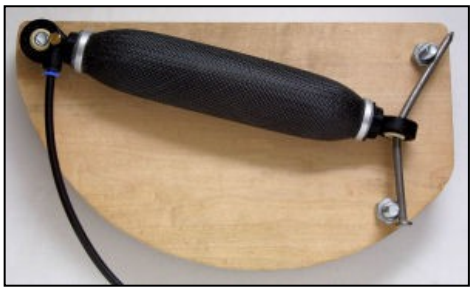

Fig. 8 Contracted state [1]

Next, the air muscle was connected to the positioning slide. The Labview program controls the slide and stretched the contracted air muscle to a distance correlating with the number of steps entered. As the slide moved, the extension distance was recorded and the results were plotted in Figure 9, showing a linear relationship between extension and force.

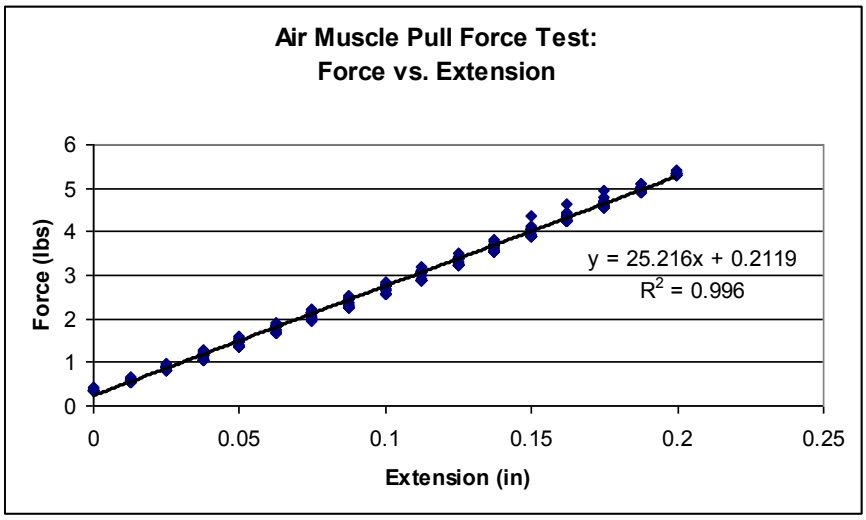

Fig. 9 Air Muscle Pull Force Plot

In order to determine the extended distance of a compressed air muscle when it is attached to the hand, the individual robotic hand air muscles were measured. When the air muscle is free to contract without an opposing force, the difference in length from the resting state to a contracted state will be less than when the muscle is contracted while attached to the fingers. The weight of the fingers, foam rubber strip, friction of the joints and wire will oppose the contracting force of the air muscle. When the hand is assembled, the length of a compressed air muscle will be extended or stretched when the fingers are in a contracted position.

Table III shows the air muscle lengths for each finger. The resting lengths of the muscles vary slightly due to human error, incurred during the assembly process. Note that the contracted length for each air muscle when connected to the hand was slightly different for the individual fingers. This suggests that the size of the finger being contracted or its wiring played a role in the force that stretches/opposes the contracted muscle.

Finger Air Muscle	Resting length (in)	Contracted length when connected to hand (in)	Contracted Length when not connected to hand (in)	Extension (in)	Pressure (psi)
Index	6	4.875	4.725	0.15	60
Middle	6	5.125	n/a		
Ring	5.875	5.25			
Little	6	5.25			
Thumb	5.875	5.125			

Table III Air Muscle Lengths

An observation from these measurements was that the index finger is different from the other fingers. This was likely due to this particular finger being removed from the hand for dimensional measurements. Another reason may be that the friction of the finger was reduced by repeated loading and unloading of the joints during handling. The joints may have loosened, resulting in the air muscle having less oppositional force from the finger and thus a smaller contracted length than the other "stiffer" fingers.

When the index finger was re-wired and re-attached to the hand, the process was likely different than the first time the hand was assembled. To address this issue, the length of wire used in reassembling the hand was carefully measured to correspond with a fully contracted finger at 60 psi. The amount of wire used for the other fingers and how much slack was allowed was not assessed. An assumption was made that the other fingers would perform comparably to the index if wired in a similar manner. Since a sample air muscle was used for the Air Muscle Pull Force Test, it was assumed that all muscles of the same resting length would result in approximately the same contracted distance when not attached to anything. This was previously confirmed by Senior Design teams.

Knowing that the extended distance of the index finger air muscle when attached and contracted is 0.15 inches, data from the Air Muscle Pull Force Test is used to calculate the pull force of the index finger. In this test, the air muscle was stretched in the same way the muscle is stretched by the finger opposing its motion. The oppositional forces to contraction include the friction of the pin joints and the foam rubber spring stiffness. Both of these were later determined and entered into Recurdyn as inputs for the dynamic model. However, the pull force is related to the extension distance and the best fit equation of the linear data is displayed in Figure 9. The equation $y = 25.216x + 0.2199$ describes the relationship between the applied force "y" and the extension distance "x". The extension distance x of the index finger is 0.15 inches, and this value was plugged into the equation. As a result, the pull force of the wire generated by the index finger air muscle, y, was 3.994 lbf. This value was the input for axial force in the dynamic model. Next, the amount of opposition provided by the foam rubber material was investigated.

The natural gum foam rubber strip attached to the top (palm facing down) of each finger acts as a tendon, or spring to return the finger to its original relaxed position after being contracted by the air muscle. In order to characterize the foam rubber material, the

spring constant is needed. A tensile test was performed in the RIT Materials Lab to generate data for determining the material spring constant.

A 2500 kg Instron machine was used for the Tensile Test. The data acquisition rate of 10 Hz was set for data collection, with an initial speed of 0.2 in/min for the machine. The acquisition rate and initial speed were suggested values for polymeric materials. Samples of the foam rubber were cut to 3 inch pieces. To prevent tearing the sample, two additional pieces of the rubber were used to reinforce the edges of the material clamped in the grippers. The amount of material showing between the grippers was recorded as the initial length. A total of four material samples were tested to failure, resulting in an average peak load of 6.93 lbf. Each rubber piece stretched to 5.8 inches on average before failing at a length approximately 330% longer than its initial length.

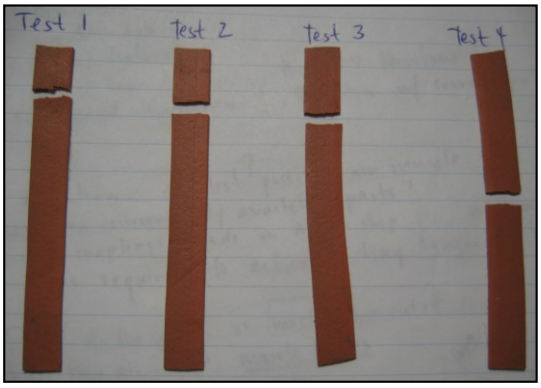

Fig. 10 Tensile Test Foam Robber Samples

While three out of four samples failed in a location close to the upper gripper, the fourth piece of rubber failed near the center of the material. (Fig. 10) The failures nearer one side could have resulted from variations due to loading of the specimen or variations in the material itself. Nonetheless the peak loads were similar for each specimen.

A plot of the applied force versus load for the fourth sample shows the results of the tensile test. (Fig. 11) This data was converted to make a stress-strain plot. (Fig. 12 & 13) According to Hooke's Law, the slope of the stress strain plot equates to the material's modulus of elasticity, E=1.0051 MPa. This number was used to calculate the spring constant of the foam rubber material. The foam rubber is mainly acting in the spaces between the phalange links, and not in the places where it is firmly adhering to the surface of the link. Thus the value of each spring force must be calculated for the individual locations on the fingers. The calculations for the index finger foam rubber springs are described below.

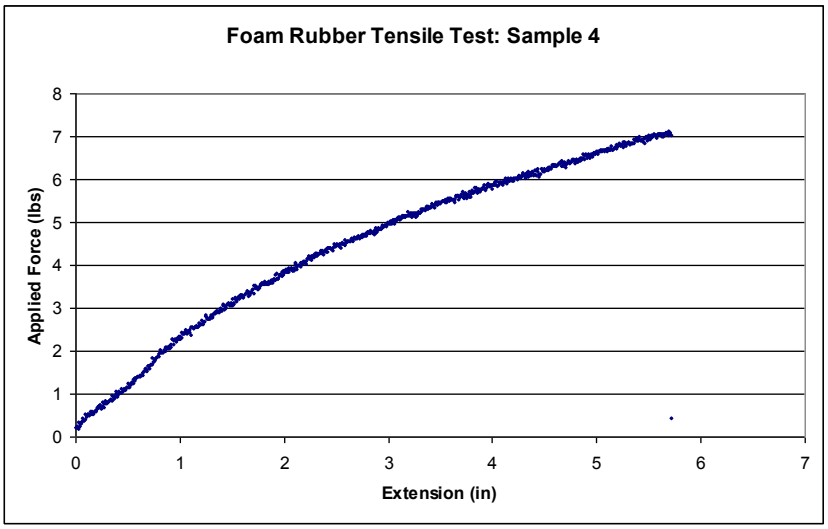

Figure 11 Applied Force vs. Extension

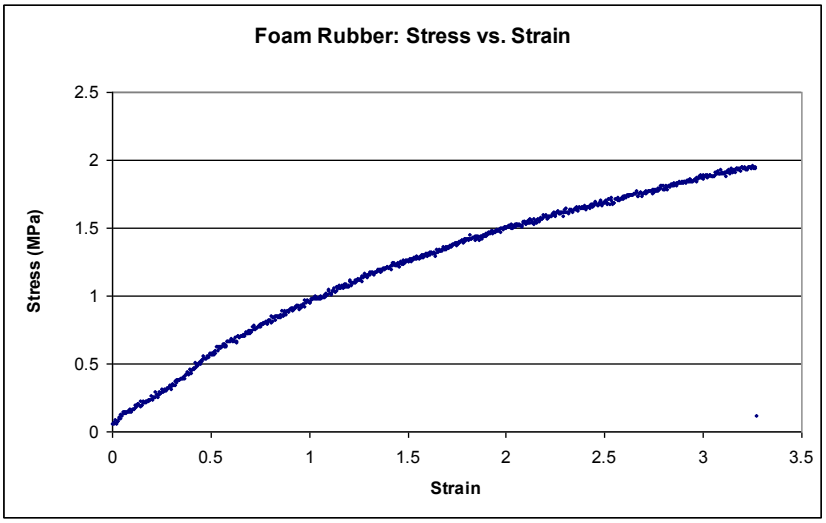

Figure 12 Stress Strain Plot for Foam Rubber Material

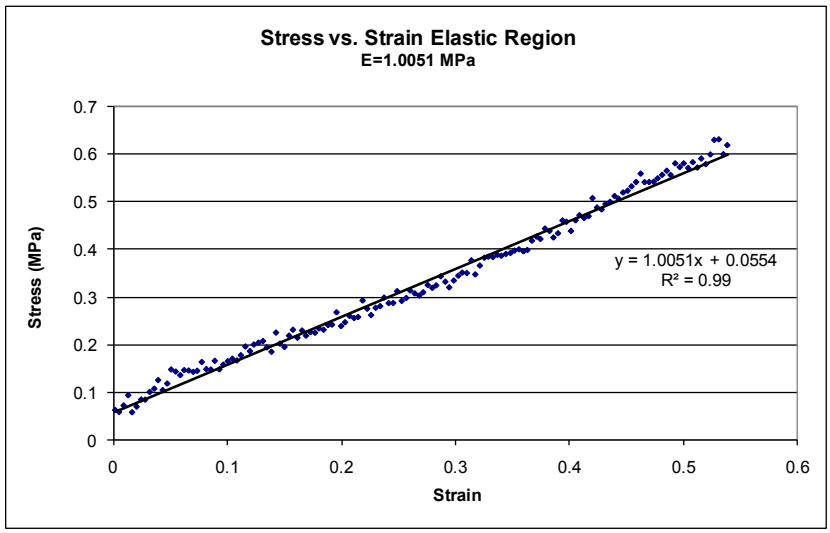

Figure 13 Elastic Region of Stress Strain Plot for Foam Rubber

There were two ways to obtain the spring constant for each spring length. The original tensile test specimen for the foam rubber was used as an example. For the sample (length=3 in.) the measured spring constant was k=2.1 lbf/in, which equates to 0.38 N/mm. This was found by reading the slope of the line from the Force vs. Extension plot, Figure 14.

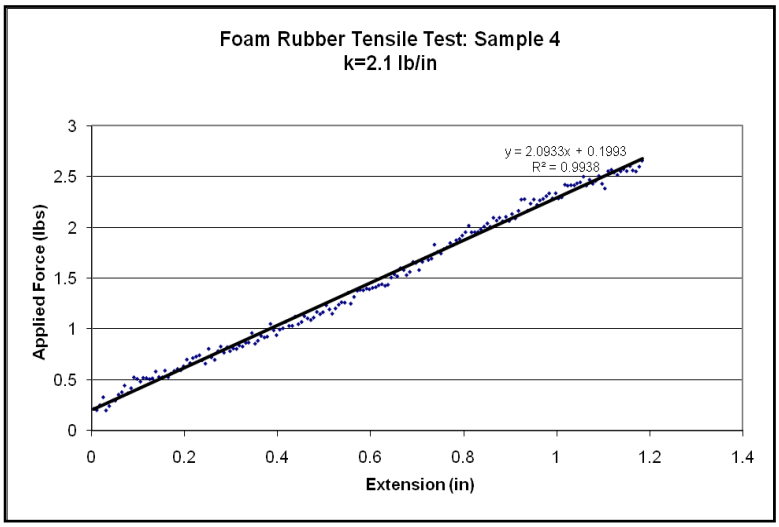

Fig. 14 Tensile Test Plot

The second method used stress and strain equations to determine the spring constant for the foam rubber. As this method is straightforward and can easily be calculated, it was the preferred method for calculating the spring rate for various length samples/springs. The calculation below for the tensile test sample also yielded the same spring rate as the previous method. Sample Calculation:

Stress σ = Force P/Cross-sectional Area A

P = 1 (N)

A = length*width, length = 0.0098 (m), width = 0.00165 (m)

σ = 1 (N) / 0.0098 (m) * 0.00165 (m) = 61842.9 (N/mm^2)

Strain ε = Stress σ/Elastic Modulus E

σ = 0.0618 (MPa)

E = 1.005 (MPa)

ε = 0.0618 (MPa) / 1.005 (MPa) = 0.0615

Change in length (extended – initial) ΔL = Strain ε * Initial length L

ε = 0.0615

L = 0.0445 (m)

$\Delta L = 0.0615 * 0.0445 \text{ (m)} = 0.0027 \text{ (m)}$

Spring constant k = Force P/Change in length ΔL

$P = 1 \text{ (N)}$

$\Delta L = 0.0027 \text{ (m)}$

$k = 1 \text{ (N)} / 2.7 \text{ (mm)} = 0.37 \text{ (N/mm)}$

In order to calculate the spring rate for each joint location, the initial length of each spring length was required. For each spring initial length, the value was plugged in to the equation for change in length ΔL. Both the stress and strain values remain the same for the material, as the cross sectional area was held constant. Table IV shows the different foam rubber lengths for each finger location and the corresponding spring constants that were applied in Recurdyn. The springs located across the three joints have slightly different spring constants, based on the distance between the links where the rubber is acting, the initial length of the spring.

	Full Sized Hand	
	initial length (m)	Spring rate k (N/mm)
Sample	0.04445	0.37
Distal	0.00743	2.18
Medial	0.00897	1.81
Proximal	0.01302	1.25

Table IV Foam Rubber Spring Lengths, Spring Constants

Simulation

The inputs for the hand model, air muscle pull force and foam rubber spring force, were identified as significant parameters by the FBD and thus were experimentally determined. The next step was to apply these values to the hand geometry in the dynamic modeling tool, Recurdyn. This software is advertised as a, "state of the art dynamics and kinematics package and gives the best performance in large scale multibody problems including contact" [41].

First, all parts of the NX hand geometry (Fig. 15) were imported into Recurdyn. (Fig. 16) A revolute joint was applied at each hinge point between phalange links. This enabled the solid links to rotate about the centerline of the pin holes. Aluminum was assigned as the material to the finger links, stainless steel to the pins. Values for both sliding and dynamic

friction were added to the properties of the revolute joints to most accurately model the pin joints.

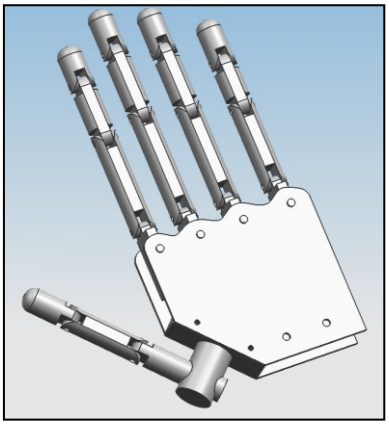

Fig. 15 Full Scale Hand Geometry, NX

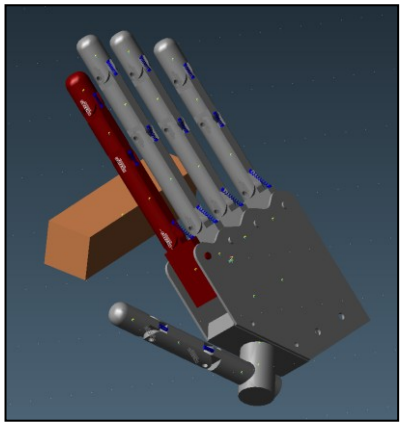

Fig. 16 Hand Geometry Imported into Recurdyn

These values, seen in Figure 17, were taken from a reference table of frictional coefficients. [42] An assumption was made that the two materials sliding on each other is the only source of friction on the joint. The friction of the wires was not accounted for in the model as it was seemingly negligible when compared with the joint friction. This difference between the parts and model was later compared with physical test results and confirmed to be minimal.

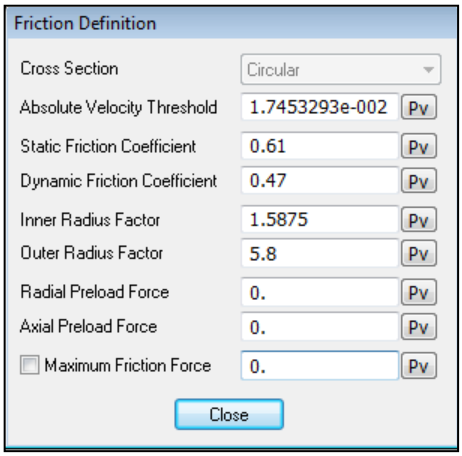

Fig. 17 Friction Coefficients

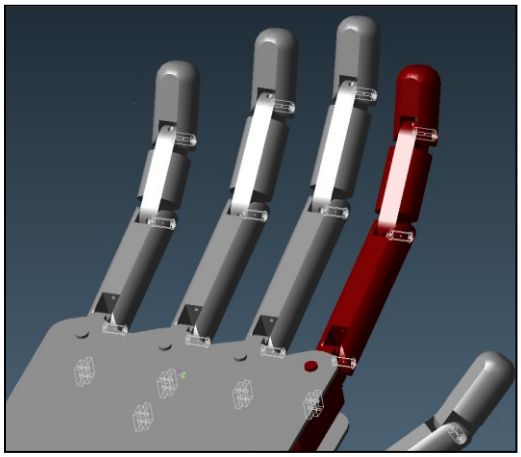

Fig. 18 Fixed and Revolute Joints

An axial force was applied between each link at the center of the wire hole to simulate the force of the wire which is pulled by an air muscle, shown in Figure 19. The calculated wire pull force of 4 lbf was applied as the value for the axial force. The foam rubber was represented as a spring force. Each spring was attached to the top of the fingers

(palm facing down) at the edge of each link. (Fig. 20) The spring constants calculated above and listed in Table IV were the values entered into the model.

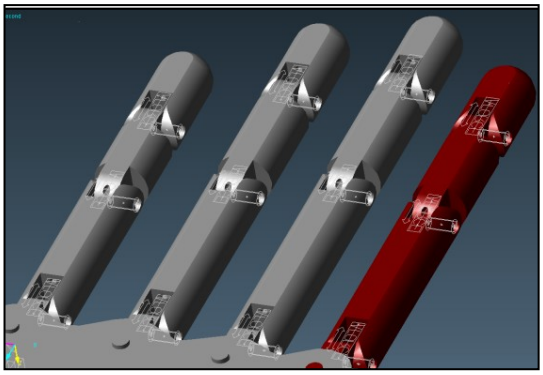

Fig. 19 Axial Force of Wire

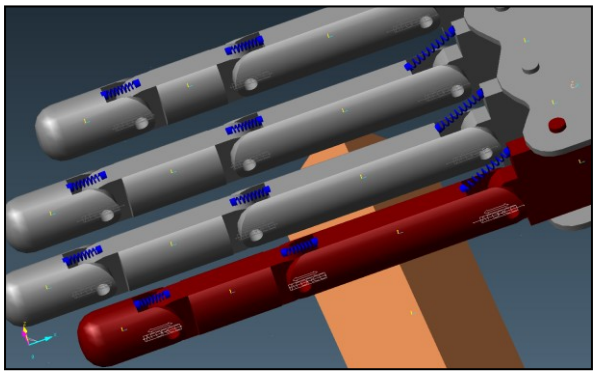

Fig. 20 Springs Representing Foam Rubber Strip

Applying the appropriate surface contact restrictions and fixing the hand in space were the last steps before the model was run. A solid rectangular body with the material property specified as rubber was added to the model, and positioned such that the finger would contact the surface similarly to the load cell in the validation test. Rubber material was used for the box, since it is an approximation of the epoxy material that covers the load cell in the experimental setup.

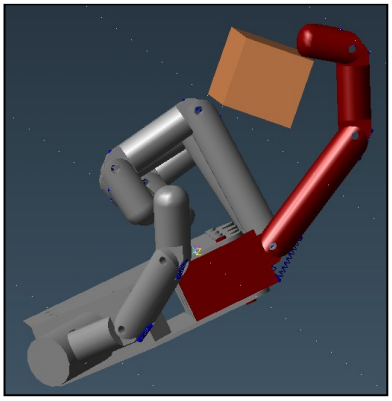

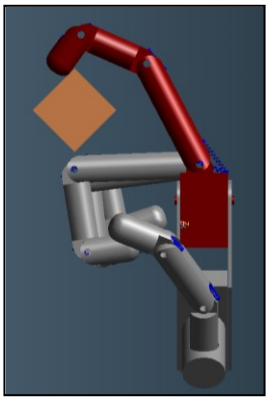

Figs. 21 & 22 Recurdyn Model- Index Finger Contact

The simulation took less time to complete when only one finger was active. Running the simulation for the index finger took 11 seconds. Running the model with all of the finger surfaces active took 3.6 minutes to complete. Thus, only the index finger results were studied since these directly correlate with the experimental data obtained. (Fig. 21 & 22) A plot of the index finger resulting contact force is shown in Figure 23. The Recurdyn results showed an initial maximum force at the time when the finger first contacted the solid body. Almost immediately after this initial contact, the force plateaued to a steady state value. The

steady state value will be referred to as the grasp or contact force of the finger, because this is the amount of force that would be exerted by the index finger upon an object when grasped by the hand. This value is of importance when evaluating the function of a grasping robotic hand.

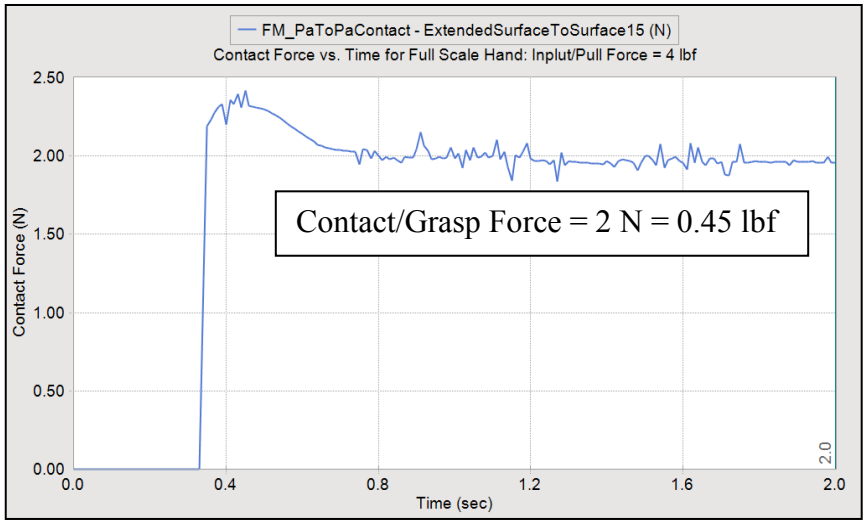

Fig. 23 Recurdyn Plot of Contact Force

Experimental Setup

In order to validate the Recurdyn model, the contact force results were confirmed with actual testing of the hardware. A test fixture was set up with a load cell for measuring the resulting contact force. The index finger was taken out of the hand assembly and mounted in the fixture for the purpose of the Contact Force Test. The finger holder was held in place by a custom machined block of aluminum. A hanger was applied to the wire so that weights could be added to contract the finger. Figure 24 shows the setup for the test and the direction of the wire pull force. In Figure 25, the finger is shown contacting the load cell. For this test, weights were used as opposed to the air muscle, so that a range of applied force could be tested.

The first weight was held above the base of the hanger and then gently dropped onto the hanger. With each new addition, all weights were removed and gently dropped onto the hanger to simulate a quick application of force similar to air muscle contraction. Dropping the weights was selected as the loading method, since it took into account the dynamic event that takes place when a finger is actuated. Figure 26 shows the finger without any applied

weight. It took 2.5 lbs of weight added to the hanger before the finger contacted the load cell. This implied the significance of the joint friction. Figure 27 shows the contact between distal phalange and the load cell.

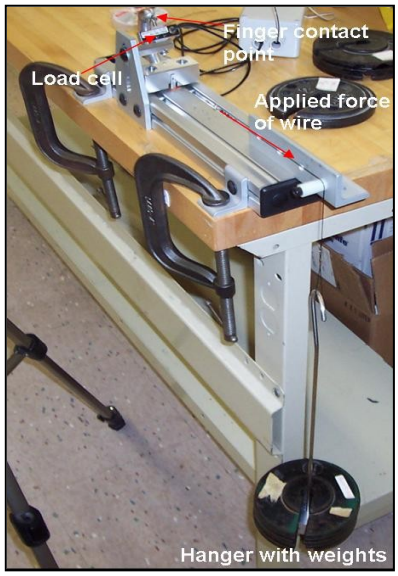

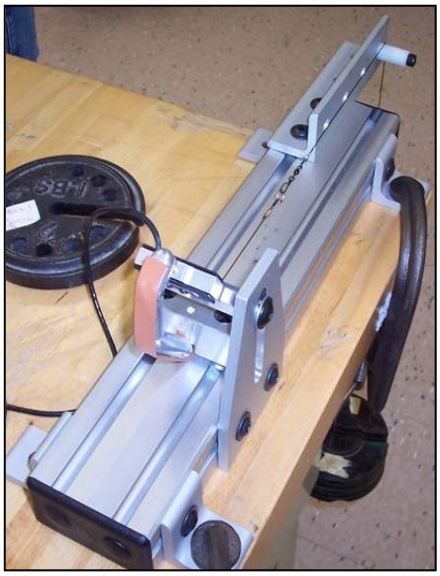

Figs. 24 & 25 Contact Force Test Equipment

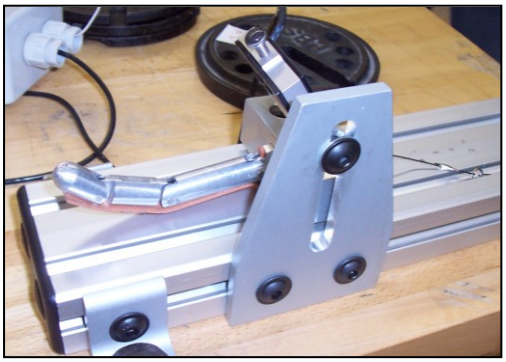

Fig. 26 Finger in the relaxed position

Fig. 27 Finger is contracted/contacting load cell

Data Analysis

The load cell measured the contact force as a voltage, where 1 Volt = 1 lbf. As the different amounts of weight were dropped in succession, the initial hit of the distal phalange on the load cell screw head was the maximum force displayed by the voltmeter. When the system came to a steady state after a time, the voltmeter displayed a "grasp" force corresponding to the applied weight. Both sets of values were recorded, and plotted in Figure 28. Weight was added, until 5.5 lbs of weight had been applied. This was determined

to be a sufficient weight since it was more than the amount of the air muscle pull force of 4 lbf required to actuate the finger.

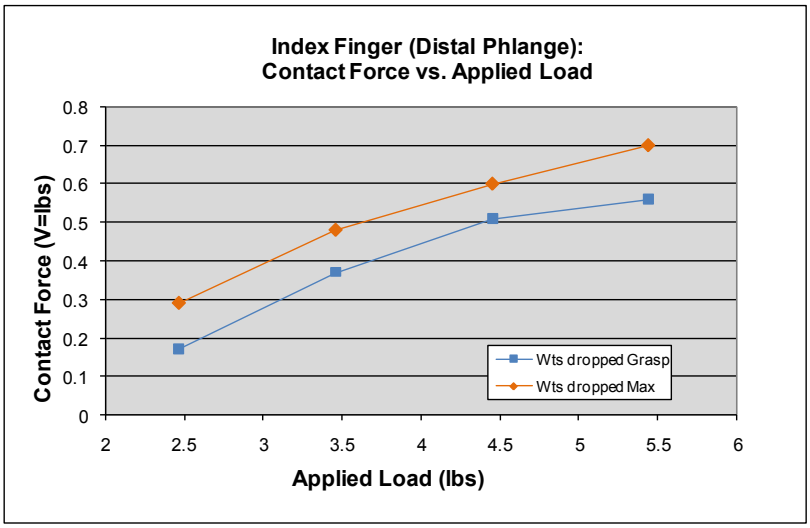

Fig. 28 Contact Force Tests Results

Interpretation of Results

Contact force results from the Recurdyn model, correspond to the observations from the experimental test. First there was an initial hit or spike of max force, before quickly leveling out to a steady state contact/grasp force as seen in Figure 23. For comparison, the contact force will be compared with the steady state grasp force determined by the Contact Force Test.

Comparing results at the actuation or pull force of 4 lbf, the initial hit or spike on the Recurdyn plot (from above) was 0.54 lbf. This was similar to results obtained from the Contact Force Test. Weights dropped maximum force data point of 0.55 lbf, as shown by the orange line in Figure 28. Also, the steady state contact or grasp force in the model was the same as was measured in Contact Force Test, with dropped weights yielding a steady state grasp data point of 0.45 lbf.

To assess how accurately the model matched the experimental test data across a range of input forces, the Recurdyn model was run for a series of applied loads. The corresponding contact force values were recorded. These data points were plotted along with the results from the Contact Force Test. Figure 29 shows good correlation between simulated and experimental results for loads up to 4.5 lbs. It is apparent that there was a non-linearity at

high applied load that the computer model did not account for. Likely this was due to the friction of the joints in the hand assembly. However, it was clear that in the actuation range of the fingers, the model closely matched the results of the tested parts. The low end of the actuation range was 2.5 lbs, which was the weight required to contract the finger to touch the load cell. The load cell was positioned such that the finger would be in a contracted state when load was applied. The higher end of the actuation range was selected as 5.5 lbs, since this weight was greater than that of the air muscle pull force.

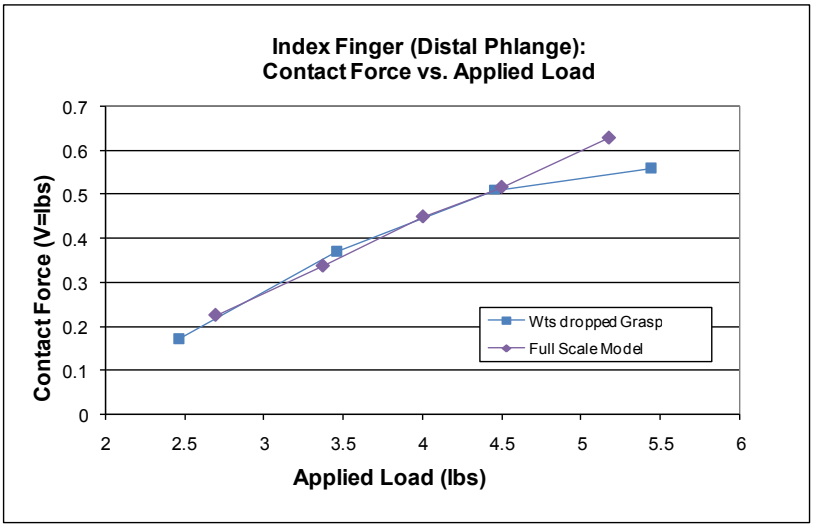

Fig. 29 Comparison of Simulation and Test Results

Scalability Study of ½-Scale Design

A correlation between the Recurdyn model and robotic hand was thus established for the full-scale (life-sized) version of the hand. These results also validated the methods for characterizing the various system inputs. The results were then used to assess the scalability of the design. An additonal goal of the project was to predict the actuation force required as well as the corresponding contact force of the design at a smaller scale.

The scaled physical model was used to determine an actuation force range. Different applications call for a range of grasp forces and corresponding acutation forces and actutation is often a limiting factor in the field of micro-robots. The amount of energy required for actuation is often large and must be external to the robot. To determine what is appropriate for the robotic hand, the index finger geometry was scaled, and the actuation force was determined using a scaled Recurdyn model. The computer model and experimental testing were used to validate the design's scalability.

First, it was important to determine the feasability of fabricating a scaled index finger. In order to begin studying the design at a smaller scale, it was decided to proceed using a ½-scale hand design. At this size, the rapid prototyping capabilities at RIT were sufficient and thus cost effective for this project. Parts were readily made in Brinkman Lab on the Elite 3D Printer. During the building process, ABS plastic is heated to a semi-liquid form and deposited by a extrusion head. The thin layers of material are bonded when the part comes out of the machine. Finally the assembly is placed into a solution that dissolves remaining support material. The machine's resolution is 0.007 inch thick layers. The clearance of the joints and wire hole diameter dimensions approached this limit, but could still be manufactured.

For ease of building via rapid prototype, the geometry was modified to include captured pin joints, shown in Figure 30. This eliminated the need to use press-fit pins and assemble the individual links post-process. The index finger assembly shown in Figure 31 was built layer-by-layer out of ABS thermoplastic.

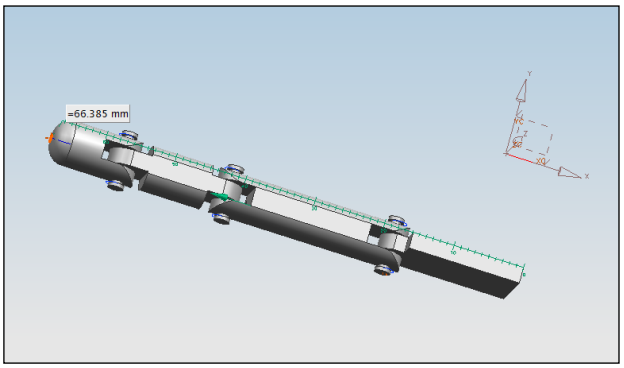

Fig. 30 NX: ½-scale finger (66.4 mm = 2.6 in)

Fig. 31 ABS rapid prototype of ½-scale finger

ABS is not an ideal material in terms of strength especially for the pin joints, as plastic is more brittle than a metal material choice. Thus the rapid prototype with captured pins may not be the most desirable option for production scale parts. However, the assembly was strong enough to use for a contact force test identical to the one performed for the full-scale hand.

A Contact Force Test of the ½-scale finger assembly was set up in the same manner as outlined above for the full-scale version. First, a piece of foam rubber was cut to size and applied to the surface of the plastic finger. Since the foam rubber was cut smaller for the smaller finger, the plastic assembly weight to "spring stiffness" ratio was different due to the

lighter finger material. It was reasoned that it may take more weight, relatively speaking, for the plastic finger to overcome the spring force than it did for the heavier, full-scale, aluminum parts. The finger assembly was mounted on the test fixture, such that the contracted finger would contact the head of the load cell as weights were applied, seen in Figures 32 and 33.

The results of the ½-scale Contact Force Test revealed that the minimum contraction force of the smaller, lighter-weight finger was twelve times less than that of the full-sized version. It took only 0.3 lbf to contract the finger and touch the load cell. The resulting contact force was a mere 0.04 lbf.

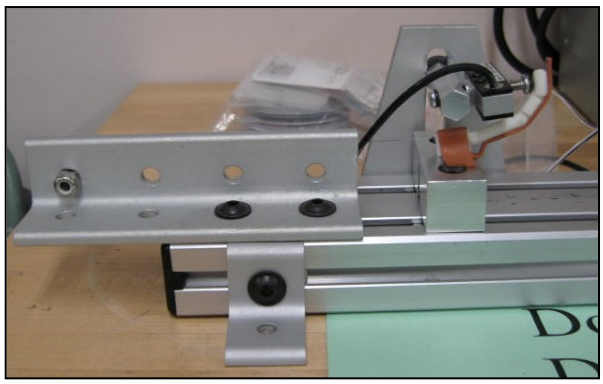

Fig. 32 ½-Scale finger assembly Contact Force Test

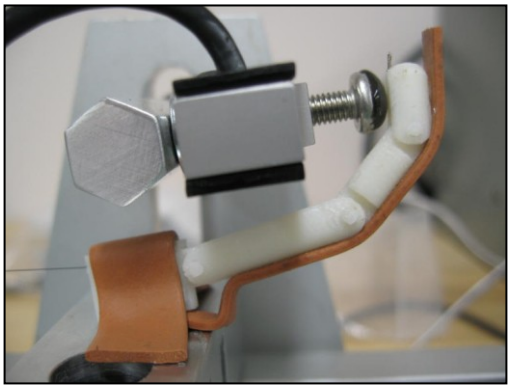

Fig. 33 Close up of contact with load cell

The two main differences between the full-scale and ½-scale fingers were the material and the design of the joints. The captured pin joints of the ½-scale finger are virtually frictionless, whereas the press fit pins of the aluminum finger contribute great resistance. Figure 34 shows the results of the Contact Force Test for the ½-scale ABS finger assembly.

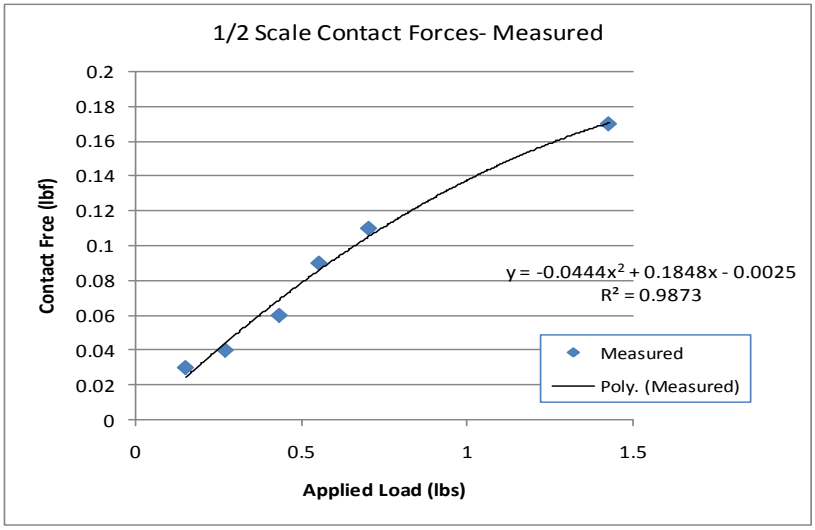

Fig. 34 ½-scale Contact Force Test Results

With the physical test complete, a new dynamic model that captures the changes of the ½-scale physical parts was made in Recurdyn. Since the calculations for the system inputs were outlined above from the full-scale design, it was easy to replicate a Recurdyn model for smaller geometry. CAD parasolid files were reduced to ½-scale and then imported into Recurdyn. (Fig. 30) The ABS material was specified in Recurdyn by its density and was assigned to the finger links. No frictional coefficients were applied to the joints, due to the modified design. The foam rubber spring forces for the smaller-sized links were calculated and input as the spring constant values for the springs in Recurdyn. To complete the ½-scale model, a solid rectangular box was added to create a contact surface for the finger.

The test of the model's usefulness was how well it correlated with the physical results. The full-scale model was already shown to accurately represent the physical system. Another benefit of modeling is the ability to easily vary the design characteristics. For example, the captured and frictionless pin joints were different for the ½-scale design. Different spring forces (foam rubbers) could be applied to the geometry to quickly determine the effects. The same could be said for varying the finger material as well, should future work require.

Once the design was modified to ½-scale, the input force or wire pull force was varied and the model was run several times to determine the resulting contact force of the finger on the green box, whose material was specified as rubber. (Fig. 35) The results are plotted in Figure 36 alongside the data from the physical test.

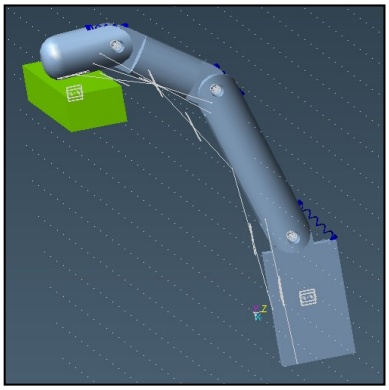

Fig. 35 ½-Scale Recurdyn Model

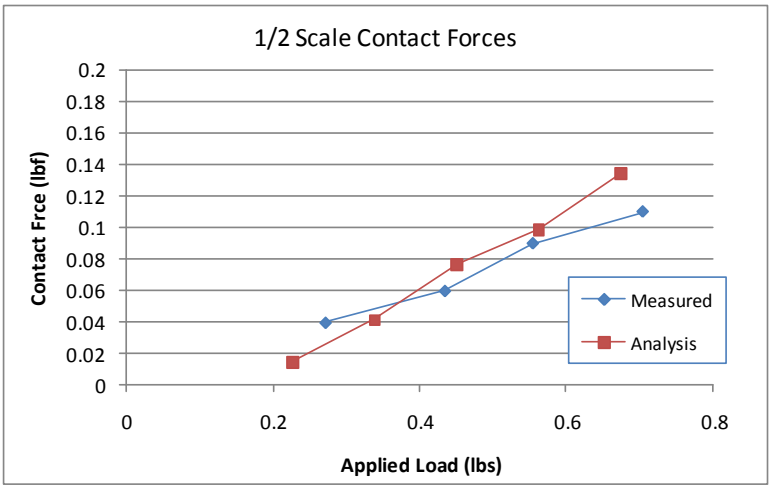

Fig. 36 ½-Scale Contact Forces: Measured, Modeled

The actuation range of the small finger was bounded on the low end by the minimum amount of force that it takes to contract the finger. The upper end of the range would be determined

by the hand's future application. During the ½-Scale Contact Force Test, it was apparent how much weight was required to contract the finger verses overstressing the assembly. Based on observed deformation, the finger was overstressed above approximately 0.75 lbf of actuation force.

The actual upper limit of actuation force would also be selected based on the strength of the hand material. For example, an ABS plastic hand would likely not be used for an application requiring a relatively large grasping force. The strength of the pin joints would not withstand the stress of grasping heavy objects. The further study of these limits would be an interesting future project to explore. Further modeling of joint stress and more physical testing could reveal a variety of applications suitable for the ½-scale hand. While the slopes of the lines for measured and modeled data were slightly different, in the range of interest (applied load = 0.3-0.75 lbf), the model was shown to predict contact forces.

Interpretation of ½-Scale Results

There were several potential sources of error in both the physical test and the model. In the physical test, it is likely that the finger was not positioned precisely normal to the top of the load cell. Any amount of variation in the contact point was likely contributing to error. While the ½-sphere shaped epoxy on the load cell was fine for the physical test, this shape was not desirable for the dynamic model. The dynamic model was simplified by using a flat surface for the contact point of the finger. It was easier to simulate the finger contacting the box normal to its flat surface. (Fig. 35)

Another source of error may have been the rapid prototyping process. There was some remaining material in the joints that prohibited movement of the links to a small degree. This bit of resistance was not accounted for in the model, which assumes frictionless joints. Due to limitations of the 3D Printer, there is a limit to the accuracy that can be achieved at this scale.

In Recurdyn, an assumption was made that there is no pre-load on the foam rubber. There was likely some human error involved in applying the foam rubber to the finger. Any amount of preload may affect the contact force results. While there are sources of error in both the testing and modeling, within the range of interest the model correlates fairly well with the measured data. When comparing linear fit equations for each line, the percent error

is about 12% between the measured and modeled values for contact force. The model and method for determining inputs has thus been validated both at the full-scale, and the ½-scale. For the ½- scale size, an actuation range was identified along with corresponding contact forces. The model could be used to further explore the topics suggested below in the Future Work section. In the short-term, it was used to investigate the feasibility of a ¼-scale model.

Fabrication of ½-Scale Hand

Due to the successful production of a ½-scale finger assembly on RIT's 3D printer, an entire hand assembly was made. The ½-scale hand assembly was made for future testing, to demonstrate the viability of the full hand design at ½-scale, and to demonstrate the capabilities and limitations of RIT's Dimension Elite 3D Printer. Manufacturing the robotic hand assembly at ½-size was successful, as seen in Figures 37 and 38, and was not seen as the break point in terms of the design's scalability. At this scale, smaller air muscles could be employed to actuate the hand. To make a production version, a CNC lathe or screw machine would be capable of turning metal finger components. The individual links would be pinned together, leaving clearance for frictionless joints, post process.


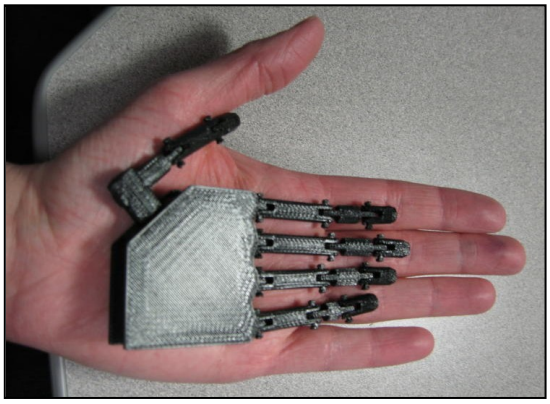

Figs. 37 & 38 ½-Scale robotic hand assy made on Dimension Elite 3D printer

A Senior Design Team at RIT built and tested several sizes of air muscles. [39] The smallest being 3 inches in length, which is half the size of the full-sized hand assembly air muscles. From their test data, it could be interpolated that an air muscle of 1.8 inches in length would provide 0.5 lbf of pull force, which is the middle of the ½-scale actuation range identified above. Further discussion of this calculation is described in the Actuation Limitations section below. However, the range of actuation forces confirmed that a ½-scale hand is both manufacturable, and could be actuated via air muscles. A goal of this project

was to determine the smallest scaled version of the current design that could be manufactured using traditional manufacturing techniques and actuated, thus scaling the robotic hand design to ½-scale was confirmed as feasible. To find the lower limit of scale for the robotic hand, the hand was sized to ¼-scale.

Scalability Study of ¼-Scale Design

An attempt to scale the robotic hand to ¼-scale was a large step towards determining the break point of the design. There were several processes that were deemed potential options for making the miniature hand components. Traditional hand machining techniques are limited by tool and drill size. Based on discussions with model makers in the RIT Machine Shop, a ¼-scale model would be difficult to produce with available tools. Thus, Swiss screw machining, investment casting, and additive manufacturing processes were considered instead.

Swiss screw machining was identified as a possible method for machining the fingers. A screw machine is a fully automated specialized lathe generally used to manufacture turned components. While there are different machines with corresponding capabilities, the bottle neck in terms of the ¼-scale hand design was drilling the 0.016 inch diameter wire holes through each finger component. Dependent upon material selection of the hand, the drill itself would become a challenge to produce. However, a machining expert at RIT believes that a 0.04 inch hole is possible to drill for this application. [43] This diameter was consequently the requirement for the ½-scale, but would not be small enough for the ¼-scale hand.

It was concluded that while it is possible to machine the ¼-scale finger parts, drilling the wire holes through the fingers to run tendon cables becomes extremely difficult at this scale. Further micro-machining techniques would be necessary to achive the design at this scale and certainly for a hand smaller than ¼-scale. The question of material selection is constrained by these processes. Aluminum would be too soft of a material to machine at the small scale. Harder materials such as titanium or delrin plastic would be possibilities.

Investment casting or the lost wax method is another that may be employed to make the ¼-scale hand components. In this process, a model of the part is made out of wax, and this is used to create an inner and outer mold. Melted wax is poured into the mold which is a

negative of the original model. This new wax model is covered with ceramic shell material, then fired. This process melts the wax which escapes out of tiny holes, finally revealing a hollow mold. Molten metal is poured into the ceramic shell to cast the final part. This process is typically used for jewelry and dental impants. Figures 39 and 40 show examples of components manufactured using investment casting. [44] Since each individual finger link would require its own mold and cast, this would be an expensive option. Based on speaking with sales representatives for two investment casting forgerys, producing the hand would cost many thousands of dollars.

Fig. 39 Original model of ring [44]

Fig. 40 Wax model to be covered by ceramic shell [44]

An additive manufacturing process is likely the most cost effective and capable method for producing a ¼-scale hand assembly. Rapid prototyping is used to visualize designs of complicated parts that would take hours to machine by conventional methods. The additive process begins with a CAD file, then uses software to dissect the file into slices. Cross-sectional slices are built up in thin layers of material to create a part or assembly. Support material is sometimes generated while building, but is later removed by post-processing. Rapid prototyping techniques are mainly defined by the way the additive layers are created. When selecting a rapid prototyping technique for parts requiring high resolution, layer thickness is the important factor.

In order to easily visualize the impact of ¼-scaled parts, an attempt was made to rapid-prototype the pieces of the index finger with RIT's 3D printer. This was the same equipment used to produce the ½-scale hand. The Dimension Elite 3D printer, lays down material in 0.007 inch layers. The ¼-scale size was slightly outside the resolution limits of the machine. The wire hole was not visible and the pin holes were not clear of excess material. After this attempt, it was apparent that a higher resolution method was required for for generating the ¼-scale parts.

Stereolithography (SLA) is known for high resolution capabilities with machines operating at 0.002 inch layer thickness. Here, a UV curable liquid and UV laser are used to bond material one layer at a time. The laser beam "writes" the part's cross section, curing the liquid into a solid. The parts are built on a platform that lowers by a layer thickness as the layers are completed. The completed part is cleaned in a chemical bath and then further cured under UV light. This process is somewhat more expensive than high resolution 3D printers, which have emerged as a cost-effective alternative.

Selecting a manufacturing process to produce a miniature robotic hand may be challenging, but could likely be accomplished. For future applications, there are other important considerations as well. Material selection for a surgical tool hinges on biocompatability. Biocompatability is defined as, "the success in use of a non-viable material in contact with biology" [45]. One would need to be familiar with the implications of material selection for specific medical applications. Finally cost also becomes a factor. Specific material choices would require further investigation based on intended applications for the hand.

Fabrication of ¼-Scale Hand

As described above, the Dimension Elite 3D printer did not have high enough resolution to create a ¼-scale hand. However, FineLine Prototyping (Raliegh, NC) offers 3D printing services with high resolution. The InVisionHR uses a multi-jet print head, and deposits 0.00125 inch layers when building parts. The features of the ¼-scale model were achievable with this process.

When assessing the smallest feature size that can be achieved by an additive manufacturing process, part orientation is of importance. A part is oriented in the xy plane such that the smallest dimension is dependent on pixels, laser spot size, and mechanical precision. The z dimension depends on the layer thickness. [46] The ¼-scale robotic hand has feature size restrictions that are important in both the xy plane and z direction. The distance between the pins and pin holes in the finger links was the most stringent at 0.006 inches of clearance, thus the part was oriented with fingers pointed upwards. The wire through holes had to be increased to 0.02 inches (from 0.016 in.) in diameter to enable the clearance of support material. This small increase in diameter did not greatly affect the

design, but showed that this dimension was a bottleneck for scalability. Thus, it was important to use the process with highest resolution for making a prototype of the hand assembly.

Different than the RIT's Dimension Elite printer, InVision uses a UV-curable liquid as the layer material. Wax support material is melted during the post-processing steps to complete the part. This level of resolution rivals the SLA process and is less expensive. In order to assess the capability of the InVisionHR, the ¼-scale design was purchased from FineLine. The cost for three hand assemblies was $92.

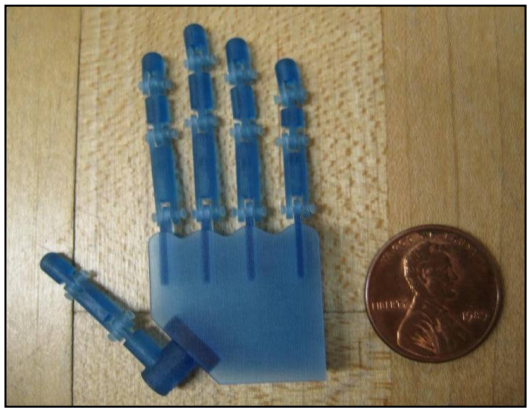

Fig. 41 ¼-Scale RIT Robotic Hand

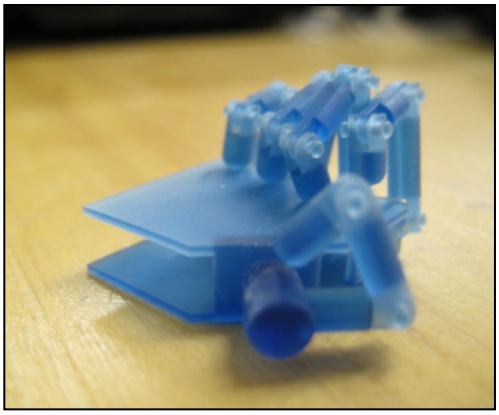

Fig. 42 ¼-Scale RIT Robotic Hand, curled

A ¼-scale assembly was achievable via rapid prototyping, however this size is the logical break point in terms of the design. The Fineline process engineer had to increase the diameter of the wire through hole to 0.02 inches in order for the support material to be removeable. As specified above, the dimension of the wire hole as dictated by the design is 0.016 in. diameter. While smaller finger parts could be made on the inVisionHR, again it is the design of the wire through-hole that limits the scalability of the robotic hand. This size is also the lower limit of scale for the RIT hand design in terms of manufacturing a durable assembly.

Upon receiving and handling the ¼-scale hand, it was observed that the assembly was delicate and would likely not stand up to strenous tasks. Selective Laser Sintering (SLS) was assessed as a method for a future iteration, since this process can produce metal parts. This process uses a laser to melt and fuse particles of powdered plastic, metal, ceramic, or glass into the desired 3D shape. Titanium is one of the materials that could be used. SLS would produce the individual finger components, then the fingers would be pinned together. A stiff piece of wire could be used to pin the links together. This would result in stronger material

for the fingers, and also metal joint pins versus the brittle ABS of the 3D printer. However, Dr. Cormier of RIT who specializes in rapid prototyping techniques, discounts SLS as a practical method. He believes that the wire hole diameter would be unachieveable by this process. [47] While the SLS process is capable of producing stronger/harder parts, the process's resolution of 0.004 inch layer thickness would not be adequate to achive the wire hole dimension. As with the screw machining process above, attempting to drill the tiny wire hole post process would be difficult.

The ¼-scale design is a unique size in terms of manufacturability. On the other side of the spectrum, this design was viewed as being on the large side of micro-scale techniques. The typical size of micro-scale devices is less than 1 mm, compared to the 180 mm size of the ¼-scale hand. Thus, the materials available and complicated processes associated with micro-fabrication would not be ideal for this particular application. [48] [49]

After evaluating several potential methods for creating a ¼-scale hand, additive manufacturing and the lost wax method emerged as the best options for manufacturing. However, each of these have drawbacks. The 3D Printer plastic hand assembly was not robust and would be limited in application. The lost wax method is expensive and may require post processing for the wire holes. Thus it was concluded that a ¼-scale hand assembly is the breaking point in terms of manufacturability for the RIT hand design. Further miniaturization would require micro-machining or redesign of the hand mechanism.

Actuation Limitations

After manufacturability, the second piece of information that is critical to the scalability of the hand design is the actuation method. At what point are air muscles no longer the preferred or practical choice for actuation? The answer to this was inferred from previous air muscle test data collected by the RIT Senior Design Team. [39] The students built three sizes of air muscles. One of the measurements taken was the resting and contracted lengths at various pressures. For the purpose of this project, only one pressure was addressed, 60 psi. This was the pressure at which the full-scale hand assembly is operated. For three different sized air muscles, the plot of contracted lengths are shown in Figure 43. The relationship between air muscle length and contraction distance is linear and

thus suggests that air muscles of similar construction, but different lengths, are scalable according to the data.

A theory was that since contraction distance versus air muscle length is a linear relationship, pull force and air muscle length may also be related linearly. An assumption was made that due to the air muscle design and operation, contraction distance and pull force are directly related, supporting the theory. With one data point from the Air Muscle Pull Force Test, the rest of the data was plotted using the same ratio of pull force to contraction distance. (Fig. 43) This assumption of a linear relationship was made since only the length of the air muscle was varied.

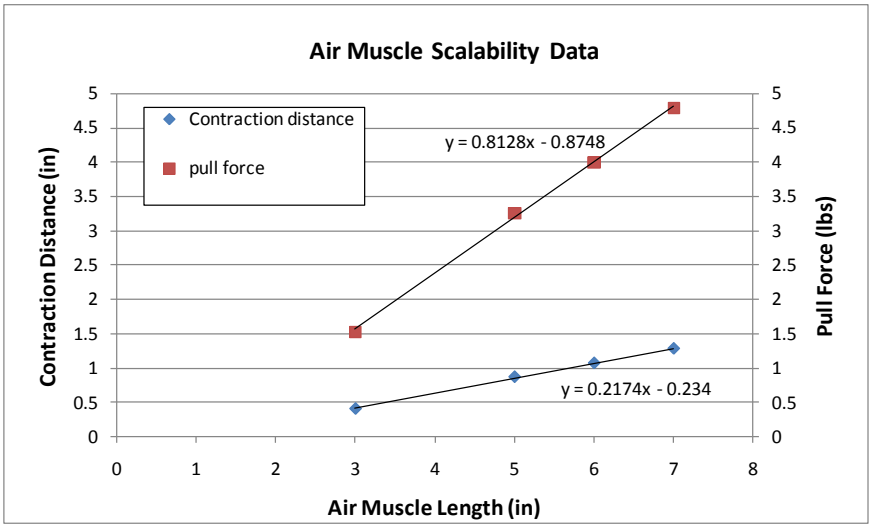

Fig. 43 Air Muscle Data

The equation for pull force is $y = 0.8128x - 0.8748$, where x is the air muscle length and y is the pull force generated by an air muscle of a specified length. Using this equation of the linear fit data for pull force, the smallest air muscle length was interpolated. In Excel, potential air muscle length values for the variable x were entered until the pull force value y was slightly greater than zero, a pull force of 0.1 lbf. The minimum length of an air muscle was found to be 1.2 inches long based on this process. The equation for contraction distance, $y = 0.2174x - 0.234$ was used to determine how much the 1.2 inch long air muscle would contract. The air muscle length is also x in this equation, and the value of 1.2 inches was plugged in. The y value of contraction distance is 0.03 inches for this length. This calculation is found in Appendix A.

Smaller radial dimensions for air muscles could likely be used. However, the study of miniature air muscle components while related, was outside of the scope of this thesis

project. Thus the limitation of air muscle acutation stood with a 1.2 inch-long air muscle able to generate 0.1 lbf. Another question was what are the pull force requirements at the smaller scale? Will this theoretical minimum-sized air muscle length and pull force be appropriate for a ¼-scale robotic hand? These questions were addressed by using the Recurdyn model to analyze the ¼-scale hand assembly.

¼-Scale Simulation

The process for modeling the robotic hand in Recurdyn was again repeated at the ¼-scale. While it was already described why it would be difficult to manufacture at this scale, this was a good test to determine whether or not the design would work in terms of the current actuation technique. The actuation force range for this size hand is a narrow one. According to the Recurdyn model, only 0.2-0.25 lbf is required to actuate the small finger. (Fig. 44) It was assumed that the ¼-scale finger actuation requirements would be less than the ½-scale finger. The Recurdyn results confirm this.

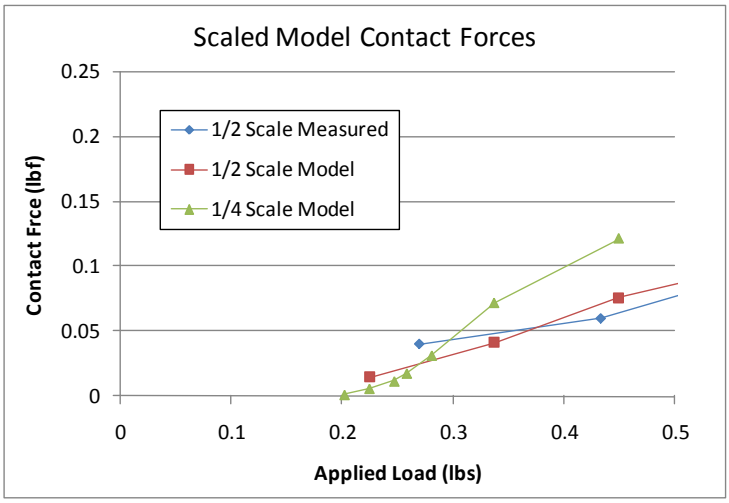

Fig. 44 Contact force results with ¼-scale

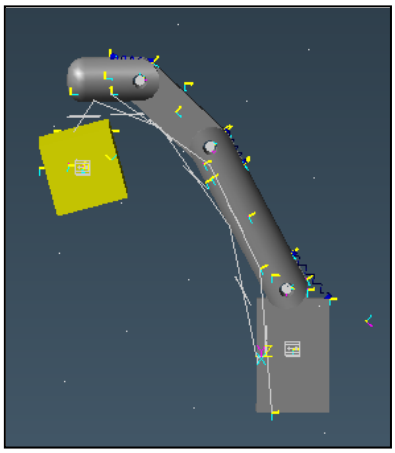

Fig. 45 ¼-Scale Recurdyn simulation

However, the plot shows that an input force of above 0.3 lbf would result in a contact force greater than that of the ½-scale assembly at the same input force. Since the ½-scale and ¼-scale parts are made of similar materials and have the same joint design, it makes sense that these results would be much closer than the full-scale and ½-scale. Yet, it is apparent that the dynamic model showed a much steeper slope for the ¼-scale than the ½-scale.

For an unknown reason, the model becomes unstable between the input force of 0.26 and 0.45 lbf. The contact force plot seen in Figure 47 for an input force of 0.28 lbf shows a

very different response than the typical plot for contact force, such as Figures 46 and 48, at 0.26 lbf and 0.45 lbf input forces respectively. Also when playing the simulation, the motion of the finger is different for the 0.28 lbf input force case. Here, the finger hits the contact surface then slides quickly across it. For all of the other input force cases, 0.26 lbf and below, and 0.45 lbf and above, the finger comes into contact with the surface and does not slide.

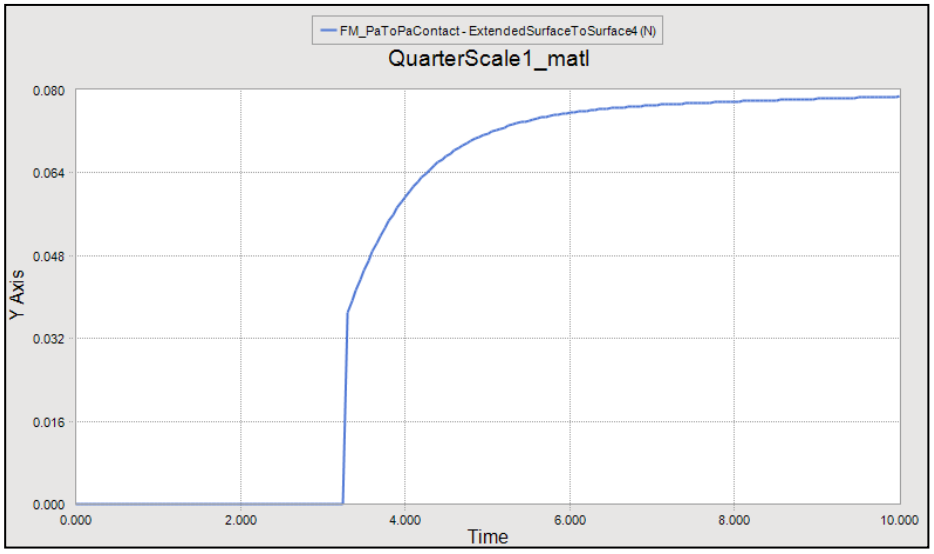

Fig. 46 Input force = 0.26 lbf

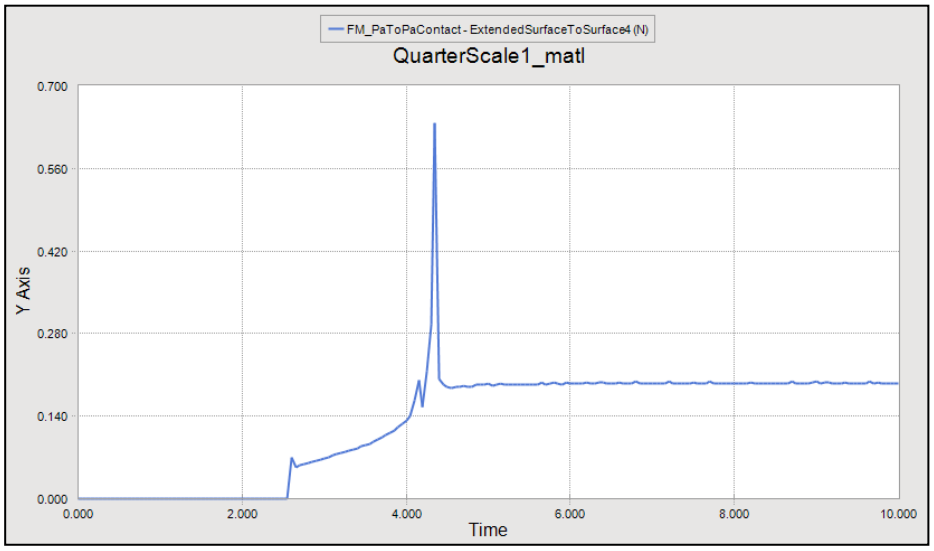

Fig. 47 Input force = 0.28 lbf

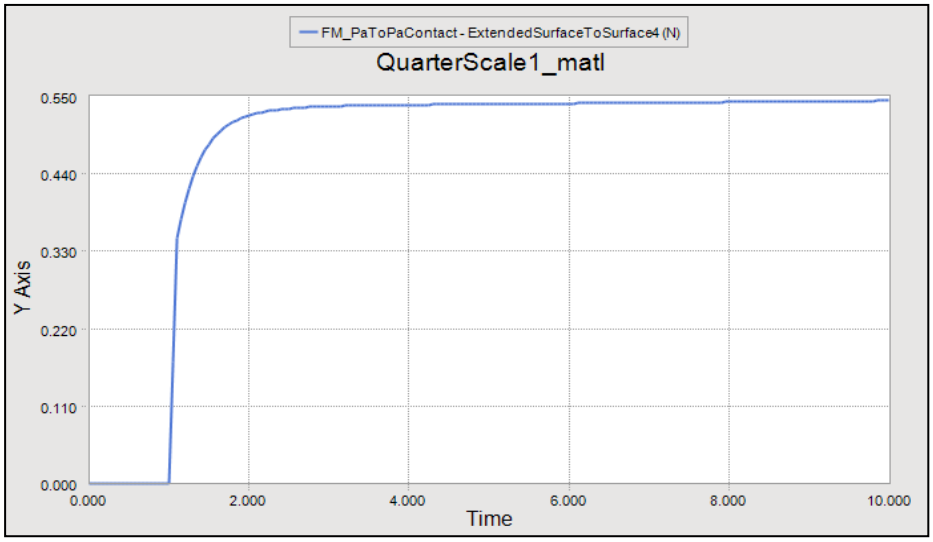

Fig. 48 Input force = 0.45 lbf

Despite the instability of the model at the point of 0.28 lbf input force, knowledge was gained about the amount of force required to actuate the ¼-scale robotic hand. For future work, the actuation pull force to begin with would be 0.26 lbf or below. It is of importance to realize that the computer model does not account for stress on the parts. If a great enough actuation force was applied to the small joints, the finger would snap and break at the pin joints. This is a lesson about modeling, where one must be careful that what the model is predicting actually makes sense. When running the simulation, it plays back the dynamic event of the finger moving and touching the block. Once the finger appeared to be slamming into the block, this was an indication that the input force was too high. The low end of the actuation range is the input force needed to contract the finger and touch the block. Figure 45 shows the ¼-scale finger before it came into contact with the yellow block.

Based on the data plotted in Figure 44, the actuation force for the ¼-scale hand was predicted to be around 0.25 lbf. Above, it was learned that the smallest air muscle is theoretically capable of producing 0.1 lbf pull force, indicating that an air muscle is likely capable of actuating a ¼-scale finger. It is unknown if a smaller air muscle could be made to produce a pull force less than 0.1 lbf. Thus a hand assembly requiring this small amount of force for its actuation requirement would likely need an alternative actuation technology. One option explored for a sub ¼-scale hand assembly is Electroactive Polymers (EAP).

Electroactive Polymers

EAPs are known in the field of micro-robotics as artificial muscles. These polymers are deformable by applying an external voltage. (Fig. 49) EAPs have a "high load bearing capacity to mass ratio, short response time, and nearly linear deformation response with respect to applied voltage" [50]. Researchers see the benefits of these materials and many applications for their use have emerged. An experiment performed at UCLA demonstrated the forces generated by a typical EAP. [50] Figure 50 shows that up to 4.5 g or 0.01 lbf of weight lifted was achievable.

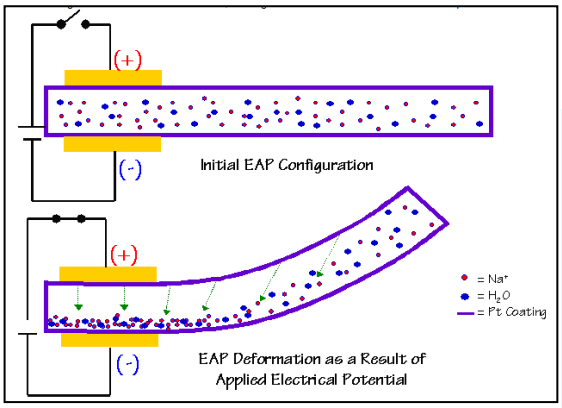

Fig.49 EAP Deformation Mechanism [50]

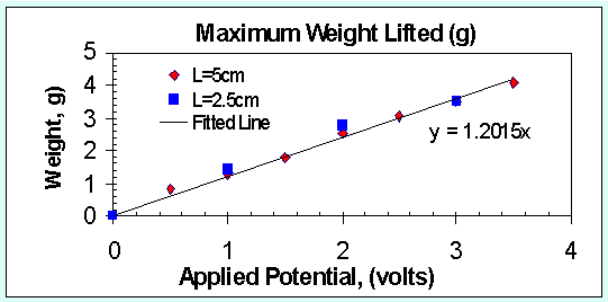

Fig. 50 EAP Lift and Strength [50]

This is about twenty-five times less than what is required to actuate the ¼-scale robotic hand. Again, this ¼-scale size was somewhat unique since it is on the edge for air muscle actuation, and would require too much force to employ EAPs. Significant changes to the robotic hand to allow for further scalability may result in a design appropriate for EAP actuation.

Degrees of Freedom and Range of Motion

In the literature, the authors usually made a point to document the number of degrees of freedom (DOF) of their device. The higher number of DOF suggested the greater dexterity that the device would have. Since the RIT hand aimed to eventually be similar in dexterity to the human hand, these were compared. The human hand is a highly articulated system with 27 DOF. Each finger is capable of flexion/extension, abduction and adduction, resulting in four DOF per finger. The thumb is further capable of circumduction for a total of five DOF. Translation and rotation of the wrist account for the final six DOF. As stated in the project introduction, the robotic hand design was limited to grasping and thus a reduced number of DOF are needed to achieve this type of motion. The full-scale, ½-scale, and ¼-

scale robotic hands each have the same number of DOF when operated as intended with the wires and air muscles. Each finger has three joints and thus three DOF for bending (flexion and extension). The thumb with only two joints makes the total 14 DOF for the robotic hand.

While the full-scale hand is currently limited by the joint construction, the rapid prototype assemblies exhibit additional DOF while not connected with wires. Due to the clearance of the joint pins, the fingers of the scaled hands also move with abduction and adduction. (Fig. 51 & 52) While this is desirable to match the human hand at the MCP joint, where the finger meets the palm, it could be considered a disadvantage to have the additional motion at the medial (PIP) and distal (DIP) joints. For a future iteration, care should be taken to ensure the smallest clearance of pin and joint hole to reduce the motion in these two joints. However, the motion of the MCP joint could be increased if the joint hole were to be elongated or slotted to allow even more abduction and adduction. When these additional DOF are included, the ½ and ¼-scale rapid prototype hands have 28 DOF each. Whether or not these additional DOF could be controlled to provide more dexterous motion would require further study. However at the quarter-scale, the robotic hand presented here is novel in terms of similarities with the human hand for a grasping function.

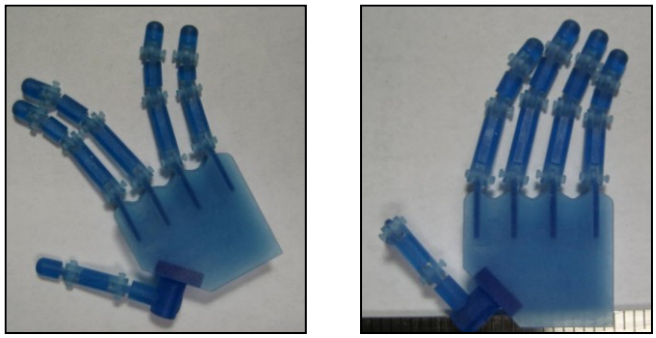

Figs. 51 & 52 ¼-Scale Hand Abduction and Adduction

The range of motion (ROM) of the human hand is also a standard to be matched by the robotic designs. This is typically measured by the range of joint motion, which is limited by hand anatomy. ROM only includes the amount of motion attainable without applying external force, such as bending fingers backwards. [51] In comparison, measuring the ROM of the ½ and ¼-scale robotic hand joints could be misleading. One must recognize that once the wires and foam rubber strips are applied to the assembly, the ROM would be drastically reduced. When operated, the air muscles pull on the wire with a force that may or may not be the maximum force to fully contract the joints to their complete extension. In order to

realistically comprehend the range of motion of the small hands, they would need to be fully assembled for operation. In the meantime, a process was created using photography to measure the ROM of the joints.

$$0° \le \theta_{MCP-F} \le 90°,$$
$$0° \le \theta_{PIP} \le 110°,$$
$$0° \le \theta_{DIP} \le 90°, \text{ and}$$
$$-15° \le \theta_{MCP-AA} \le 15°.$$

Fig. 53 Human Hand Range of Motion [51]

Again, while the robotic fingers could easily be bent backwards much further than a human hand, this was not the intention of the design. When the wire applies the external force, the fingers only flex in one direction, towards the palm of the hand. With this understood, the process to measure the joint angles was used for a non-assembled hand system. The plastic hands were measured to the full range of their joint motion. This process could be repeated for the robotic hand assembly with wires and foam rubber.

The ½ and ¼-scale hand assemblies were aligned with a straightedge ruler. First the MCP joint was positioned to one extreme of its range, and then photographed. (Fig. 54) The finger was rotated to the bent-backwards position, and photographed. (Fig. 55) Cropping the pictures, aligning the points of rotation of the joint, and drawing a straight line along the axis of the proximal phalange allows for the joint angle to be measured with a protractor. (Fig. 56)

The process was repeated for the remaining joints. Appendix C contains the complete set of pictures. The results are summarized in Table V. Since there are no restrictions on the ROM of the ½-scale hand such as tendon cables and foam rubber, the robotic hand ROM is vastly greater than that of the human hand. It is expected that once these restrictions are added, the ROM of the robotic hand will more closely match that of the human hand.

Fig. 54 MCP Joint Position 1

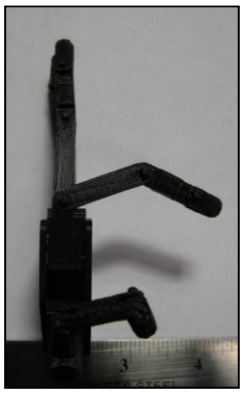

Fig. 55 MCP Joint Position 2

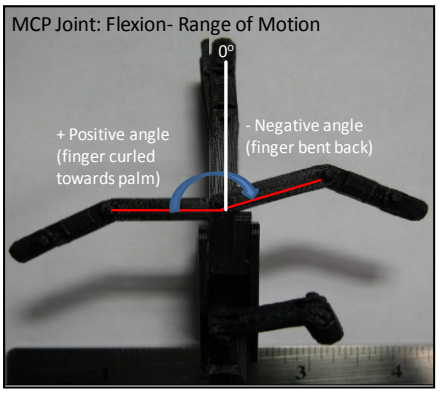

Fig. 56 MCP Joint Combined Pictures

1/2 Scale Hand		Abduction/Adduction	
Flexion ROM of Joints	Range (°)	ROM of Joints	Range (°)
$-75^{o} \leq \theta_{MCP\text{-}F} \leq 90^{o}$	165	$-12^{o} \leq \theta_{MCP\text{-}AA} \leq 12^{o}$	24
$-90^{o} \leq \theta_{PIP\text{-}F} \leq 90^{o}$	180		
$-133^{o} \leq \theta_{DIP\text{-}F} \leq 90^{o}$	223		
1/4 Scale Hand		Abduction/Adduction	
Flexion ROM of Joints	Range (°)	ROM of Joints	Range (°)
$-100^{o} \leq \theta_{MCP\text{-}F} \leq 80^{o}$	180	$-15^{o} \leq \theta_{MCP\text{-}AA} \leq 15^{o}$	30
$-130^{o} \leq \theta_{PIP\text{-}F} \leq 100^{o}$	230	$-11^{o} \leq \theta_{MCP\text{-}AA} \leq 11^{o}$	22
$-100^{o} \leq \theta_{DIP\text{-}F} \leq 110^{o}$	210	$-10^{o} \leq \theta_{MCP\text{-}AA} \leq 10^{o}$	20

Table V Robotic Hand ROM

Design Recommendations

During the course of handling, testing, and modeling the RIT robotic hand assemblies, several future design recommendations for scalability can be made. The life-sized robotic hand designed and built by the RIT Senior Design Team is dexterous with human-like motion and as this study shows, was scalable. The actuation method and controls make the hand capable of performing an automated grasping motion. Having a successful design as a starting point is a benefit to those who pursue continuing research.

The Scalability Study aimed to optimize the grasping hand without drastically changing the design. However, since the "gold standard" of robotics is to mimic the counterpart in the human body, one suggestion is anatomical corrections. If the life-size hand were to be redesigned, closer attention could be paid to the length of each phalange and angle of the finger holders. In order to get the best hold on an object, typically fingers are splayed in order to cover more surface area of the object being grasped. Positioning the finger holders in the palm plates to mimic the human hand may improve the robotic hand's dexterity.

The major change made to the hand during the Scalability Study was the design of the joints. As mentioned above, the press fit pins of the life-sized hand created significant friction that opposed both flexion and extension of the fingers. In the smaller assemblies, the joints were converted to captured pins and friction was reduced to virtually nothing. This was a design change that the full-scale assembly could test relatively easily. The Recurdyn

model could be modified to predict changes in the contact force if joint friction was to be reduced.

Another change to the joints could be made to improve dexterity. Although originally intended for grasping only, creating more DOF in the hand would only improve the hand's functionality. For example, the pin joints of the MCP could be changed to allow for abduction and adduction. This way the robotic hand would more closely match the DOF of the human hand. One suggestion for accomplishing this would be to slot the pin holes on the finger holder, Figure 57. Controlling this motion could require more wires and air muscles.

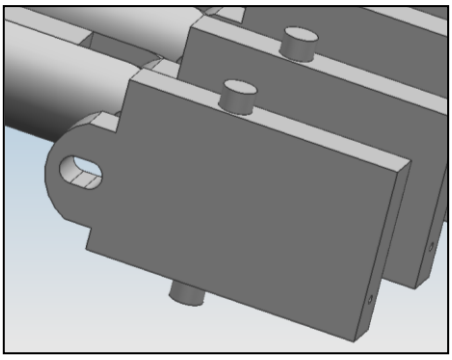

Fig. 57 Proposed slotted finger holder

While the plastic hand assemblies have a large range of motion without wire and foam rubber, this is not representative of the complete hand system. Once fully assembled with air muscles and constrained by foam rubber, the ROM for the robotic hand is similar to that of the human hand. Should an external force be applied to bend back the fingers of the robotic hand, the ROM is much greater than for the human hand. Whether or not this is irrelevant for the operation of the robotic hand may depend upon the application.

Another observation of the full size hand that will translate to the smaller scaled hands is the wire at the tip of the distal phalange is essentially unattached. (Fig. 58 & 59) When the wire is threaded through the wire holes of each phalange, the wire is terminated at the tip of the distal phalange with a small metal cylinder. This cylinder is pinched around the wire to keep the wire from being pulled out of the finger. It appears that this metal terminal became lodged in the wire hole effectively securing it in place. The terminal was cut down so to be flush with the finger. While this works, there is the chance of the wire terminal coming loose from the wire hole.

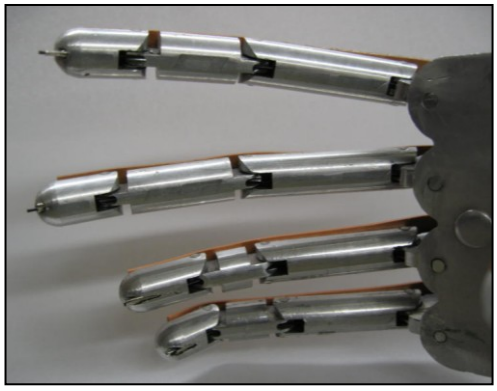

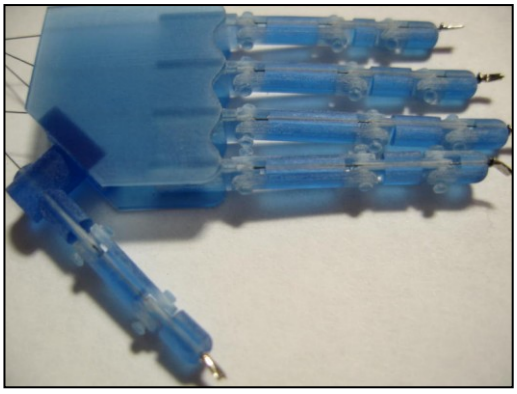

Figs. 58 & 59 Metal terminal sticks out at tip of phalange

A design recommendation is to create a recess in the tip of the distal phalange to allow room for the metal terminal. (Fig. 60) Then this recess and the metal terminal could be covered with material such as epoxy and filled. The wire would be firmly attached to the tip of the finger, and the potentially sharp metal terminal encapsulated. This process could be achieved simply by increasing the radius of the wire hole at the tip of the distal phalange so that the wire terminal would seat into the finger. Potentially this change could work for each sized assembly. One drawback of this is if the hand needs to be re-wired, or if the wire pulls out of the metal terminal. Especially at the smaller scale, it may be difficult to repair the wiring.

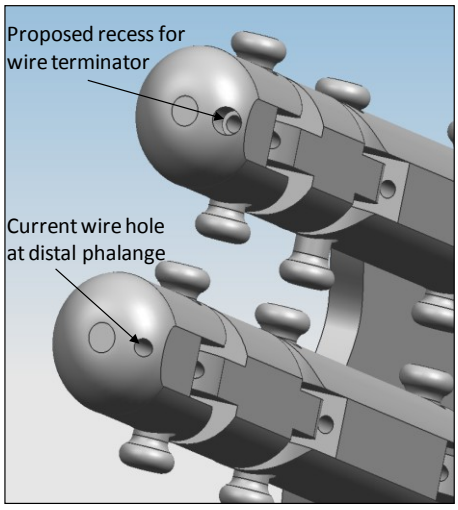

Fig. 60 Fingertip recess for wire terminal

To improve robustness of the ¼-scale plastic hand, the individual finger links could be made separately on a high resolution 3D printer, then assembled with metal pins. By increasing the strength of the pin material, this would greatly improve the sturdiness of the

overall assembly. This is under the assumption that the narrow plastic pins would be the weakest point of the plastic assembly. Attempts could be made with either press fit pins, or captured pins, depending on frictional requirements.

In order for the life-sized hand to be reproduced, the screw machine in the Brinkman Lab at RIT could be used to turn the finger parts. An attempt to make the ½-scale hand assembly on this machine would be interesting as well. Several eyeglass screws available from the company QTE North America could be used as potential pin joints for the ½-scale hand. A robust ½-scale hand assembly could be used to continue testing with smaller scale air muscles and attempt to increase dexterity at the smaller scale.

Finally a few considerations for improving the ¼-scale hand design include identifying the best wire to actuate and perhaps a less-stiff foam rubber. As mentioned briefly above, consideration for the finger weight to spring stiffness ratio may merit a look at different foam rubbers. The mass of the index finger for each robotic hand was calculated based on the part volumes. Next the spring constant 2.1 lb/in that was calculated for the 3 inch sample piece of foam rubber was used to establish a ratio. These numbers are arbitrary, but showed the great difference between applying the same foam rubber material to the aluminum full-scale hand parts and the lightweight ¼-scale plastic parts. (Fig. 61) The foam rubber has a much bigger impact on the finger at the small scale, and would require more force to overcome, relatively speaking. Appendix A contains the details of the calculation.

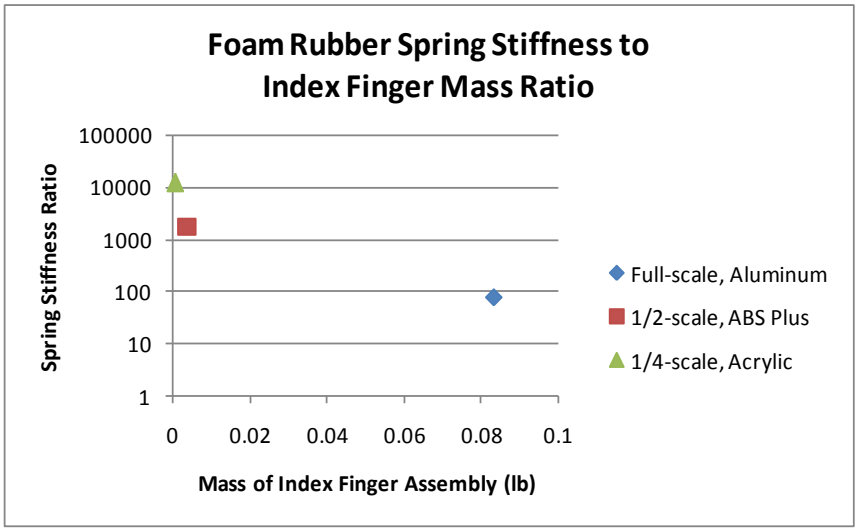

Fig. 61 Foam Rubber Stiffness Ratio

Further research into investment casting would reveal if this is a cost-effective option for making the small fingers out of metal. Another option is to investigate the requirements for micromachining. The company Norman Noble states that, "Our unique micromachining and finishing capabilities enable the manufacturing of your newest designs of Medical Devices, Components, and Implants. We specialize in micromachining of exotic materials to very complex geometries with dimensional tolerances to +/-.0001" [52]. This sounds promising for the manufacture of a ¼-scale robotic hand assembly, or potentially smaller.

Conclusions

- Manufacturability: The design of the RIT robotic hand is limited by the size of the wire hole dimensions and joint construction
    - Potential manufacturing methods for a ¼-scale hand are investment casting and additive manufacturing
    - Below the ¼-scale would require micro-fabrication techniques
- Actuation: Air muscle actuation could be employed to actuate the ½ and ¼-scale rapid prototype robotic hands
    - Below the ¼-scale, alternative methods may be required
- Dexterity: The degrees of freedom of the robotic hand are comparable to the human hand in terms of a grasping function
    - Additional DOF would require a design (joints) change

The overall goal of this thesis project was to explore the scalability limitations of the RIT robotic hand design. A review of literature related to robotic hands, simulation tools, micro-manipulators, and robotic surgery set the stage for an aspect of these fields that was missing. By bridging the gap between a complex robotic hand design and low DOF micro-manipulators, the scalability limitations of the RIT robotic hand design were determined. Testing and computer modeling were the tools employed to gain further knowledge of the design's capabilities. By breaking down the system into components, the inputs were identified and values determined. These included optimized hand geometry, actuation force, and spring-return force. The hand geometry was re-sized, by changing the RIT robotic hand

design to more closely resemble the anatomical average dimensions of a human hand. The solid models of the robotic hand were created in CAD, NX.

A free body diagram was used to identify the input parameters that characterize the robotic hand system. The force that contributed to actuation, the air muscle pull force was determined experimentally using a positioning slide and Labview program. Results of the Air Muscle Pull Force Test were used to calculate the pull force generated by an air muscle. The air muscles were measured in several states, and the difference in length was used to calculate the pull force of a specific air muscle, the one attached to the robotic hand index finger. The pull force of the 6 inch long air muscle with an extended distance of 0.15 inches when attached to the index finger was 4 lbf.

The foam rubber strip attached to the fingers of the robotic hand was used to retract or relax the fingers from a contracted position. Thus, this counteracts the motion of actuation when the hand operates to grasp an object. The return force was meant to act primarily when the air muscles are not in operation, thus the impact of this force on the hand was less significant than the air muscle pull force. However it was important to quantify this parameter and this was done primarily by a tensile test.

The tensile test provided the raw data used to calculate the spring constant for the rubber material. The extension of the rubber piece as it was stretched by the Instron machine was recorded as a function of applied force. This data was converted to a stress-strain plot, using equations for stress and strain. Since the material was determined to be elastic, a linear fit of the data provided an equation whose slope was the elastic modulus of the material. This material property was used in Hooke's Law relating stress and strain to calculate the spring constant for a specific length of rubber. For the robotic hand, each joint had a different length of foam rubber, and thus a different spring constant related to the initial length of the rubber. Two different methods were used to calculate the spring constant value for a specific length of rubber, and both yielded the same value, thus validating methods.

The two previously unknown inputs of pull force and the spring return force for each joint were determine experimentally for use in a dynamic computer model of the hand system. The other parameters identified by the free body diagram were the weight of the finger and friction of the joints and wire. The weight of the material was specified for each component of the hand in Recurdyn. The fingers are aluminum, and the pins are stainless

steel. These two materials have known frictional coefficients for both sliding and dynamic friction. The values for these were added to the properties of the revolute joins in the dynamic model. The friction of the wire through the finger was neglected in the computer model, as observation showed that this was minimal when compared with joint friction.

The metric used to compare results of testing and modeling was the contact force generated by the finger assembly. When the simulation was run for a particular pull force, the result was a plot of the contact force of the finger on a flat surface. These results were compared with an experimental test. A custom fixture was set up for the Contact Force Test of the index finger. Weights were used to simulate the air muscle pull force, and the resulting contact force was measured by a load cell. The data from this experiment was compared with Recurdyn results. The contact forces in each case were similar, thus the model and methods for characterizing the parameters were validated.

These steps were necessary groundwork before the scalability of the robotic hand was assessed. Theoretically, the dynamic model could be used to predict contact forces of a smaller system. An objective of this work was to show this capability of the dynamic model. Thus, a ½-scale model was created and validated with experimental testing. In order to carry out the physical testing, a ½-scale rapid prototype of the index finger assembly was fabricated on a 3D printer. This assembly was different from the full-scale version, since the joints were redesigned to be captured pins with clearance, versus the press fit pins of the full-scale hand. A Contact Force Test was performed with the ½-scale finger, and these results were compared with a scaled Recurdyn model.

Changes to the computer model included the material type, and the joints were frictionless. Even with these significant changes, the results of the experimental testing and dynamic model were similar. Thus, the dynamic model was scalable, and its accuracy was relatively uninfluenced by changes in material or frictional forces. Based on this success, an entire hand assembly was fabricated on the 3D printer and ½-scale was not deemed as the smallest feasible size for the robotic hand. Thus, the next step was to assess the design at ¼ size of the human hand.

The ¼-scale presented a more significant problem in terms of manufacturing. The conventional methods for machining were not capable of meeting the small feature sizes,

especially the wire holes at 0.016 inch diameter. Several methods were discussed including Swiss screw machining, investment casting, and multiple additive manufacturing techniques. This investigation of several possible manufacturing processes revealed additive manufacturing as the most probable for success. A novel ¼-scale human-like robotic hand was made on a high resolution 3D printer. This assembly was capable of being wired just as the full scale fingers are done. (Fig. 59) Several design recommendations were made to improve the robustness and operation of this mini hand.

Actuation limitations were also assessed for the ¼-scale robotic hand. This was accomplished by using air muscle data relating muscle length and the contraction distance when compressed. The ratio of pull force to contraction distance was known for the specific air muscle length of 6 inches. This ratio was applied to the other air muscle lengths to define an equation for pull force and air muscle length. The new equation was used to calculate the minimum length dimension of an air muscle. This muscle could be theoretically built to operate a small-scale robotic hand. A model of the ¼-scale index finger was done in Recurdyn to determine if the air muscles would be adequate for the required actuation predicted by the computer model. Results of the model showed that 0.2 lbf was required to actuate the ¼-scale hand, and the smallest air muscle was capable of generating a pull force of 0.1 lbf. The equation for air muscle length and pull force was used to determine that an air muscle 1.3 inches long would generate a pull force of 0.22 lbf capable of actuating a ¼-scale hand. Thus, the actuation method is near the edge of its capability, but still possible to be used at the ¼-scale. Below the ¼-scale would likely require an alternative actuation method.

Although the design works well at the macro level, both life-sized and ½-scale, the design began to break down around the ¼-scale mark. Near and below this point manufacturability and actuation became difficult to keep with current/conventional means. Further study could reveal improvements for the ¼-scale design. These may include material selection, foam rubber selection, and actuation method.

There are many applications suitable for a robotic hand, and the dynamic model is a useful tool when determining requirements at the scale of operation. A job requiring accuracy and smaller grasp forces could be performed better by a ½-scale hand. Optimizing a ¼-scale design would open up the possible applications even further.

There has been rapid growth in the field of cell manipulation, but there are still many challenges to overcome, particularly in the development of a micro-hand. One of the main obstacles involves the actuation of a small-scale robot. Using a tool to predict the actuation forces of a design would be beneficial to such research. The Recurdyn model created for this Scalability Study is one more tool to be used in developing a low-cost, robotic hand. Furthermore, the knowledge gained and methods developed in this thesis provide a solid framework for future work.

Reccomendations for Future Work

This section provides a summary of further research that is relatable to this thesis project. These topics could be avenues for which the RIT Robotic Hand Platform could expand and improve. In order to advance in bio-robotics, it is important to remember the scope of the large biological field. Narrowing biomedical engineering down to only mimicking a human hand is a broad and daunting task. Valero-Cuevas writes, "There is still much work to be done to identify the features (anatomical and neural) responsible for, and instrumental to, the specific functional features of versatile hand function" [53]. One of the goals of the RIT Hand Platform is a dexterous design closely resembling human hand movements. This would provide the greatest opportunity and benefit, as it would be intuitive to humans to operate a robot that acts like their own hands. While it is likely impossible to achieve such accuracy and control, the human hand is the benchmark for which researchers aim to imitate.

Ogahara et. al introduced a new driving mechanism for a robotic hand using "elastic torsion springs and hinges as joints, and the finger is wire-driven from actuators placed outside the robot hand" [54]. The mechanism was tested on a one-joint finger, and then was applied to a ½-scale robot hand. The aim was to increase the DOF of a miniature hand, thus the work focused on controlling the individual joints. The ½-size robotic hand presented "is designed to have a maximum output force of at least 1.0 N at the fingertip" [54]. Compared with the RIT life-sized hand, which exhibited 2.0 N of contact force at the fingertip. Modifying the design of the RIT hand to control each joint would be beneficial for improving the hand's dexterity.

As mentioned above, EAPs would be an option for a micro-scale robotic hand. Air muscles could theoretically actuate the ¼-scale hand, but there may be alternatives for this uniquely sized hand. Flexible Microactuators (FMA) "consists of fiber-reinforced rubber structure with multi air chambers and realizes bending motion pneumatically" [55]. Since being developed in 1980, FMAs have been used in miniature robotic applications. However, the process to fabricate these is complicated due to the fiber reinforcements. In 2009, Wakimoto et al. published work describing, "a rubber pneumatic actuator realizing very large bending motion in two directions" [55]. By removing the fibers from the material, the fabrication process was simplified. They presented a miniature soft hand with three fingers that is comparable in size to the ¼-scale RIT hand.

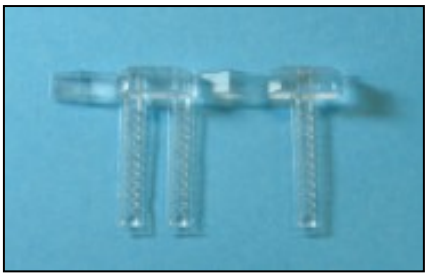

Fig. 62 Soft Hand Before Folding [55]

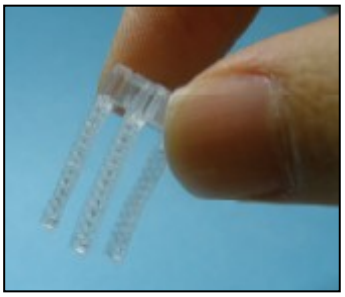

Fig. 63 Finished State of Soft Hand [55]

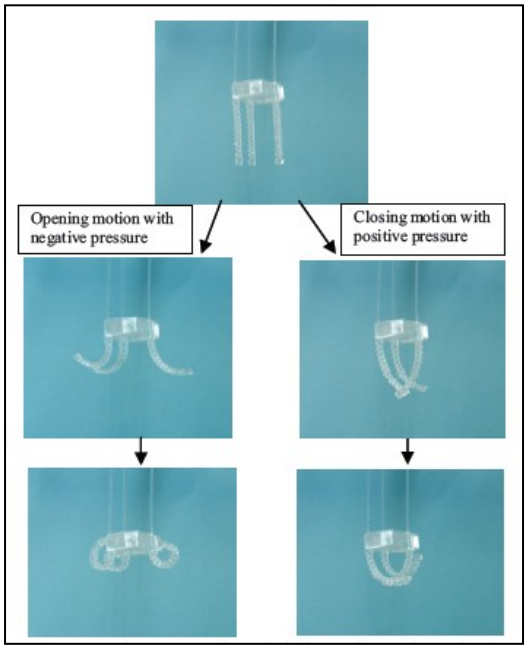

Fig. 64 Experiments of Opening and Closing Motions [55]

These rubber actuators could possibly be attached to the RIT hand's fingers as the foam rubber strip is now, and function as both actuator and spring return, since the actuator

was capable of bending in two directions. Controlling the bending motion could be another project leveraged from this work.

One developing feature of the hands described in the Literature Review was the incorporation of haptic feedback. The ability to sense that an object is being touched and the corresponding ability to adjust the force on the object would provide a much more advanced system. Tactile feedback refers more to sensing an object's size and texture, which is one aspect that most micro-manipulators lack. On the other hand, force feedback or force reflection has nearly become obligatory technology when it comes to development of robotic surgery systems. Work has continued surrounding this problem. For example the development of a "new sensing element… which has a columnar feeler and eight conical feelers. The tactile sensor is validated by scanning surfaces of fine abrasive papers… It is concluded that the sensor has sufficient dynamic sensing capability to detect normal and shearing forces" [56].

Another aspect of grasping force control that was not discussed for the RIT hand is the "issue of translational and rotational slippage that occurs when a robot hand grasps and object" [57]. Since the plastic prototypes made during the Scalability Study were not tested for grasping function, this aspect may be an interesting future project. One might assume that without very strong grasping forces an object could slip against the smooth plastic parts.

Research has been ongoing to address this problem. In order to deal with this, Saito et al. have tried mounting a flexible contact sensor on the robotic hand noting that, "A sufficient condition for grasping an object against translational and rotational slippage is derived on condition that no additional sensors, such as tactile sensors, are required" [57]. After mounting their flexible contact sensor, they set up an experiment to test the grasping performance. A known grasping force was applied to an object, which was supported on the bottom. The support was removed and then an additional rotational moment was applied. Since the object's position did not change significantly, it was concluded that, the object was held against translational and rotational slippage. [57]

Other work described a different approach with the development of a "partial slip sensor contains strain gages in several ridges placed on the curvature contact surface of the elastic body" [58]. More recently, researchers have incorporated tactile sensing to detect slippage and control grasping force accordingly. One article described using "thin, flexible,

lightweight two-dimensional center of pressure (CoP) tactile sensors that can be mounted on a robot hand. CoP sensors can measure the center position of a distributed load applied to the surface of a sensor and the total load itself" [59] thus achieving rapid slip detection.
One benefit of the flexible CoP sensors was that they could be used on curved surfaces such as a robotic hand fingertip. The construction of this sensor is relatively simple. (Fig. 65)
The installation of the sensor on a robotic finger is shown in Figure 66.

Based on their test results "it is clear that immediately before slip displacement occurs, the CoP sensors show changes in force output" [59]. Thus a method was developed for anti-slip control. More testing confirmed that this method was effective. Perhaps this type of tactile sensor could be incorporated with the RIT hand to set it apart as a dexterous, scalable design that is capable of processing haptic feedback.

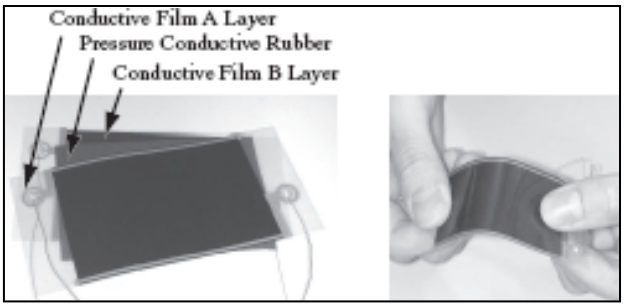

Fig. 65 (left) Structure of CoP sensor [59]
Fig. 63 (right) Installation of CoP sensor [59]

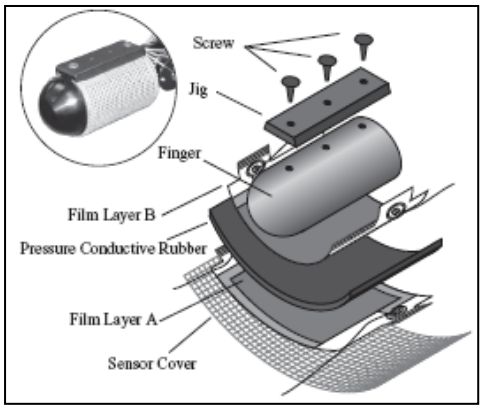

Works Cited

[1] *Shadow Robot Company Ltd.* N.p., 14 Nov. 2007. Web. 2 Feb. 2008. <http://www.shadowrobot.com//>.

[2] *Robonaut Hands*. NASA, n.d. Web. 2 Feb. 2008. <http://robonaut.jsc.nasa.gov/.htm>.

[3] Miller, A, et al. "From Robotic Hands to Human Hands: A Visualization and Simulation Engine for Grasping Research." *Industrial Robot* 32.1 (2005): 55-63. Print.

[4] Girot, Maxime, Mehdi Boukallel, and Stephane Regnier. "Towards a Non-Destructive In Vitro Biomechanical Characterization." *IEEE Bio Micro and Nanosystems Conference* (Jan. 2006): 68-73. Print.

[5] *Wikipedia*. Wikimedia, n.d. Web. 16 Apr. 2010. <http://www.wikipedia.org/>.

[6] Grace, Kenneth W, et al. "A Six Degree of freedom Micromanipulator for Ophthalmic Surgery." *IEEE international Conference on Robotics and Automation* 1 (May 1993): 630-635. Print.

[7] Ramadan, Ahmed A, et al. "New Hybrid Two-Fingered Micro-Nano Manipulator Hand: Optimization and Design." *IEEE International Conference on Mechatronics and Automation* (Aug. 2007): 2524-2529. Print.

[8] Han, Kyungnam, et al. "Fabrication of the Micro-gripper with a Force Sensor for Manipultaing a Cell." *SICE-ICASE International Joint Conference* (Oct. 2006): 5833-5836. Print.

[9] Tam, Michael C.S., Shahram Payandeh, and Ash M Parameswaran. "Design and Development of a Multiple DOF Compliant Robot." *IEEE International Conference on Advanced Robotics* (July 2005): 876-881. Print.

[10] Wejinya, Uchechukwu C, et al. "Development of Pnumatic End Effector for Micro Robotic Manipulators." *IEEE/ASME International Conference on Advanced Intelligent Mechatronics* (July 2005): 558-563. Print.

[11] Xi, Ning, Uchechukwu Wejinya, and Yantao Shen. "End Effector for Nano Manufacturing." *IP Services, Patent*. World Intellectual Property Organization, 2 Jan. 2007. Web. 2 Feb. 2008. <http://www.wipo.int///.jsp?IA=WO2007014095&DISPLAY=STATUS>.

[12] Favre-Bulle, Bernard. “Hyper-Redundant Robotic Micro-Grippers with Neural Control.” *IEEE Conference on Emerging Technologies and Factory Automation* 2 (Sept. 2005): 197-203. Print.

[13] Burdick Group Robotics and BioEngineering Research dept. home page. *California Institute of Technology*. N.p., 1 Nov. 2005. Web. 2 Feb. 2008. <http://robotics.caltech.edu/>.

[14] Truper, T, et al. “Transporting Cells with Mobile Microrobots.” *IEE Procedings Nanobiotechnology* 151.4 (2004): 145-150. Print.

[15] Brufau, J, et al. “MICRON: Small Autonomous Robot for Cell Manipulation Applications.” *IEEE International Conference on Robotics and Automation* (Apr. 2005): 844-849. Print.

[16] Tagliareni, F, et al. “Manipulating Biological Cells with a Micro-robot Cluster.” *IEEE/ RSJ International Conference on Intelligent Robots and Systems* (Aug. 2005): 1414-1419. Print.

[17] Li, Wen J, and Ning Xi. “Novel Micro Gripping, Probing, and Sensing Devices for Single-Cell Surgery.” *IEEE International Conference of the Engineering in Medicine and Biology Society* 4 (Sept. 2004): 2591-2594. Print.

[18] Tie, Zhang, Li Lin, and Xie Cunxi. “Research of Inarticulate Micro-manipulator Robot Driven by Magnetic Levitation Force.” *IEEE International Conference on Systems, Man and Cybernetics* 6 (2004): 5221-5226. Print.

[19] Wang, Xiaoyun, et al. “A Test-Bed for Visual Servo Control of Artificial Muscle Micro-Robot with Parallel Architecture.” *IEEE International Conference on Mechatronics and Automation* (June 2006): 848-853. Print.

[20] Mitsuishi, Mamoru, et al. “A Tele-micro-surgery System Across the Internet with a Fixed Viewpoint/Operation-Point.” *IEEE/RSJ International Conference on Intelligent Robots and Systems* 2 (Aug. 1995): 178-185. Print.

[21] Mitsuishi, Mamoru, et al. “Remote Operation of a Micro-surgical System.” *IEEE International Conference on Robotics & Automation* 2 (May 1998): 1013-1019. Print.

[22] Ikuta, Koji, Keiichi Yamamoto, and Keiji Sasaki. "Development of Remote Microsurgery Robot and New Surgical Procedure for Deep and Narrow Space." *IEEE International Conference on Robotics & Automation* 1 (Sept. 2003): 1103-1108. Print.

[23] Berkelman, Peter J, et al. "A Miniature Microsurgical Instrument Tip Force Sensor for Enhanced Force Feedback During Robot-Assisted Manipulation." *IEEE Transactions on Robotics and Automation* 19.5 (2003): 917-922. Print.

[24] Wang, Shuxin, et al. "A Robotic System with Force Feedback for Micro-Surgery." *IEEE International Conference on Robotics and Automation* (Apr. 2005): 199-204. Print.

[25] *PHANTOM Desktop Haptic Device*. Sensable Technologies, Inc., 2008. Web. 2 Feb. 2008. <http://www.sensable.com/phantom-desktop.htm>.

[26] Mitsuishi, Mamoru. "Medical Robot and Master Slave System for Minimally Invasive Surgery." *IEEE/ICME International Conference on Complex Medical Engineering* (2007): 8-13. Print.

[27] Mitsuishi, Mamoru, Naohiko Sugita, and Phongsaen Pitakwatchara. "Force-Feedback Augmentation modes in the Laparoscopic Minimally Invasive Telesurgical System." *IEEE/ASME Transactions on Mechatronics* 12.4 (2007): 447-454. Print.

[28] *Proportional Integral Derivative PID Controllers*. High Tech Services, 30 Jan. 2008. Web. 2 Feb. 2008. <http://www.htservices.com///.htm>.

[29] "Robotics: the Future of Minimally Invasive Heart Surgery." *Division of Biology and Medicine*. Brown University, 3 May 2000. Web. 16 Apr. 2010.

[30] "da Vinci Surgery." *da Vinci Surgery*. Intuitive Surgical, Inc., 2008. Web. 16 Apr. 2010. <http://www.davincisurgery.com/>.

[31] Yang, Tian, et al. "Motion Planning and Error Analysis in Robot Assistant Micro-Surgery System." *IEEE Proceedings of the 6th World Congress on Intelligent Control and Automation* 2 (June 2006): 8819-8823. Print.

[32] Pak, Nicola Ng, et al. "Electrolytic Silicone Bourdon Tube Microactuator for Reconfigurable Surgical Robots." *IEEE International Conference on Robotics and Automation* (Apr. 2007): 3371-3376. Print.

[33] Kitagawa, Masaya, et al. “Analysis of Suture Manipulation Forces for teleoperation with Force Feedback.” *MICCAI 5th International Conference on Medical Image Computing and Computer Assisted Intervention* (Sept. 2002): n. pag. Print.

[34] Pillarisetti, Anand, et al. “Evaluating the Role of Force Feedback for Biomanipulation Tasks.” *IEEE Symposium on Haptic Interfaces for Virtual Environment and Teleoperator Systems* (Mar. 2006): 11-18. Print.

[35] Riviere, Cameron N, Wei Tech Ang, and Pradeep K Khosla. “Toward Acive Tremor Canceling in Handheld Microsurgical Instruments.” *IEEE Transactions on Robotics and Automation* 19.5 (2003): 793-800. Print.

[36] Davies, Brian, et al. “Active-Constraint Robotics for Surgery.” *IEEE Proceedings* 94.9 (2006): 1696-1704. Print.

[37] *Acrobot*. The Acrobot Company Limited, 2007. Web. 2 Feb. 2008. <http://www.acrobot.co.uk/>.

[38] Kasper, Jonathan, et al. *Air Muscle Artificial Limb*. Rochester: Rochester Institute of Technology, 2008. N. pag. Print.

[39] Moore, Aaron, et al. *Air Muscle Artificial Limb*. Rochester: Rochester Institute of Technology, 2008. N. pag. Print.

[40] Freivalds, Andris. *Biomechanics of the Upper Limbs*. Boca Raton: CRC Press, 2004. Print.

[41] “Recurdyn Multi-Body Simulation & FEA.” *FunctionBay*. Siemens AG, 2010. Web. 16 Apr. 2010. <http://functionbay.de/>.

[42] "Friction Coefficients." *Engineers Handbook*. N.p., 2006. Web. 16 May 2010. <http://www.engineershandbook.com/Tables/frictioncoefficients.htm>.

[43] Bonzo, John. Personal interview. 8 Apr. 2010.

[44] Brecher, Hugh, prod. “A Glimpse of Model Making.” *South East Casting*. N.p., 2007. Web. 16 Apr. 2010. <http://jewelry-casting.net/models.html>.

[45] Vogler, Erwin A. “Courses.” *Erwin Vogler*. The Pennsylvania State University, n.d. Web. 16 Apr. 2010. <http://www.ems.psu.edu/~vogler/.htm>.

[46] "Glossary." *Redeye Express*. Stratasys, 2010. Web. 16 May 2010. <http://express.redeyeondemand.com/Glossary.aspx>.

[47] Cormier, Denis. Personal interview. 8 Apr. 2010.

[48] Sarrran, Michael. “RIT Recieves $400K Grant For Computer-Wafer Processing Technique.” *University News*. Rochester Institute of Technology, 8 Sept. 2004. Web. 16 Apr. 2010. <http://www.rit.edu//?r=44415>.

[49] Raisanen, Alan. Personal interview. Fall-Winter 2009.

[50] Cohen, J Y. “Electroactive Polymers as Artificial Muscles.” *Polymers and Separations Research Laboratory*. University of California, 9 Nov. 2004. Web. 16 Apr. 2010. <http://www.polysep.ucla.edu/%20Advances//_polymers_as_artifi.htm>.

[51] Lin, John, Ying Wu, and Thomas S Huang. *Modeling the Constraints of Human Hand Motion*. Urbana: University of illinois at Urbana-Champaign. N. pag. PDF file.

[52] *Norman Noble, Inc.* Norman Noble, Inc., 2009. Web. 16 Apr. 2010. <http://www.nnoble.com/>.

[53] Valero-Cuevas, Francisco J. "Why the Hand?" *Progress in Motor Control* (2009): 553-557. Print.

[54] Ogahara, Yoichi, et al. "A Wire-Driven Miniature Five Fingered Robot Hand using Elastic Elements as Joints." *IEEE/RSJ*. Proc. of Intl. Conference on Intelligent Robots and Systems. Las Vegas: n.p., 2003. 2672-2677. Print.

[55] Wakimoto, Shuichi, et al. "Miniature Soft Hand with Curling Rubber Pneumatic Actuators." *IEEE*. Proc. of Intl. Conference on Robotics and Automation. Kobe: n.p., 2009. 556-561. Print.

[56] Ohka, Masahiro, Hiroaki Kobayashi, and Yasunaga Mitsuya. *Sensing Characteristics of an Optical Three-axis Tactile Sensor Mounted on a Multi-fingered Robotic Hand*. Nagoya: IEEE, n.d. N. pag. Print.

[57] Saito, Naoki, Toshiyuki Satoh, and Hideharu Okano. *Grasping Force Control in Consideration of Translational and Rotational Slippage by a Flexible Sensor*. Akita: IEEE, 2006. 3892-3897. Print.

[58] Koda, Yuta, and Takashi Maeno. "Grasping Force Control in Master-Slave System with Partial Slip Sensor." *IEEE/RSJ*. Proc. of Intl. Conference on Intelligent Robots and Syatems. Bejing: n.p., 2006. 4641-4646. Print.

[59] Gunji, Daisuke, et al. "Grasping Force Control of Multi-fingered Robot Hand based on Slip Detection Using Tactile Sensor." *SICE*. Proc. of SICE Annual Conference. N.p.: n.p., 2008. 894-899. Print.

Appendix A

Calculations

1. Optimized Phalange Lengths
2. Air Muscle Contraction
3. Spring Stiffness Ratio

Appendix B

Drawings

1. Free Body Diagram
2. ¼-Scale Details

Appendix C

Pictures

1. Range of Motion